

TYCO



TYCO LABORATORIES, INC., BEAR HILL, WALTHAM, MASSACHUSETTS 02154 TELEPHONE 617 899-1650

AD 628071

ELECTROCHEMISTRY OF FUEL  
CELL ELECTRODES

FINAL REPORT

Contract No. Nonr-3765(00)

ARPA ORDER NO. Nonr-3765(00)

Project Code 9800

Task No. NR 359-443

Prepared for:

OFFICE OF NAVAL RESEARCH  
Materials Sciences Division  
Washington 25, D. C.

**BEST  
AVAILABLE COPY**

Tyco Laboratories, Inc.  
Bear Hill  
Waltham, Massachusetts 02154

ELECTROCHEMISTRY OF FUEL CELL ELECTRODES

FINAL REPORT

Contract No. Ncr-3765(00)

ARPA ORDER NO. 302-62

Project Code 9800

Task No. NR 359-443

Prepared for:

OFFICE OF NAVAL RESEARCH  
Materials Sciences Division  
Washington 25, D.C.

Reproduction in Whole or in Part is Permitted by the U.S.  
Government. Distribution of This Document is Unlimited.

Tyco Laboratories, Inc.  
Bear Hill  
Waltham, Massachusetts 02154

ELECTROCHEMISTRY OF FUEL CELL ELECTRODES

FINAL REPORT

Contract No. Nonr-3765(00)

ARPA ORDER NO. 302-62

Project Code 9800

Task No. NR 359-443

Prepared for:

OFFICE OF NAVAL RESEARCH  
Materials Sciences Division  
Washington 25, D.C.

## CONTENTS

	<u>Page No.</u>
I. Abstract	1
II. Summary of Research and Findings	2
A. Electrocatalysis	2
B. Kinetics of Oxidation of Organic Fuels	6
C. Oxygen Reduction	8
III. Abstracts of Work Performed Under this Contract	10
A. Electrocatalysis	11
1. Electrochemical Behavior of Nickel Compounds I. The Hydrogen Evolution Reaction on NiSi, NiAs, NiSb, NiS, NiTe <sub>2</sub> , and their Constituent Elements	11
2. The Hydrogen Reaction on Nickel in Alkaline Solutions	17
3. Hydrogen Evolution at Dilute Platinum and Palladium Amalgam Electrodes	18
4. Hydrogen Evolution at a Dropping Indium Amalgam Electrode	22
5. Hydrogen Evolution at a Solid Indium Electrode	25
6. Activity Coefficients of Liquid Indium-Mercury Amalgams at 25°C	29
7. The Electrical Double Layer on Indium Amalgams in 0.1 M HClO <sub>4</sub> at 25°C	34
8. Interfacial Tension of Indium Amalgams in 0.1 M HClO <sub>4</sub> at 25°C	39
9. A Curve-Fitting Method for Calculating Interfacial Tension by the Sessile Drop Method	45
10. Temperature Dependence of Hydrogen Overvoltage on Indium Amalgams	48
11. The Potential of Zero Charge on Indium Amalgams in Perchlorate Solutions	54

## CONTENTS (Cont.)

	<u>Page No.</u>
12. The Electrical Double Layer on Thallium Amalgam Electrodes	57
13. Hydrogen Overvoltage at a Dropping Thallium Amalgam Electrode	61
14. Hydrogen Evolution and the Electrical Double Layer on Gallium and Gallium Alloy Electrodes	64
15. On the Relation Between Heat of Adsorption of Hydrogen and Hydrogen Overpotential	67
B. Kinetics of Oxidation of Organic Fuels	68
16. Adsorption and Oxidation of Formic Acid on Smooth Platinum Electrodes in $\text{HClO}_4$ Solutions	68
17. The Use of Large Anodic Galvanostatic Transients to Evaluate the Maximum Adsorption on Platinum from Formic Acid Solutions	73
18. Galvanostatic Transient Studies of Carbon Monoxide Adsorption on Platinum Electrodes	77
19. Comparison of Adsorbed Formic Acid and Carbon Monoxide on Platinum Electrodes	81
C. Oxygen Reduction	83
20. Electrochemical Behavior of Nickel Compounds II. Anodic Dissolution and Oxygen Reduction in Perchlorate Solutions	83
21. Kinetics of Redox Reactions on Passive Electrodes	90
22. Kinetics of the Ferric-Ferrous Reaction on Iron-Chromium Alloys	96
23. Surface Oxidation of Gold Electrodes	102
24. Ageing Effects on Thin Anodic Oxide Films on Gold in $\text{N HClO}_4$	107

## I. ABSTRACT

This report is essentially an extended abstract of the main results of the research program initiated in April 1962 under Contract Nonr-3765(00), ARPA Order No. 302-62, and carried out between that time and October, 1965. The program dealt with the electrochemistry of fuel cell reactions, and included studies of the hydrogen reaction, the oxidation of organic fuels, and oxygen reduction. The clarification of the role of the electrode in catalyzing fuel cell reactions was the central theme of this work.

In order to establish the relation of electrocatalytic activity to electrode composition it is necessary first to understand in detail the mechanism of the reaction of interest. The simplest reaction studied was the hydrogen reaction, and in this case, it was possible to show that electrocatalytic activity is dependent on the electronic structure rather than the surface composition of the electrode. The oxidation of organic fuels and oxygen reduction are more complicated reactions and the work with these reactions was directed primarily towards elucidating their kinetics and mechanisms.

A summary of the main experimental results, of the conclusions reached, and of the implications of these studies in the development of fuel cells is given in Section II of this report. Detailed abstracts of the work done under this contract, and published in various journals, are given in Section III.

## II. SUMMARY OF RESEARCH AND FINDINGS

### A. Electrocatalysis

#### 1. Electrocatalytic Activity and Electrode Composition

In attempting to understand, control, and eventually predict the dependence of electrocatalytic activity on electrode composition, it is convenient to distinguish between geometric, chemical, and electronic factors. The geometry of a catalyst surface is always important and in some cases crucial in determining the extent of interaction between reactants and substrate. The roles of the chemical composition of the surface and of the electronic structure of the bulk material are less directly perceived and more difficult to establish. It is particularly difficult to separate these factors and to establish unambiguously their relative importance. However, a distinction between these factors is extremely useful in providing a framework within which a rational search for superior electrode materials can be conducted.

By a "chemical factor" in electrocatalysis we mean: specific interactions between surface atoms and reactants which lead to distinct intermediate chemical compounds. In contrast, we speak of "electronic factors" if the bulk electronic structure of the catalyst or of the surface layer is important in the catalytic reaction. The chemical, or atomic, approach to electrocatalysis implies that reactivity is determined by the intrinsic chemical properties of the individual surface atoms, and is only slightly influenced by neighboring atoms in the crystal. This approach appears to be valid in certain cases: for example, in the chemisorption of oxygen on metalloid surfaces, and in the oxidation and dissolution of covalent intermetallic compounds. On the other hand, the electronic, or continuum, approach has been used extensively to interpret chemisorption and catalysis by transition metal alloys; and is particularly relevant to metals and semiconductors whose electronic structure (expressed, for example, by their electrical conductivity) appears to be intimately related to their catalytic properties.

A study of the relative contribution of atomic and of continuum factors in the electrocatalysis of the hydrogen reaction was undertaken using amalgam electrodes. The hydrogen reaction was chosen because it is relatively simple. The determination of the rates of individual steps in its mechanism is also straightforward. By using a dropping liquid amalgam electrode we were able to obtain a clean, reproducible surface whose chemical composition and electrical properties could be determined unambiguously.

The first alloy systems studied were homogeneous, liquid solutions of platinum and palladium in mercury. Both platinum and palladium are extremely active catalysts for the hydrogen reaction, whereas mercury is a very poor one. Using the exchange currents on the pure metals, we calculate that if platinum atoms were to exert their electrocatalytic effect independent of their surroundings, a nearly saturated amalgam (0.03 mole % Pt) would have an exchange current of about  $3 \times 10^{-7}$  amp/cm<sup>2</sup>, as compared to only  $1 \times 10^{-12}$  for pure mercury. Similarly, palladium amalgams (0.006 mole % Pd) are expected to have an exchange current of about  $6 \times 10^{-9}$  amp/cm<sup>2</sup>. Surprisingly, our experiments showed that the hydrogen reaction on these amalgams proceeded at essentially the same rate as on pure mercury. In attempting to understand the complete absence of catalytic effects by platinum and palladium when these are dispersed in mercury, we examined the electrode capacity as a function of frequency. This measurement gives the extent of adsorption of hydrogen atoms formed as intermediates in the over-all reaction; the results showed that the discharge step on platinum atoms dissolved in mercury must be at least ten times slower than on platinum atoms in pure platinum.

These experiments showed that the electrocatalytic properties of platinum and palladium are greatly modified when they are present as dilute solutions in mercury, and therefore that the atomic approach to catalysis of this reaction is a poor approximation to reality. Thus they provided strong support for a continuum approach in which the electronic structure of platinum plays a dominant role.

In order to understand in greater detail the continuum factors which determine electrocatalytic activity, we studied the hydrogen reaction using amalgams of indium and thallium, which have wide ranges of solubility in mercury, and of gallium. These studies were directed towards establishing the relation of the reaction rate to the surface charge on the electrode, the potential drop in the double layer, of the bulk electronic properties of the electrode (such as the work function). In addition, measurements of electrode capacity and interfacial tension permitted us to obtain the Gibbs surface excess of the amalgam components and to establish whether any relation exists between this quantity and catalytic activity.

The results in the case of the indium amalgams confirmed the continuum approach. Although the surface composition calculated from the Gibbs surface excess showed complex maxima and minima, the exchange current and enthalpy of activation were smooth monotonic functions of bulk composition. For comparisons, the electronic properties of the amalgams, such as electrical conductivity, temperature coefficient of resistivity, Hall Coefficient, and optical reflectivity, all are smooth monotonic functions of composition. These results confirm our previous conclusion that the actual surface composition of a homogeneous electrode has very little influence on the electrocatalytic properties of that electrode: these are determined by electronic properties which reflect the structure of the bulk of the material, and which are cooperative properties of the components, rather than independently additive ones.

One important conclusion which results from a rigorous analysis of the influence of electrode composition on the rate of the hydrogen evolution reaction concerns the influence of the work function of the electrode material on the exchange current for the reaction. From the knowledge that the rate-determining step is transfer of an electron from the electrode to a hydrogen ion at the surface, one might conclude that the work function is a primary factor in determining the rate, but such

is not the case. A cancellation arises if the zero-charge potential of the electrode is a linear function of the work function, with unit slope. This relation holds if the dipolar structure of the interface is independent of electrode composition, as has often been suggested in the literature; but the evidence to back it up has been sketchy, and of low accuracy. We have made accurate measurements of the zero-charge potentials of indium amalgams over the entire range of composition from 0 to 70% indium, and the correlation of these data with accurate measurements of the photoelectric work functions of these same amalgams is crucial in determining the influence which work function may have on electrocatalytic activity. The deviation of the results from the ideal correlation reflects changes in the dipolar structure of the amalgam and the aqueous solution at the metal-electrolyte interface.

## 2. The Role of the Double Layer in Electrode Reactions

All electrode reactions take place in a region within a few angstroms of the interface between metal and solution, and as we have seen, an understanding of the structure and properties of this region is crucial to a rational approach to electrocatalysis. We have carried out studies of the electrical double layer on indium and thallium amalgams to supplement our studies of the hydrogen reaction.

Two important questions have been answered by these studies. First: what effect does a shift in zero-charge potential of the electrode have on the rate of the hydrogen discharge reaction? We have shown that the effect of the diffuse double layer is relatively large, but that differences between amalgams are small primarily because the larger double layer of the more concentrated amalgams tends to cancel the effect of a smaller difference between the electrode potential and zero-charge potential.

Second: is the specific adsorption of ions on the electrode appreciably influenced by the electrode composition? We have shown, by studying the zero-charge potential and double layer capacity of indium amalgams in perchloric acid and sodium fluoride solutions, that although

the fluoride ion is specifically adsorbed on mercury only at very large positive surface charges, it is strongly adsorbed on indium amalgams even at negative surface charges. The perchlorate ion was found to be much less strongly adsorbed on indium amalgams than was the fluoride ion, even though the reverse is true in mercury. These effects show that the composition of the electrode is crucial in determining specific adsorption, and that the properties of the double layer on electrodes cannot in general be predicted from results for mercury. Further studies with other electrode materials will make useful correlations possible, but the influence of electrode composition on the structure of the electrical double layer is a field which has barely been touched.

Our studies of electrocatalysis of the hydrogen reaction show therefore that the continuum electronic structure of the electrode is the principal factor in determining electrode activity: it controls the reaction rate by controlling the extent of adsorption of intermediates and by determining the composition of the double layer in any given solution. Therefore, research on fuel cell catalysts must emphasize the role of electronic structure and must concentrate on intermetallics and other compounds where a controlled variation of electronic structure can be achieved.

#### B. Kinetics of Oxidation of Organic Fuels

Meaningful correlations between electrode composition and electrode activity presuppose a detailed knowledge of the reaction mechanism. The kinetics of oxidation of organic fuels are complex and largely unknown. Therefore, we undertook to study a relatively simple reaction - the oxidation of  $\text{HCOOH}$  to  $\text{CO}_2$  - which could be used as a model reaction in electrocatalytic studies with organic fuels.

A significant problem in studying these reactions is the difficulty of obtaining reproducible measurements. This is due to the difficulty of defining the surface structure and, most importantly, to the sluggishness of attaining a steady state for ad-species. To overcome this, very careful preparation and purification techniques were used and, in

addition, a procedure of electrode pre-anodization was adopted to ensure a well-defined, clean surface. Both galvanostatic cleaning pulses, and potentiostatic pulses, which avoid any possible interference from  $O_2$  evolved during the cleaning process, were used to pretreat the electrode.

The crucial and significant findings of the work with formic acid were: i) adsorption onto Pt from acid solutions of HCOOH is slow - much slower than the diffusion-limited rate; ii) the adsorption rate is potential-dependent; iii) the product of adsorption interferes with the oxidation process.

The self-poisoning characteristic of this reaction is of general significance to electrochemical oxidation of organic fuels since it is encountered with all organic fuels. Giner has described a species, which he calls "reduced  $CO_2$ ", which is formed on the reductive adsorption of  $CO_2$  on Pt. He found a qualitative similarity between this species and a species which is adsorbed on Pt from solutions of a number of simple oxygenated organic fuels. Recently, he has shown that the same species is found on working hydrocarbon electrodes. The studies carried out by us show that this conclusion may be too simple, but it does point up the intimate relation between these reactions and the reactions of hydrocarbons.

Further work was thus centered on efforts to identify this adsorbing "poison" for HCOOH oxidation. The experimental work was primarily concerned with trying to make an accurate determination of the characteristics of the film adsorbed on smooth Pt from HCOOH solutions and comparing them with those found for CO, which has been suggested as the poison. (This CO is supposed to originate from the decomposition of HCOOH).

The difficulty in characterizing  $Q_{HCOOH}$  (the charge to oxidize the species adsorbed from HCOOH solutions) is that the species can only be oxidized in a potential region where the electrode itself oxidizes. Thus, there are three faradaic processes which can contribute to the anodic charge passed during the oxidation of the adsorbate. These are: (1) oxidation of adsorbate, (2) oxidation of species in solution, and (3) surface oxidation of the electrode. In order to separate these and to

determine (1), a new method was developed, involving the application of a series of pulses to the surface of the electrode. Then, an effective separation of these processes can be made for HCOOH and CO, and accurate values of  $Q_{\text{HCOOH}}$  ( $285 \mu\text{coul/cm}^2$ ) and  $Q_{\text{CO}}$  ( $365 \mu\text{coul/cm}^2$ ) can thus be made. The difference between  $Q_{\text{HCOOH}}$  and  $Q_{\text{CO}}$  and a comparison of the oxidation kinetics showed that  $\text{CO}_{\text{ads}}$  and " $\text{HCOOH}_{\text{ads}}$ ", while similar, are not the same. The question of the identity of the adsorbing poison is, thus, still open.

These studies form a basis on which to attempt to establish the detailed kinetics of oxidation of organic fuels eventually leading to the efficient electrochemical oxidation of common fuels, similar to gasoline or diesel oil. It appears that platinum will not turn out to be the best catalyst for this electrochemical reaction and that alternative electrodes must be found. This suggests in turn that less drastic conditions than concentrated phosphoric acid and elevated temperatures must be developed, particularly if materials outside the noble metal group are to be explored.

### C. Oxygen Reduction

In a number of fuel cell systems, such as  $\text{H}_2/\text{O}_2$ , the oxygen electrode limits the attainable efficiency and power density. Oxygen reduction is a highly irreversible process with complex kinetics which are still largely unknown even for simple electrodes. The kinetics are further complicated by side reactions (e. g.  $\text{H}_2\text{O}_2$  production) and by reactions with the substrate (surface oxide formation). In order to clear up at least some of the ambiguities in studies of this reaction, we undertook to examine the general role of surface oxide films in determining the kinetics of electrochemical reactions at electrodes. This work was extended later to include studies of the kinetics of formation and reduction of oxides and particularly of the factors which determine their steady state thickness and their electrochemical properties.

Aside from specific effects, e. g. changes in the energy of adsorption of reactants or of intermediates, superficial oxides may influence the kinetics of an electrochemical reaction by providing a barrier to electron

transfer between the metal and an ion or molecule at the oxide/electrolyte interface. A simple way of examining the general electrochemical effects of surface oxides is to compare the kinetics of an elementary electron transfer reaction on oxide-covered and oxide-free electrodes. Specific effects, e. g. adsorption, should be at a minimum for the redox couple chosen. The ferric-ferrous couple was selected in this study because its kinetic behavior on oxide-free electrodes is straightforward. Overpotential measurements for this couple on passive nickel, iron, chromium, titanium, and iron-chromium alloys were carried out in solutions of fixed ionic strength but of varying pH. Tafel lines were generally obtained with exchange currents between  $10^{-7}$  and  $10^{-5}$  amp/cm<sup>2</sup> and cathodic transfer coefficients of about 0.45. The anodic transfer coefficients were less, particularly with Ti and Fe electrodes. A limiting anodic current, which was unrelated to diffusion in solution, was observed under certain conditions on Fe and Ti. In general, the surface oxide film has rectifying properties, the easy direction of electron flow being from metal to solution. This rectification is additional to the usual faradaic rectification observed with most electrochemical reactions. The apparent transfer coefficients, calculated from the anodic and cathodic polarization curves, yield sums significantly less than unity. The results demonstrate the existence of a potential drop across the surface oxide film, the magnitude of the drop being dependent on the thickness and composition of the film.

These studies suggest that one condition for optimum performance of a material as an oxygen electrode is either the absence of an oxide film or the restriction to a minimum thickness (e. g. by suitable alloying or choice of electrolyte) of any surface oxide film which may be formed in the relevant potential region.

III. ABSTRACTS OF WORK PERFORMED  
UNDER THIS CONTRACT

## A. Electrocatalysis

### 1. Electrochemical Behavior of Nickel Compounds I. The Hydrogen Evolution Reaction on NiSi, NiAs, NiSb, NiS, NiTe<sub>2</sub>, and Their Constituent Elements

A. K. M. Shamsul Huq and Arthur J. Rosenberg

Submitted as Technical Memorandum No. 1 (April, 1963).

Presented at the Boston Meeting of the Electrochemical Society, May, 1963.

Published: J. Electrochem. Soc. 111, 270-278 (1964).

The objective of the studies was to clarify the influence of crystal environment on the electrochemical, and particularly the electrocatalytic, properties of a transition metal atom. We chose to examine several compounds of nickel with elements from groups IVB, VB, and VIB of the Periodic Table. The use of such compounds was favored for two reasons: the clear chemical differences between the component elements, and the highly ordered atomic coordination.

The cathodic polarization behavior of NiSi, NiAs, NiSb, NiTe<sub>2</sub>, and NiS at room temperature was determined in 1M perchlorate solutions at pH 0.04 and pH 10.8 up to -1.0v vs. the reversible hydrogen electrode. Measurements were also made on Ni, Si, Sb, Te, and on Ni electrodes exposed to As<sub>2</sub>O<sub>3</sub> and H<sub>2</sub>S. Sb, Te, Si, and Ni + As<sub>2</sub>O<sub>3</sub> exhibit kinetic peculiarities which are probably attributable to hydride formation, but these features are not generally shown by the corresponding nickel compounds. With the exception of Si in acid solution, all of the electrodes show an extended Tafel line indicating the hydrogen evolution reaction with the following characteristics. In alkaline solution, the Tafel slope is greater than 100 mv for all metals, while the exchange current is between 10<sup>-5</sup> and 10<sup>-8</sup> amp/cm<sup>2</sup>. In acid solution, Ni, Sb, NiSi, NiSb, and Ni + As<sub>2</sub>O<sub>3</sub> have slopes close to 120 mv, while Te, NiTe<sub>2</sub>, Ni + H<sub>2</sub>S, and NiS show slopes between 50 and 80 mv. The exchange currents in acid solution vary from about 10<sup>-5</sup> for Ni to about 10<sup>-11</sup> amp/cm<sup>2</sup> for Te. The data are shown in Figs. 1-1 - 1-6 and Table 1-1.

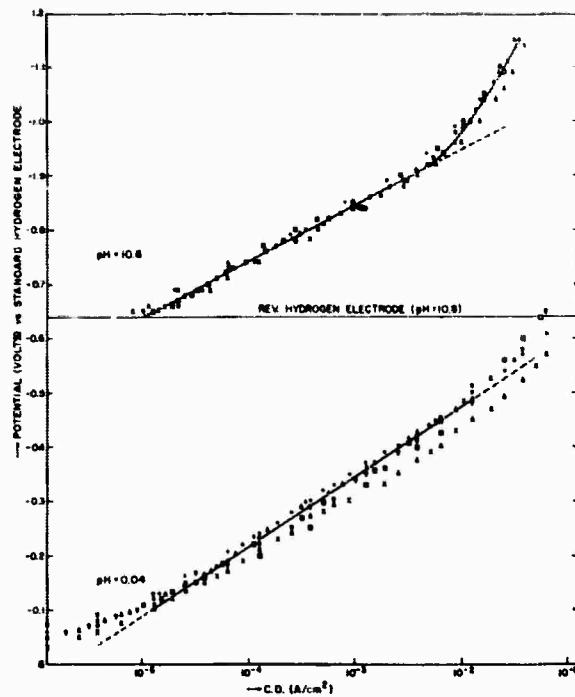


Fig 1-1. Hydrogen evolution reaction on nickel in 1M  $\text{HClO}_4$ , pH 0.04 and in  $1\text{M NaClO}_4 + 10^{-2}\text{M NaOH}$ , pH 10.8 at  $25^\circ\text{C}$ . Solution preelectrolyzed at 30 ma for 6 hr. Results of ten runs at pH 0.04 with mean  $b = 0.125\text{v}$ ,  $i_0 = 2 \times 10^{-6}\text{ amp/cm}^2$  and of six runs at pH 10.8 with  $b = 0.105\text{v}$ ,  $i_0 = 1 \times 10^{-5}\text{ amp/cm}^2$ .

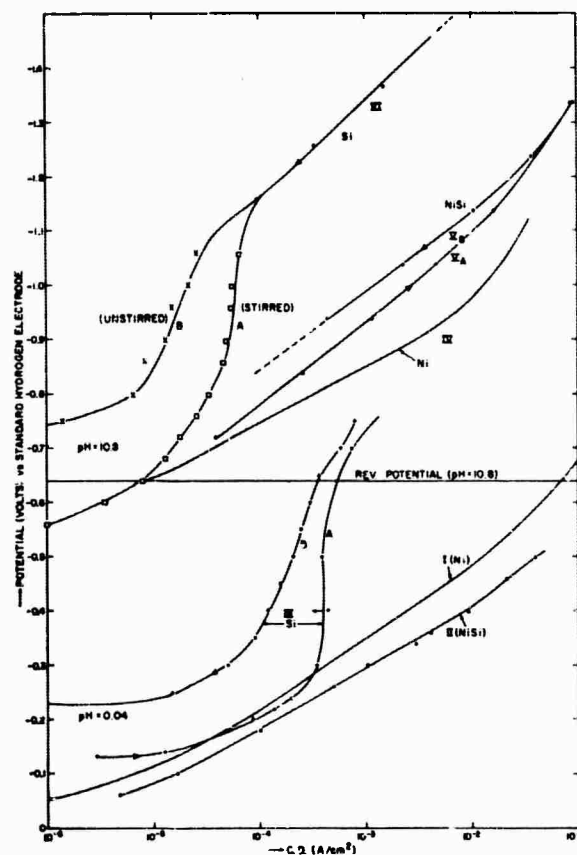


Fig. 1-2. Cathodic polarization curves (log current density vs. potential) for NiSi and Si in  $1\text{M HClO}_4$ , and in  $1\text{M NaClO}_4 + 10^{-2}\text{M NaOH}$ , pH 10.8 at  $25^\circ\text{C}$ . At pH 0.04, I, Ni (for comparison); II, NiSi; III<sub>A</sub>, Si toward higher cathodic potentials (up); III<sub>B</sub>, Si, toward lower cathodic potentials (down). At pH 10.8, IV, Ni (for comparison); V<sub>A</sub>, NiSi (up); V<sub>B</sub>, NiSi (down); VI, Si (A, stirred, B, un stirred).

TABLE 1-1

Tafel Parameters for the Hydrogen Evolution Reaction

	<u>pH 0.04</u>		<u>pH 10.8</u>	
	<u>b, mv</u>	<u><math>-\log i_{o,2}</math> amp/cm<sup>2</sup></u>	<u>b, mv</u>	<u><math>-\log i_{o,2}</math> amp/cm<sup>2</sup></u>
Ni	125	5.3	105	5.0
Ni + As <sub>2</sub> O <sub>3</sub>	120	8.0	no effect on Ni	
NiAs	56	7.3	155	6.1
Si	no Tafel region		168	7.5
NiSi	113	5.4	145	5.4
Sb	170	5.7	260	5.3
NiSb	108	7.6	245	5.0
Te	48	11	-	-
NiTe <sub>2</sub>	55	8	-	-
Ni + H <sub>2</sub> S	80	9.4	no effect on Ni	
NiS	62	7.2	100	4.9

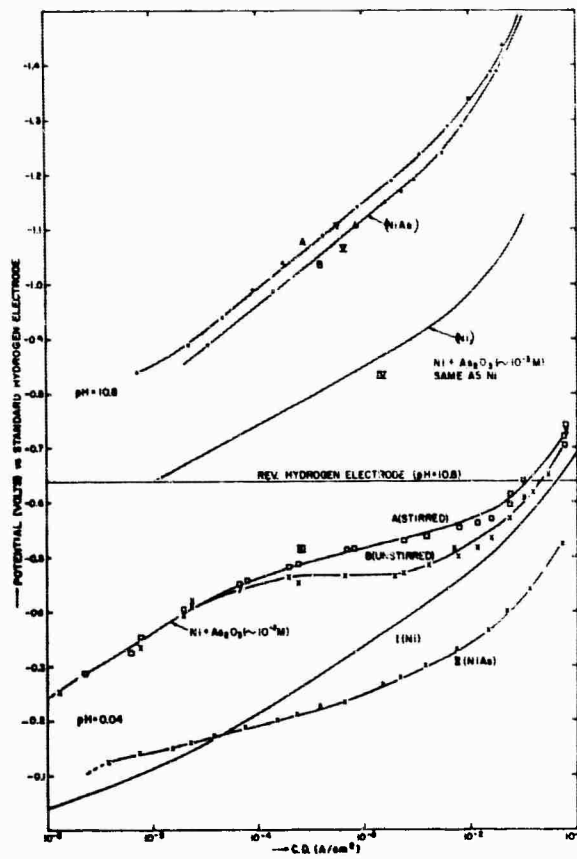


Fig. 1-3. Cathodic polarization curves for NiAs and Ni +  $10^{-3}$ M  $As_2O_3$  in 1M  $HClO_4$ , pH 0.04, and in 1M  $NaClO_4$  +  $10^{-2}$ M  $NaOH$ , pH 10.8 at 25°C. At pH 0.04, I, Ni; II, NiAs, mean of 5 runs; III, Ni with addition of  $\sim 10^{-3}$ M  $As_2O_3$  in solution; (A stirred, B, unstirred). At pH 10.8, IV, Ni, no effect of  $\sim 10^{-3}$ M  $As_2O_3$  added to solution. V, NiAs (A, "up"; B, "down").

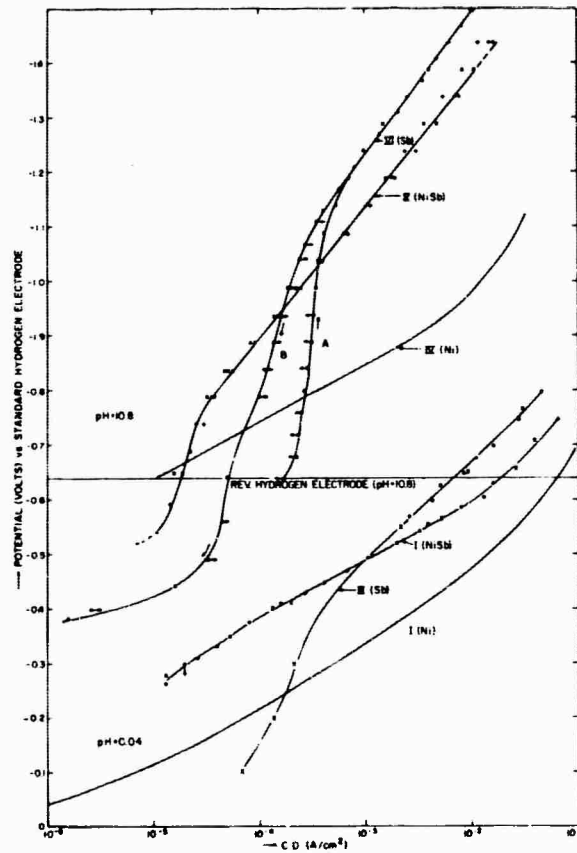


Fig. 1-4. Cathodic polarization curves for NiSb and Sb in 1M  $HClO_4$ , pH 0.04 and in 1M  $NaClO_4$  +  $10^{-2}$ M  $NaOH$ , pH 10.8 at 25°C. At pH = 0.04, I, Ni; II, NiSb; III, Sb. At pH = 10.8, IV, Ni; V, NiSb; VI, Sb. (A, "up"; and B, "down").

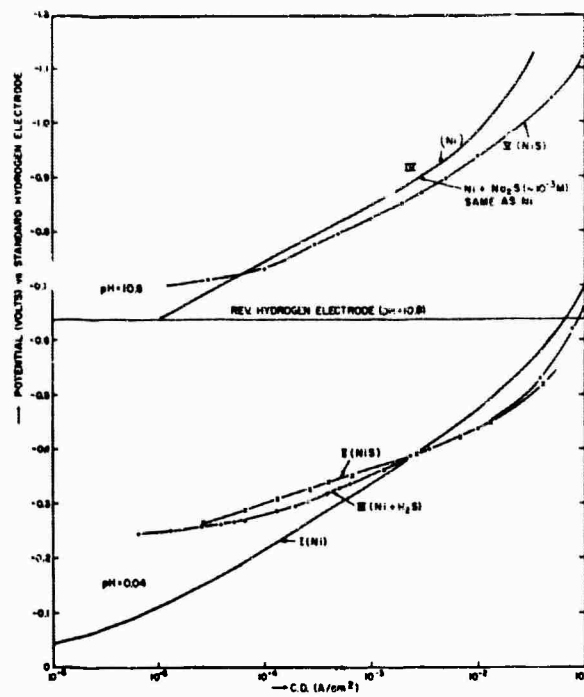


Fig. 1-5. Cathodic polarization curves in  $1M HClO_4$ , pH 0.04 and in  $1M NaClO_4 + 10^{-2}M NaOH$ , pH 10.8 at  $25^\circ C$ . At pH = 0.04, I, Ni; II, NiS (odor of  $H_2S$  in the effluent gas); III, Ni in presence of  $H_2S$ , added as  $Na_2S$ . At pH = 10.8, IV, Ni; V, NiS, no effect of addition of  $\sim 10^{-3}M Na_2S$ .

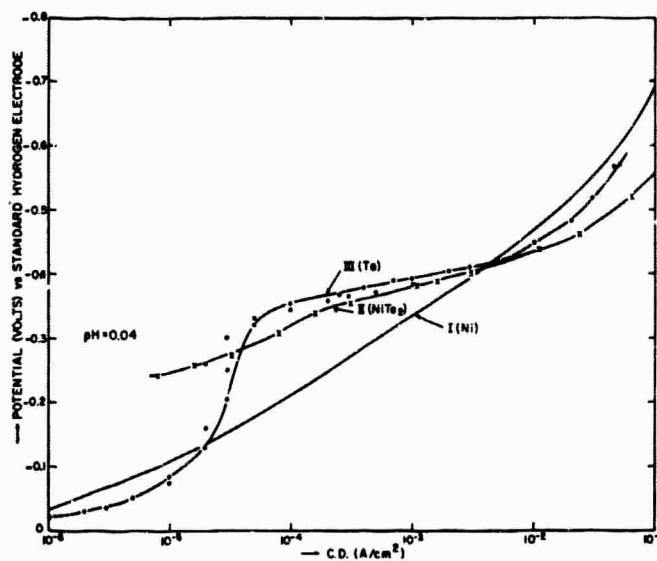


Fig. 1-6. Cathodic polarization curves in  $1M HClO_4$ , pH 0.04, at  $25^\circ C$ . I, Ni; II,  $NiTe_2$ ; III, Te.

In the cases of NiAs, NiTe<sub>2</sub>, and NiSi in acid solution, there are potential regions where the current densities on the compounds are greater than on either of the component elements. This immediately rules out the simple atomic description since the surface concentration of either component, regardless of crystallographic orientation, does not exceed that of its elemental form. For the remaining cases under study, it is also evident that the over-all rate of the hydrogen evolution reaction is not a specific atomic property, and that interactions between the surface atoms or between adsorbed hydrogen atoms at neighboring sites on the crystal surface play a prominent role.

It was concluded, therefore, that the electrocatalysis of the hydrogen evolution reaction on nickel compounds cannot be explained in terms of the intrinsic chemical properties of the surface atoms. Further work along these lines, together with complementary studies of the electronic properties and gas phase chemisorption characteristics, is needed to elucidate the electronic factors governing electrocatalytic activity.

## 2. The Hydrogen Reaction on Nickel in Alkaline Solutions

A. C. Makrides

Submitted: J. Electrochem. Soc.

The hydrogen reaction on nickel was studied at a number of NaOH and Na<sub>2</sub>SO<sub>4</sub> concentrations at 30°C. The exchange current, Tafel slope, stoichiometric number, and hydrogen oxidation current depend on the polarization history of the electrode. The initial electrode state, characterized by a relatively low exchange current and high Tafel slope and by a stoichiometric number of 2 is transformed, upon anodic-cathodic cycling, to a state with a higher exchange current, low Tafel slope, and a stoichiometric number of 1. These changes are attributed to the formation of a superficial oxide which is not easily reduced. This oxide is in some respects unique since it enhances the rate of cathodic hydrogen evolution although it inhibits hydrogen oxidation. The original electrode state can be regenerated by extreme cathodic polarization ( $> 100 \text{ ma/cm}^2$ ).

### 3. Hydrogen Evolution at Dilute Platinum and Palladium Amalgam Electrodes

---

J. N. Butler and A. C. Makrides

Submitted as Technical Memorandum No. 7 (October, 1963).

Presented at the Toronto Meeting of the Electrochemical Society  
May, 1964 .

Published: Trans. Faraday Soc. 60, 938-946 (1965).

Studies of electrocatalysis by solid alloy electrodes are complicated by the problem of obtaining a clean, reproducible surface. Almost any operation designed to remove adsorbed material from the surface of a solid alloy changes the structure or composition of the surface to some extent. For this reason, studies of electrocatalysis by liquid alloys at a dropping electrode provide a more direct approach to the influence of alloy composition on electrode activity. We have made the present study to determine the extent to which platinum or palladium exerts an electrocatalytic effect for the evolution of hydrogen, when present as a dilute alloy in mercury, an inactive metal.

We have measured hydrogen overpotential and differential capacity on an amalgam containing 0.028 atom percent platinum and an amalgam containing 0.006 atom percent palladium. A conventional three-compartment pyrex cell was fitted with a capillary in place of the working electrode, and housed in an air thermostat. All measurements were made in 0.100 molar perchloric acid at 25°C. The electrolyte was saturated with hydrogen throughout the experiment. Extreme care was taken to eliminate any impurities in the solution.

Measurements of hydrogen overpotential were made using an electronic potentiostat to fix the potential of the drop with respect to a reversible hydrogen electrode in the same solution, and the current was displayed on an oscilloscope. From the known growth rate of the drop, the drop area was calculated. Galvanostatic measurements were made by fixing the current passing between the drop and a counter electrode,

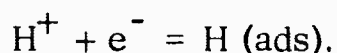
and measuring the potential of the drop with respect to a reference electrode with the oscilloscope. Both methods gave the same results for current densities higher than  $10^{-4}$  amp/cm<sup>2</sup>, and the results for mercury agreed with the best literature values.

Differential capacity measurements were made using a platinized platinum screen which surrounded the drop. The method was essentially that of Grahame [J. Am. Chem. Soc. 71, 2975 (1949)]. Measurements were made at a fixed point in the drop lifetime, balancing a series resistance and capacitance decade in an impedance bridge. For mercury, the values agreed with those obtained by Grahame.

As can be seen from Figs.3-1 and 3-2, the hydrogen overvoltage and differential capacity values obtained with the platinum and palladium amalgams were identical with that of pure mercury within the experimental error. The differential capacity showed no frequency dependence between 500 cycles and 10 kilocycles.

Platinum and palladium are extremely active catalysts for the hydrogen evolution reaction, and mercury is a relatively poor one. The exchange current on platinum is  $10^{-3}$  amp/cm<sup>2</sup> and on mercury  $1.5 \times 10^{-12}$  amp/cm<sup>2</sup>. If platinum atoms were to exert their electrocatalytic effect independently of their surroundings, an alloy containing 0.03 atom percent platinum in a catalytically inactive metal might be expected to have an exchange current about 0.03% of that observed on pure platinum, or  $3 \times 10^{-7}$  amp/cm<sup>2</sup>. This is  $2 \times 10^5$  times larger than the exchange current actually observed. For the palladium amalgam, since the exchange current on pure palladium is  $10^{-4}$  amp/cm<sup>2</sup>, the expected exchange current is  $4 \times 10^3$  larger than the value actually observed.

From the measurements of differential capacity, we can set an upper limit for the exchange current for the discharge reaction



This must be smaller than  $1.6 \times 10^{-5}$  amp/cm<sup>2</sup> for the platinum amalgam. The expected value for this quantity if platinum atoms behaved independently

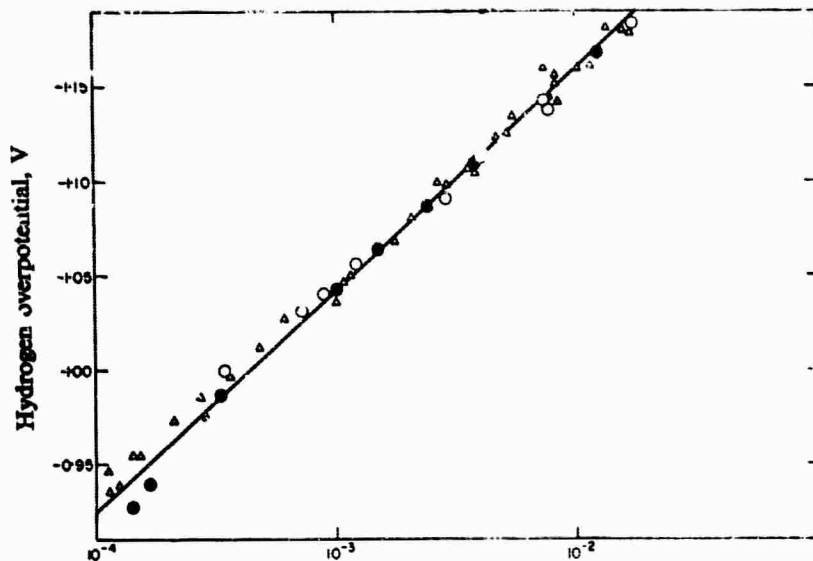


Fig. 3-1. Hydrogen overpotential on platinum amalgam (0.028 mole %), palladium amalgam (0.006 mole %), and pure mercury. O, platinum amalgam; ●, palladium amalgam; Δ, pure mercury. The Tafel line has a slope of 118 mv and an exchange current of  $1.5 \cdot 10^{-12}$  A/cm<sup>2</sup>.

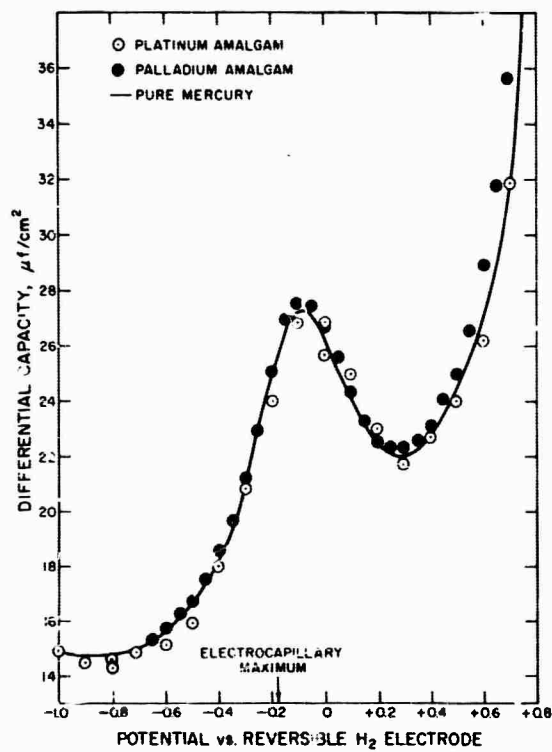


Fig. 3-2. Differential capacity on platinum amalgam (0.028 mole %) and palladium amalgam (0.006 mole %). The line represents the data for pure mercury.

of their surroundings is more than ten times as large. Furthermore, the over-all rate of the hydrogen evolution reaction at a platinum atom in the amalgam cannot be more than 100 times greater than the over-all rate of hydrogen evolution at a mercury atom, or a significantly lower over-potential would have been observed. When normalized to the fraction of the surface actually occupied by platinum atoms, this result shows that the over-all rate of hydrogen evolution at a platinum atom in the amalgam is approximately  $10^{-7}$  of what it is at a platinum atom in pure platinum. An analogous series of arguments can be made regarding the palladium amalgam.

These experiments on the electrocatalysis of hydrogen evolution by dilute platinum and palladium amalgams have shown that the electrocatalytic properties of platinum and palladium are greatly modified when they are present as dilute solutions in mercury. This lends support to the idea that electrocatalysis is primarily a cooperative property of the continuum structure of an alloy rather than an independently additive atomic property.

#### 4. Hydrogen Evolution at a Dropping Indium Amalgam Electrode

James N. Butler and A. C. Makrides

Submitted as Technical Memorandum No. 10 (February, 1964).

Presented in part at the Philadelphia Meeting of the American Chemical Society, April, 1964.

Published: Trans. Faraday Soc. 60, 1664-1676 (1954).

We have continued our studies of electrocatalysis by liquid metal alloys, using indium amalgams. Indium-mercury alloys can be prepared which are liquid at room temperature and which contain up to 63.7 atom percent indium. We have measured the hydrogen overpotential, the double-layer impedance, and the potential of zero charge on a series of these amalgams varying in composition from 0.0001% to 63.7%.

A conventional three-compartment pyrex cell was fitted with a capillary in place of the working electrode, and housed in an air thermostat. All measurements were made in 0.100 molar perchloric acid at 25°C. The electrolyte was saturated with hydrogen throughout the experiment. Extreme care was taken to eliminate any impurities in the solution.

Measurements of hydrogen overpotential were made using an electronic potentiostat to fix the potential of the drop with respect to a reversible hydrogen electrode in the same solution, and the current was displayed on an oscilloscope. From the known growth rate of the drop, the drop area was calculated. Galvanostatic measurements were made by fixing the current passing between the drop and a counter electrode, and measuring the potential of the drop with respect to a reference electrode with the oscilloscope. Both methods gave the same results for current densities higher than  $10^{-4}$  amp/cm<sup>2</sup>, and the results for mercury agreed with the best literature values. The results are shown in Fig. 4-1.

The potential of zero-charge was measured by the streaming electrode method. At these potentials, the capacity was frequency-

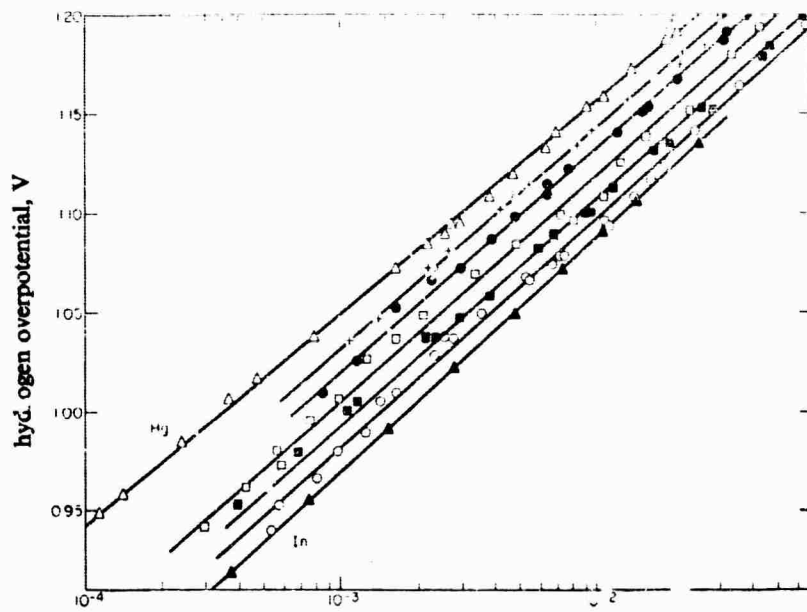


Fig. 4-1. Tafel plot of experimental results for mercury, indium, and the amalgams.

▲, pure Hg; +, 8.4% In; ●, 16.3% In; □, 30.4% In;  
 ■, 52.2% In; ○, 64.4% In; ▲, pure In (solid)

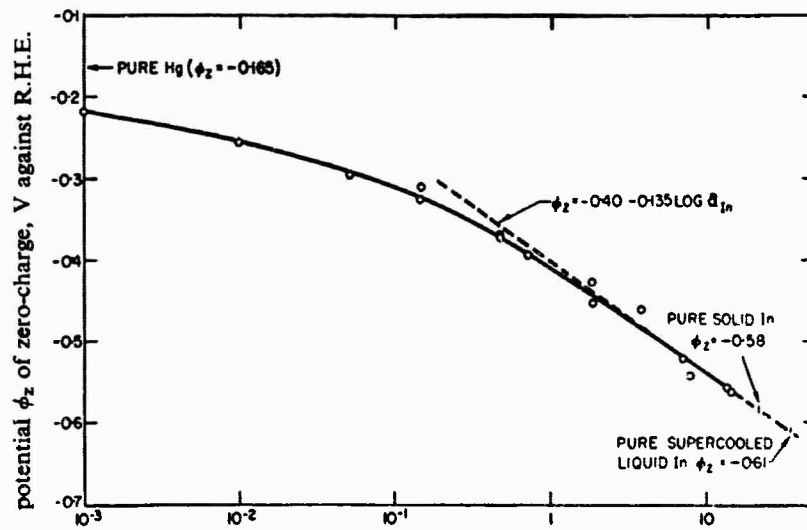


Fig. 4-2. Potential of zero charge shown as a function of the activity of indium in the amalgam.

independent, indicating an ideally polarized electrode, and the values measured for mercury agreed with those in the literature. The values are shown as a function of the activity of indium in the amalgam in Fig. 4-2.

Using the values of the zero-charge potential and some preliminary measurements of the double-layer capacity, corrections were made for the effect of the diffuse double layer on the reaction, and the experimental results were found to fit the theoretical relation with a cathodic transfer coefficient  $\alpha = 0.50$ .

Because there is virtually no change in the impedance at large negative potentials as the composition is varied, and because the Tafel slope is independent of composition, the mechanism of the hydrogen evolution reaction on indium amalgams is probably the same as on mercury: the rate determining step being the discharge of a hydrogen ion.

Two extreme viewpoints may be taken in predicting the electrocatalytic properties of alloys. According to the "atomistic" viewpoint, the electrocatalytic properties of an alloy result from short-range interactions, and to the first approximation are a linearly additive property of the components of the alloy. At the other extreme, from the "continuum" viewpoint, the electrocatalytic properties of an alloy result from cooperative properties of the material, such as its electronic band structure. Both viewpoints have been useful in explaining electrocatalysis by alloys.

The rate of hydrogen evolution on indium amalgams at a given potential varies almost linearly with the composition; but this results from two factors: The potential across the solution-electrode interface, and the purely catalytic effects. By taking the current at the potential of zero charge, the effects of excess surface charge can be separated from the purely catalytic effects. The current at the potential of zero charge varies with composition over four orders of magnitude in a very non-linear fashion. Thus, the purely catalytic properties of the amalgams have been shown to be a cooperative property, rather than a simple additive atomic one.

## 5. Hydrogen Evolution at a Solid Indium Electrode

James N. Butler and Manfred Dienst

Submitted as Technical Memorandum No. 11 (April, 1964).  
Presented at the Washington Meeting of the Electrochemical Society, October, 1964; and at the Western States Combustion Meeting, Salt Lake City, October, 1964.  
Published: *J. Electrochem. Soc.* 112, 226-232 (1965).

Indium offers an unusual opportunity for a detailed study of hydrogen overvoltage, since its zero-charge point lies within the range of potentials where hydrogen evolution is the principal reaction. We have made accurate measurements of hydrogen overpotential on indium in 0.1 molar perchloric acid at temperatures from 21°C to 59.5°C. Typical results are shown in Fig. 5-1. These results have been analyzed in terms of the structure of the electrical double layer at the indium-electrolyte interface, and the transition state theory of reaction rates.

The hydrogen evolution reaction on indium is very sensitive to traces of oxygen. In order to remove the oxide film initially present on the electrode and to obtain reproducible measurements of hydrogen overvoltage, it was necessary to polarize the electrode cathodically for 16 hours at 30°C. The oxide film was removed more rapidly at higher temperatures. Current-potential curves measured in oxygen-saturated solutions indicate that the hydrogen evolution reaction occurs at the same rate on clean or oxidized electrodes, but that oxygen reduction is more rapid on a clean electrode.

The slow step in the mechanism of hydrogen evolution is probably discharge of a hydrogen ion. The exchange current is approximately  $10^{-11}$  amp/cm<sup>2</sup> at 30°C, and the cathodic transfer coefficient is 0.50. These values are similar to those observed on mercury and lead, for which the slow-discharge mechanism is well-established. Addition of iodide ion decreases the overvoltage; and the effect of acid concentration on overvoltage is also in accord with a slow-discharge mechanism.

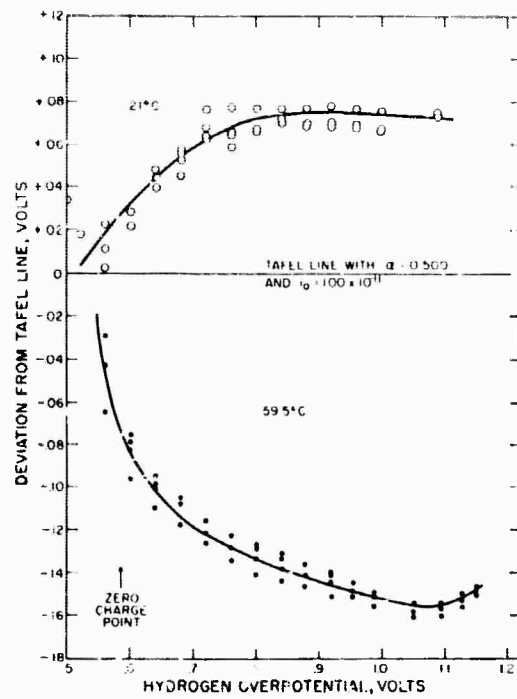


Fig. 5-1. Deviation of experimental current-potential curve from an arbitrary Tafel line with  $\alpha = 0.500$  and  $i_0 = 1.00 \times 10^{-11}$ .

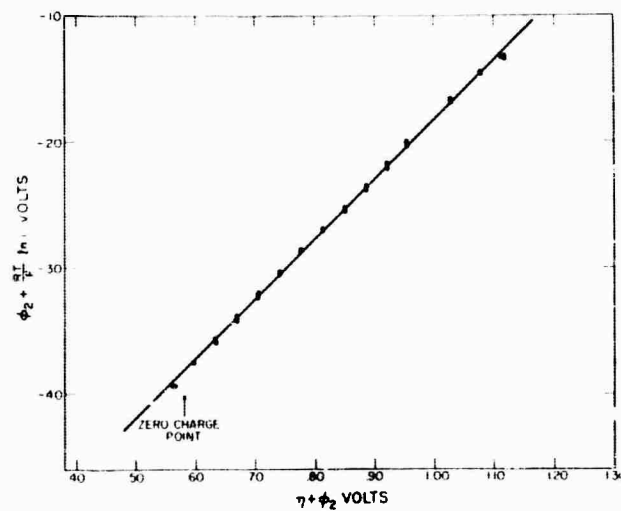


Fig. 5-2. Fit of experimental data to Eq. [ 2 ] . The temperature was  $32^{\circ}\text{C}$ , and the capacity function (Eq. [ 1 ] ) was used to calculate  $\phi_2$ . The correlation coefficient for the least-squares straight line is 0.9995. The best values for the parameters are  $\alpha = 0.472 \pm 0.003$  and  $-\log i_0' = 16.82 \pm 0.05$ .

The capacity of the electrode was measured and found to be given approximately by the equation

$$K = 8.9 + 2.75\phi_0 + 1.25\phi_0^2 \quad (1)$$

where  $K$  is the integral capacity ( $\mu\text{f}/\text{cm}^2$ ) and  $\phi_0$  is the potential with respect to the zero charge point of indium.  $\phi_2$ , the potential of the outer Helmholtz plane, was calculated using this capacity function and the experimental data was fitted to the Frumkin equation

$$\eta = \frac{1-\alpha}{\alpha}\phi_2 - \frac{RT}{\alpha F} \ln(i/i_0') \quad (2)$$

where  $i_0'$  is the corrected exchange current and is given by:

$$\ln i_0' = (1-\alpha) \ln[H^+] + \frac{\alpha F}{RT} g_H + \text{const.}$$

In these equations,  $\eta$  is the hydrogen overpotential,  $\alpha$  is the cathodic transfer coefficient,  $[H^+]$  is the concentration of hydrogen ion in the electrolyte, and  $g_H$  is the free energy of adsorption of a hydrogen atom on the electrode. The values of the parameters  $\alpha$  and  $i_0'$  are given in Table 5-1. The fit of a typical set of data is shown in Fig. 5-2.

The temperature dependence of the current at constant potential gives the enthalpy of activation for the discharge reaction. At the reversible hydrogen potential, this is  $14.1 \pm 0.5$  kcal/mole, and at the zero charge point it is  $10 \pm 0.2$  kcal/mole. Using a theoretical curve calculated by Parsons and Bockris [Trans. Faraday Soc. 47, 914 (1951)] using the transition state theory, the heat of adsorption of hydrogen atoms on indium is estimated from these values to be  $50 \pm 10$  kcal/g atom.

TABLE 5-1

Parameters of the Current-Potential Curve for  
Hydrogen Evolution on Indium  
 (Errors are 95% Confidence Limits)

Temp °C	corrected <sup>(a)</sup>		uncorrected <sup>(b)</sup>	
	$\alpha$	$-\log i'_0$	$\alpha$	$-\log i'_0$
21.0	.389 ± .011	10.19 ± .14	.445 ± .009	10.74 ± .12
25.0	.449 ± .003	10.86 ± .04	.498 ± .002	11.15 ± .03
30.0	.489 ± .004	10.83 ± .06	.530 ± .004	11.19 ± .07
41.0	.495 ± .005	10.77 ± .07	.538 ± .005	11.14 ± .07
50.5	.502 ± .006	10.44 ± .08	.546 ± .006	10.81 ± .09
59.5	.510 ± .006	10.22 ± .07	.552 ± .006	10.57 ± .08

a) using the capacity given by equation (1)

b) assuming  $\phi_2 = 0$  in equation (2)

5. Activity Coefficients of Liquid Indium-Mercury  
Amalgams at 25°C

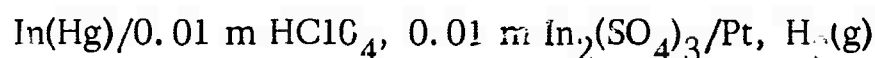
James N. Butler

Submitted as Technical Memorandum No. 9 (January, 1964).

Published: J. Phys. Chem. 68, 1828-1833 (1964),

Although indium amalgams have been used in a number of electrochemical investigations, no accurate measurements of the activity coefficients in these liquid solutions are readily available. During the course of investigations at this laboratory on electrocatalysis by indium amalgams, we had occasion to measure these activity coefficients. The results are summarized in this paper.

Potentiometric measurements were made using the following cell:



at 25.0°C. Amalgams were prepared from triple-distilled mercury and 99.999% pure indium by weighing out the required quantities of mercury and indium and combining them under an atmosphere of nitrogen. For amalgams containing from 1 to 30% indium, the potential could be reproduced to within 0.01 mv.

The measurements of cell potential and the activity coefficients calculated from these measurements are given in Table 6-1. These were found to fit the equation

$$\log \gamma_{\text{In}} = B (1 - X_{\text{Hg}}^2)$$

which describes regular solutions, for which the entropy of mixing is ideal. In equation (1),  $\gamma_{\text{In}}$  is the activity coefficient of indium in the amalgam, referred to infinite dilution, B is a temperature-dependent parameter, and  $X_{\text{Hg}}$  is the mole fraction of mercury in the amalgam.

Using literature data for the heat of fusion and heat capacity of indium, together with the activity of pure indium, a value  $B = 1.50$  at 25°C

TABLE 6-1

Emf. Measurements and Calculated Activity Coefficients, 25.0°

<u>Mole % indium</u>	<u>Cell emf, mv.</u>	<u>Activity based on Henry's law, mole fraction</u>	<u>Activity, coefficient</u>
100.0 <sup>a</sup>	266.7	21.6	--
70.0 <sup>b</sup>	266.8	21.8	31.2
64.41	264.30	16.37	25.4
63.60	263.03	14.07	22.1
52.22	258.95	8.73	16.7
50.00	258.31	8.10	16.2
39.98	251.80	3.78	9.46
30.40	245.50	1.812	5.96
30.00 <sup>c</sup>	245.35	1.780	5.94
20.00 <sup>c</sup>	237.06	0.678	3.38
16.26	234.70	0.514	3.16
10.00 <sup>c</sup>	226.46	0.196	1.96
8.41	223.31	0.1358	1.612
5.00 <sup>c</sup>	217.90	0.0723	1.447
3.28	214.40	0.0480	1.238
1.00 <sup>c</sup>	201.44	0.01057	1.059
0.920	200.68	0.00968	1.051
0.0940	179.0	0.000946	1.006
0	---	0	1.000

<sup>a</sup>Pure solid indium. <sup>b</sup>Saturated amalgam with excess solid indium present. <sup>c</sup>Most precise measurements,  $\pm 0.01$  mv.

was calculated. The values of B obtained directly from the activity coefficient data were compared with those calculated from the emf data of other workers<sup>(1, 2)</sup>. The solutions appear to be regular throughout the composition range, as can be seen from Fig. 6-1; and the temperature dependence of the coefficient B is consistent with a zero value for the entropy of mixing (Fig. 6-2).

In both the dependence of the activity coefficient on composition, and in the ideal entropy of mixing, mercury-indium mixtures behave approximately like regular solutions. In one respect, however, they are not completely regular. A large negative volume change ( $1 \text{ cm}^3/\text{mole}$ ) is observed on mixing mercury and indium, and its magnitude suggests that a negative excess entropy of approximately 5 joules/deg. should be observed. It is possible that the compensating positive entropy arises from repulsive interactions between partially shielded  $\text{In}^+$  ions in the metal.

The large activity coefficients (indicating large negative deviations from Raoult's law), as well as the large negative heat of mixing, indicate that indium-mercury interactions are much stronger than mercury-mercury or indium-indium interactions. Whether or not an actual compound species such as  $\text{InHg}$  exists in the liquid phase cannot be unambiguously decided from thermodynamic measurements alone, but such a compound certainly exists in the solid phase. Phase diagram studies show that in the composition range where liquid amalgams can be obtained at room temperature, two compounds,  $\text{InHg}$  and  $\text{InHg}_6$ , are probably formed; but only  $\text{InHg}$ , melting at  $-18.5^\circ$ , is agreed upon by all investigators. The solid solution range of  $\text{InHg}$  is only about 2 mole %, which indicates the possibility of specific bond formation between In and Hg in the liquid.

Kozin<sup>2</sup> observed discontinuities in the slope of his emf-concentration curves at compositions corresponding to  $\text{InHg}_3$  and  $\text{InHg}$ , which he interpreted as evidence for the formation of stoichiometric compounds in the liquid phase. Such discontinuities are possible, and when observed have been interpreted as indicating strong ordering in the liquid phase. However, only Kozin's data of part 1 show the breaks prominently. His

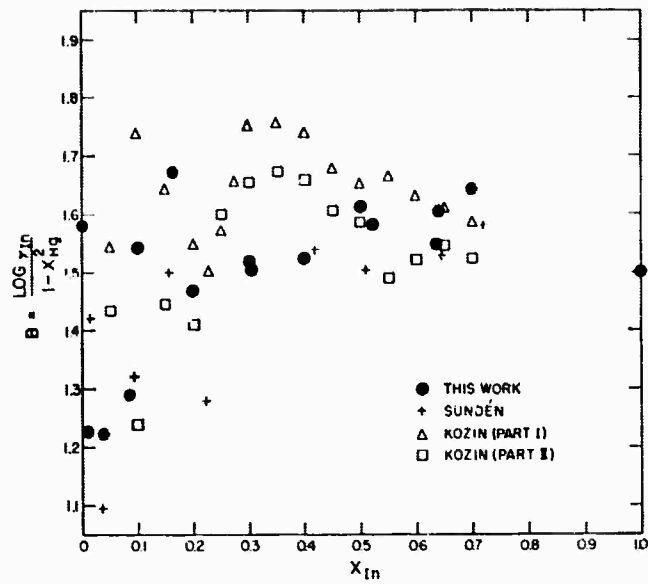


Fig. 6-1. Fit of experimental activity coefficient data to the empirical equation  $\log \gamma_{In} = B(1 - X_{Hg}^2)$ . The best value of B obtained from our data (circles) is 1.54, from Sundén's data (crosses) is 1.46, from Kozin's data (part I, triangles) is 1.64 and (part II, squares) 1.53. The value of B calculated from the heat of fusion of indium and the activity coefficient of pure solid indium is 1.50.

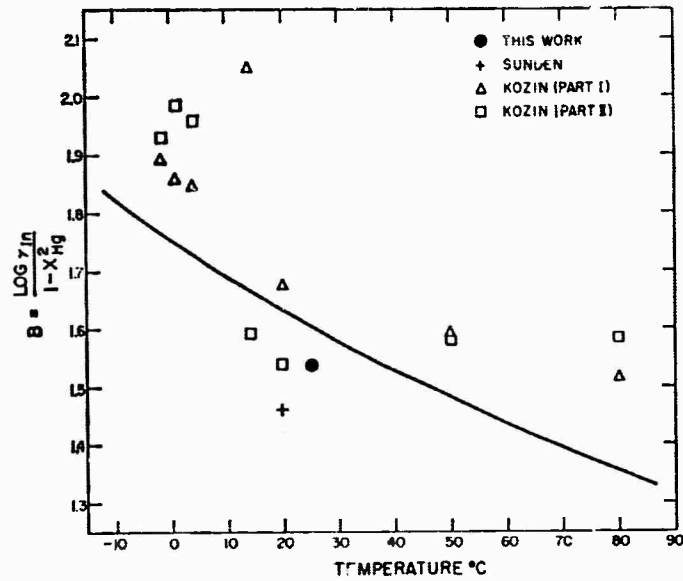


Fig. 6-2. Temperature dependence of the coefficient B. The curve was calculated from the known heat of mixing of indium and mercury, with the assumption that the excess entropy of the solution was zero.

data of part II show them to a much smaller extent and at compositions considerably different from  $\text{InHg}_3$  and  $\text{InHg}$ . Neither our data nor Sunden's data show any such breaks. Since the variations which are interpreted as breaks in the slope of the emf-concentration curve are probably within experimental errors (see Fig. 6-1), they cannot be considered adequate evidence for the formation of compounds in the liquid phase.

The consistent description of the thermodynamic properties of these solutions by the theory of regular solutions argues against the formation of any specific compound other than  $\text{InHg}$ . According to statistical mechanical theory, zero excess entropy is obtained with a single potential of interaction with nearest neighbors of a given kind, and compound formation as such need not be postulated.

#### References:

1. N. Sunden, Z. Elektrochem. 57, 100 (1953).
2. L. F. Kozin, Tr. Inst. Khim, Nauk, Akad. Nauk Kaz. SSR 9, 71, 81 (1962).

7. The Electrical Double Layer on Indium Amalgams in  
0.1 M HClO<sub>4</sub> at 25°C

James N. Butler, Mary L. McEhan, and A. C. Makrides

Submitted as Technical Memorandum No. 15 (September, 1964)

Presented at the Chicago Meeting of the American Chemical Society, September, 1964.

Published: J. Electroanal. Chem. 9, 237-250 (1965).

Indium amalgams provide an excellent system for studying the effect of electrode composition on the structure and properties of the electrical double layer. At room temperature, liquid amalgams containing up to 70 mole % indium can be prepared, and accurate capacity measurements can be made at the clean, reproducible surface obtainable at a dropping electrode.

Differential capacity was measured in perchloric acid solutions at 25°C, by the method of Grahame [J. A. C. S. 71, 2975 (1949)]. A platinized platinum screen surrounding the drop was used as a potential-fixing electrode. Measurements were made at a fixed point in the drop lifetime, balancing a series resistance and capacitance decade in an impedance bridge. The area of the drop was calculated from the measured mass flow rate and density of the amalgam, with correction for back-pressure due to interfacial tension.

The potential of zero charge was measured by observing the potential at which no current flowed between the drop and screen. At this potential, the polarization resistance and capacity was frequency independent, indicating that the electrode was ideally polarized. Under these conditions the current results entirely from charging the double layer as the drop changes area, and hence the zero-current point corresponds to the zero-charge point.

At very small concentrations of indium (Fig. 7-1), the capacity of the double-layer is nearly identical to pure mercury; but at concentrations above 0.001%, the diffusion-controlled rate of dissolution of indium exceeds the rate of dissolution of mercury, and a large pseudo-capacity

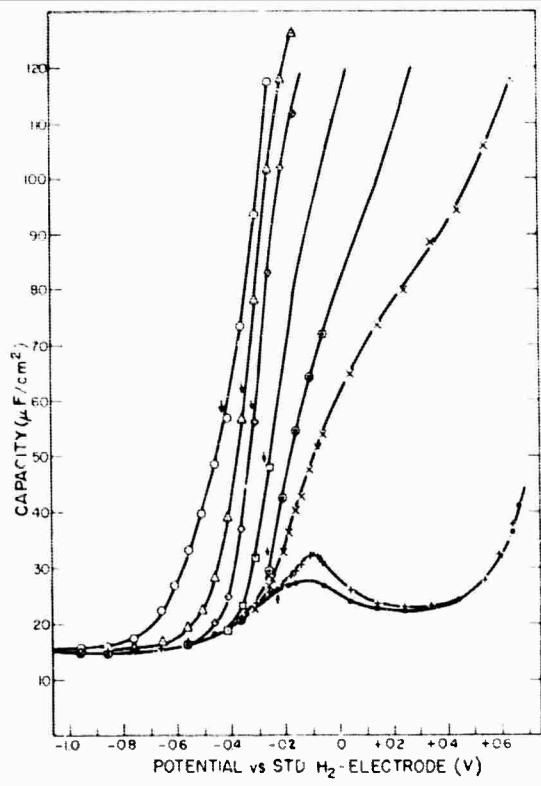


Fig. 7-1. Differential capacity of indium amalgams containing up to 16.3 mole % In, at 1 kc. O, 15.3%;  $\Delta$ , 3.9%;  $\diamond$ , 1.0%;  $\square$ , 0.1%;  $\bullet$ , 0.01%; X, 0.005%; +, 0.002% In;  $\circ$ , 0.001% In (and pure Hg). The potentials given on the figure are 0.065 v. more negative than those in the tables, because of the different reference electrode.

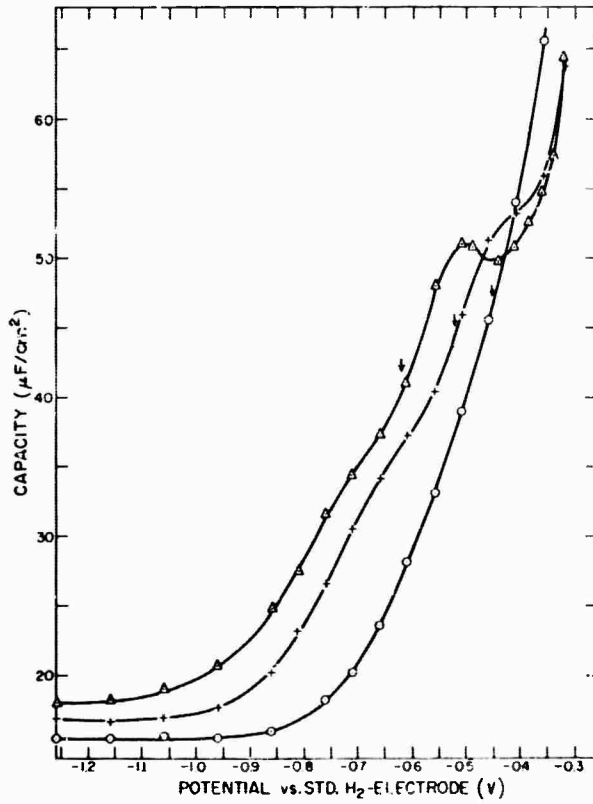


Fig. 7-2. Differential capacity of concentrated In amalgams at 10 kc.  $\Delta$ , 64%; +, 40%; O, 20%.

and polarization resistance is observed at potentials positive with respect to the zero-charge point. At negative potentials, the capacity is identical to that of mercury.

At higher concentrations of indium (Fig. 7-2), the zero-charge point shifts to more negative values. The zero-charge point of a 70% indium amalgam is approximately 0.4 volts more negative than the zero-charge point for mercury. If capacity curves are compared at the same rational potential (potential with respect to the zero-charge point), the shape of the curves at negative values of potential remains relatively constant, but the capacity increases by about 30% as the composition changes from pure mercury to 70% indium.

The capacity curves were integrated to obtain the surface charge (Fig. 7-3). At negative values of surface charge, the behaviour of capacity as a function of surface charge is similar to the behaviour of capacity as a function of rational potential. At positive values of surface charge, however, the capacity goes through a maximum as the concentration of indium increases, as a result of changes in anion adsorption in the inner part of the double-layer. The capacity at  $+10 \mu\text{ coul/cm}^2$  for 65% indium amalgam is approximately twice that for mercury at the same surface charge, but the curve shows the same "hump" (attributed to changes in the dielectric properties of water) near zero surface charge in both cases.

The values obtained for the potential drop across the diffuse double layer were used in a revised interpretation of our previous measurements (part 4 of this report) of hydrogen overvoltage on indium amalgams and the influence of the electrode composition on the rate of the discharge reaction was shown to be similar to that obtained from the uncorrected current-potential curves. The Gouy-Chapman theory was adequate for calculation of the potential drop across the diffuse double-layer, as indicated by the excellent fit of the experimental data to the theoretical current-potential curve.

In Fig. 7-4 we have compared the values of corrected exchange current ( $\log i_0'$ ) obtained from a least-squares fit of the Frumkin equation

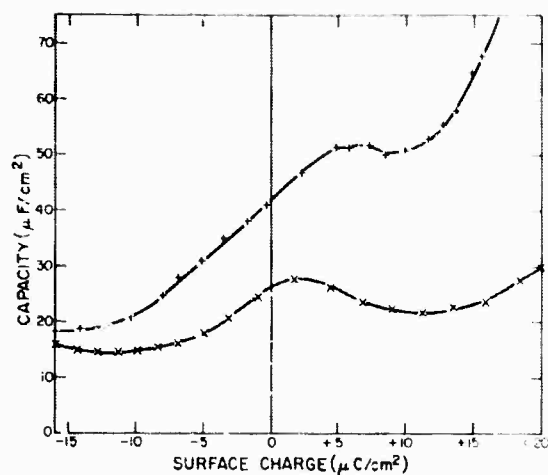


Fig. 7-3. Comparison of capacity as a function of surface charge for mercury (X) and 63.6% In amalgam (+). Note that the "hump" occurs at approximately the same surface charge.

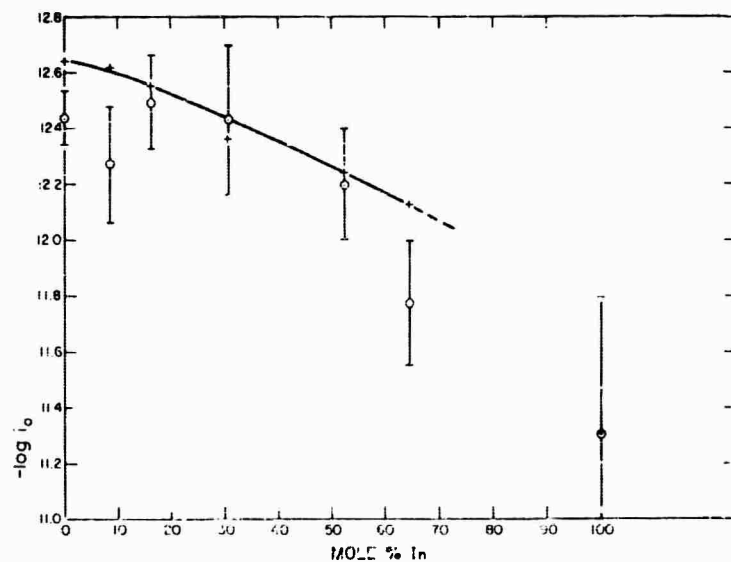


Fig. 7-4. Exchange current for the hydrogen evolution reaction (corrected for double-layer effects) as a function of amalgam composition. The crosses were calculated with the transfer coefficient,  $\alpha$ , fixed at 0.500. The circles were calculated from a least-squares fit of Frumkin's equation to the data. The vertical bars indicate 95% confidence limits.

with values calculated assuming a fixed value of the transfer coefficient  $\alpha = 0.500$ , as was done in part 5 of this report. The values of  $-\log i_0'$  calculated assuming  $\alpha = 0.500$ , show an almost linear dependence on indium concentration, whereas the values obtained by the least-squares fit show a rather non-linear dependence, and perhaps even go through a maximum at about 20% In.

This preliminary study leaves many questions still unanswered. Although we have assumed that there is no specific adsorption of ions in the Helmholtz layer, this is not rigorously correct, and perchlorate ion is almost certainly adsorbed to some extent at positive surface charges. Whether or not this specific adsorption is entirely responsible for the large change in capacity with indium concentration at constant surface charge (Fig. 7-3), we cannot unambiguously decide at the present time. The capacity difference might also result from differences in the In-Hg dipole layer in the metallic phase, or from differences in dipole orientation of water in the aqueous phase.

8. Interfacial Tension of Indium Amalgams in  
0.1 M HClO<sub>4</sub> at 25°C

James N. Butler

Submitted as Technical Memorandum No. 19 (April, 1965).

Published: J. Phys. Chem. 69, 3817-3825 (1965).

One of the factors which may influence the rate of an electrocatalytic reaction at an alloy electrode is the chemical composition of the surface. Because of the different surface energies of the components of an alloy, the surface composition will, in general, be different from the bulk composition and will change in a way which minimizes the total surface energy. It is difficult to determine the surface composition of a solid electrode, but, for a liquid electrode, the measurement of interfacial tension as a function of bulk composition can give important information about the surface composition.

The interfacial tension is related to the surface composition by the Gibbs adsorption isotherm

$$\Gamma_i = - \frac{\partial \gamma}{\partial \mu_i} \quad (1)$$

where  $\gamma$  is the interfacial tension,  $\mu_i$  is the chemical potential of a component in one phase, and  $\Gamma_i$  is the surface excess of that component with respect to a standard component (usually Hg in amalgams and H<sub>2</sub>O in aqueous electrolytes). The surface excess is not a true surface concentration but is the total difference in composition of the surface region from that of the bulk. The region of integration extends from the physical surface to where the composition equals that of the bulk. Although thermodynamic measurements cannot give the true surface composition, they can, with additional assumptions, give a quantity which approximates the surface composition.

Interfacial tension was measured by the sessile drop method, using a traveling microscope which could be read to  $\pm 0.00002$  in. A complete set of measurements of one drop consisted of approximately

20 readings of vertical coordinates, together with the 40 corresponding left and right horizontal coordinates. From these data, the interfacial tension was calculated by fitting the experimental points to a theoretical curve for the shape of a sessile drop, using a computer program (see part 9 of this report). The results obtained are given in Table 8-1.

Although interfacial tension can be measured directly as a function of potential and composition, more precise results can be obtained by integrating measurements of double-layer capacity. If the composition of both the amalgam and the aqueous phase are held constant, the differential capacity is the second derivative of the interfacial tension with respect to potential

$$C = 0.1 \frac{\partial^2 \gamma}{\partial \phi^2} \quad (2)$$

where C is the differential capacity in  $\mu\text{f.}/\text{cm.}^2$ ,  $\gamma$  is the interfacial tension in  $\text{erg}/\text{cm.}^2$ , and  $\phi$  is the potential with respect to a reference electrode.

We have made measurements of zero-charge potential and double-layer capacity for indium amalgams in 0.1 M  $\text{HClO}_4$  solutions at  $25^\circ$  (see part 7 of this report). With the additional experimental values of interfacial tension at the zero-charge potential, measured in the present work, we can obtain by integration the complete field of data required to calculate surface excess as a function of potential and electrode composition.

Figure 8-1 shows the surface excess curves calculated from the slopes of interfacial tension-activity curves, which were obtained by integrating the capacity measurements. Note that the surface is deficient in indium, the surface deficiency passes through a maximum at approximately 20 mole % indium, and an increase in bulk composition beyond this point causes the surface deficiency to decrease in magnitude. As with thallium amalgams (see part 12 of this report) the surface excess of indium amalgams was found to be potential dependent.

One of the principal objects of this investigation was to relate the surface composition of indium amalgams to the observed electrocatalytic

TABLE 8-1

Interfacial Tension of Indium Amalgams in 0.1M HClO<sub>4</sub> at 25°

Mole % In	Potential, <sup>a</sup> v.	Density, g/cm <sup>3</sup>	Parameters of sessile drop shape		Std. dev. <sup>b</sup>	$\gamma$ , ergs/cm <sup>2</sup>
			$\beta$	b, cm		
0.0	-0.165	12.534	9.88	0.586	1.21	426.0
5.97	-0.310	12.168	5.15	0.433	0.82	434.5
10.00	-0.333	11.92	6.68	0.500	0.86	437.9
20.00	-0.388	11.305	12.22	0.707	1.46	454.0
39.83	-0.480	10.03	3.75	0.432	0.85	491.0
63.02	-0.558	8.52	2.86	0.418	0.55	510.8

<sup>a</sup>Zero-charge potential, with respect to a reversible H<sub>2</sub> electrode in 0.1M HClO<sub>4</sub>. <sup>b</sup>Standard deviation of experimental points from theoretical curve, in microns.

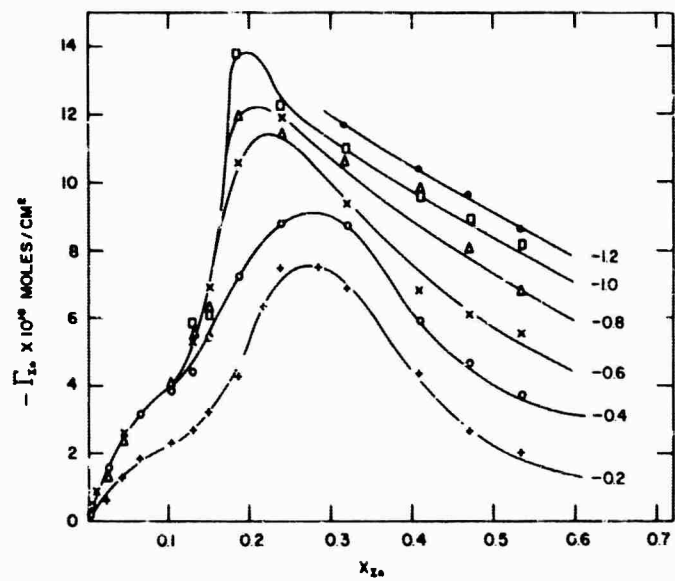


Fig. 8-1. Surface excess calculated from the slopes of interfacial tension-activity curves. The scatter of the points gives some indication of the random errors involved.

activity. The rate of the hydrogen evolution reaction, as reflected by the exchange current  $i_0'$  (see parts 5 and 7 of this report), is a smooth monotonic function of composition. In the region from 10 to 30% indium, no salient features appear which might be correlated with the maximum surface deficiency seen in Fig. 8-1.

Two alternative explanations may be made of this lack of correlation: the first, that the surface composition is essentially that of the bulk, and the second, that the electrocatalytic properties are more closely related to the bulk electronic properties of the alloy than to the surface composition.

If the composition profile in a direction perpendicular to the surface is so slowly varying that the observed surface deficiency is spread over more than 20 atomic layers, the surface composition would be essentially that of the bulk. Such a diffuse surface structure seems unlikely. No evidence for specific long-range ordering in liquid Hg-In amalgams has been found by X-ray diffraction or thermodynamic methods (see part 6 of this report). The mean free path of electrons in mercury-indium alloys is only about 2.5 interatomic distances, so that appreciable space charge is unlikely. The diffusion coefficients of metals in amalgams are comparable to the diffusion coefficients of solutes in nonassociated solutions. Thus a more reasonable estimate would be that the surface deficiency arises in the first four or five atomic layers.

In contrast to the complex way in which the surface composition (Fig. 8-1) varies, the electronic properties of mercury-indium alloys show relatively simple behavior. The resistivity, temperature coefficient of resistivity, and Hall coefficient all decrease monotonically as the concentration of indium increases. The optical reflectivity increases monotonically with increasing indium concentration. None of these properties agrees precisely with the values calculated from a free-electron theory, even though pure mercury and pure indium both are well described by such a theory. The only property which shows a complex behavior is the thermoelectric power, which goes through an

unexplained maximum at approximately 3 atom % indium. From our results (parts 4, 7, and 10 of this report) we have found that the exchange current and probably the enthalpy of activation for the hydrogen evolution reaction decrease monotonically as the concentration of indium increases.

We have previously made a dichotomy between the "atomic approach" and the "continuum approach" to electrocatalysis. The atomic approach assumes that the electrocatalytic properties of an alloy result from independently additive properties of the surface atoms; the continuum approach assumes that the electrocatalytic activity of an alloy is a cooperative property and may bear little relation to the properties calculated on the basis of the atomic approach. In our studies of hydrogen evolution at platinum and palladium amalgam electrodes (part 3 of this report), we showed that the continuum approach was probably closer to the truth since the atomic approach gave an answer which was many orders of magnitude different from the experimental results.

The results of the present study on indium amalgams also indicate that the continuum approach is the fruitful one. We have seen that the electronic properties of these alloys are virtually all simple monotonic functions of the bulk composition, as are the electrocatalytic properties. The surface composition, on the other hand, shows very complex behavior and does not correlate well with electrocatalytic activity. It would thus seem likely that electrocatalytic activity is more closely related to the cooperative electronic properties of an alloy rather than to its surface composition.

9. A Curve-Fitting Method for Calculating Interfacial Tension by the Sessile Drop Method

James N. Butler and Burton H. Bloom

Submitted in part as Technical Memorandum No. 19 (April, 1965).

Published: Surface Science 4, 1-17 (1966).

The equilibrium shape of a cylindrically symmetric sessile drop (Fig. 9-1) is governed by the equation

$$\frac{b}{R} = \left(\frac{b}{x}\right) \sin \phi = 2 + \beta \left(\frac{z}{b}\right) \quad (1)$$

where

$$\beta = \frac{gb^2}{\gamma} (d_1 - d_2) \quad (2)$$

In these equations,  $R$  is the radius of curvature in the vertical plane at the point  $(x, z)$ ,  $b$  is the radius of curvature at the origin,  $\phi$  is the angle made by the radius of curvature with the  $z$  axis,  $g$  is the acceleration of gravity,  $d_1$  and  $d_2$  are the densities of the denser and lighter fluid, respectively, on each side of the interface, and  $\gamma$  is the interfacial tension.

This form of the equation is especially useful because the linear dimensions  $R$ ,  $x$ , and  $z$  appear as ratios to the maximum radius of curvature  $b$ . Thus, a given value for the constant  $B$  gives the same drop shape, regardless of drop size, and changing  $b$  influences only the size of the drop without altering its shape. Of course, changing the size of the drop while holding the surface tension and density constant causes both  $\beta$  and  $b$  to change simultaneously.

Both  $R$  and  $\phi$  can be expressed in terms of derivatives of  $z$  with respect to  $x$ , and Eq. 1 can be transformed into the nonlinear differential equation

$$b \frac{d^2z}{dx^2} + \frac{b}{x} \left\{ 1 + \left(\frac{dz}{dx}\right)^2 \right\} \frac{dz}{dx} = \left( 2 + \frac{\beta z}{b} \right) \left\{ 1 + \left(\frac{dz}{dx}\right)^2 \right\}^{3/2} \quad (3)$$

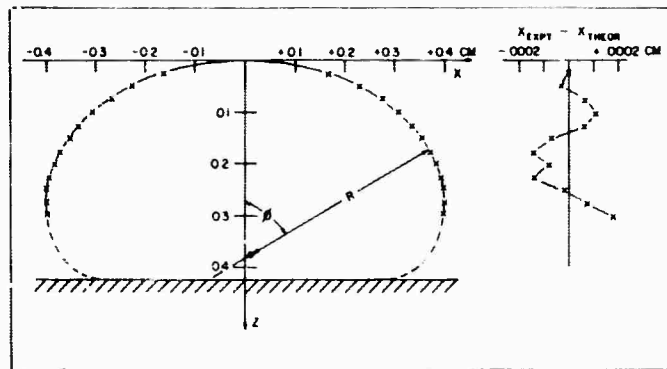


Fig. 9-1. The shape of a typical sessile drop. The shaded area indicates the surface on which the drop rests. The curve was calculated from the equations in the text assuming  $\beta = 5.397$  and  $b = 0.5766$  cm. The crosses indicate the experimental measurements obtained for a 63.0% indium amalgam.

This equation cannot be solved in terms of any conventional functions. Some solutions of this equation have been tabulated by Bashforth and Adams ["An attempt to Test the Theories of Capillary Action", Cambridge University Press, 1883].

For our purposes, however, we want to fit a number of experimental measurements of  $x, z$  pairs to the theoretical drop contour and to obtain the best values of  $b$  and  $\beta$  consistent with these experimental values. Neither the tables of Bashforth and Adams nor the empirical approximations derived by various other workers are sufficiently accurate to assure that the best possible fit of the parameters is obtained.

We have, therefore, devised a computer program which generates the function  $z(x, b, \beta)$  defined by Eq. 3 by an iterative solution of the differential equation. The parameters  $b$  and  $\beta$  are then adjusted so that the best fit is obtained for the experimental data. The interfacial tension is then calculated using Eq. 2. An example of the fit obtained to experimental measurements is shown in Fig. 9-1.

10. Temperature Dependence of Hydrogen Overvoltage  
on Indium Amalgams

James N. Butler and Mary L. Meehan

Submitted as Technical Memorandum No. 18 (March, 1965).

Published: Trans. Faraday Soc. 61, 2521-2530 (1965).

This paper presents a study of the temperature dependence of hydrogen overvoltage for amalgam electrodes containing 10, 20, 40 and 63% indium. From these results, the enthalpy of activation, which is closely related to the heat of adsorption of a hydrogen atom on the electrode surface, can be obtained, and its relation to the composition of the electrode determined. The method described previously (part 4 of this report with refinements such as charging current corrections) was used, and current-potential curves were measured for the four amalgams over the temperature range from 15°C to 65°C. A typical set of data is shown in Fig. 10-1.

The experimental values were fitted to the Frumkin equation

$$\eta = \frac{1 - \alpha}{\alpha} \phi_2 + \frac{RT}{\alpha F} \ln \left( \frac{i}{i_0'} \right) \quad (1)$$

by the least-squares method described in part 5 of this report. The potential  $\phi_2$  of the outer Helmholtz plane was calculated from capacity measurements made at 25°C, assuming no specific adsorption of perchlorate ion, as described in part 7 of this report. Eq. 1 was cast into the form of a straight line, whose slope was equal to the cathodic transfer coefficient  $\alpha$ , and whose intercept gave the corrected exchange current  $i_0'$ . In Eq. (1),  $R$  is the gas constant,  $T$  is the absolute temperature, and  $F$  is the Faraday constant.

The variations in  $\alpha$  for the various current-potential curves cause large variations in the least-squares values of  $-\log i_0'$ , which obscure the influence of temperature and composition. To show the effects of temperature and composition more clearly, we have calculated

TABLE 10-1

Enthalpy of Activation

(Errors are 95% Confidence Limits)

amalgam <u>% In</u>	$\Delta H_0^\ddagger$ <u>(a)</u>	$\Delta H_Z^\ddagger$ <u>(a)</u>	$\Delta H^\ddagger$ <u>(<math>\eta = 1.000</math> V)</u>
0.0 <sup>(b)</sup>	22.3 $\pm$ .4	20.3 $\pm$ .4	11.0 $\pm$ .4
10.0	20.8 $\pm$ 1.6	16.5 $\pm$ 1.6	11.2 $\pm$ 1.2
20.0	21.9 $\pm$ .8	17.0 $\pm$ .8	11.1 $\pm$ .4
40.0	21.9 $\pm$ .6	16.0 $\pm$ .6	11.2 $\pm$ .2
63.0	19.5 $\pm$ 1.5	12.5 $\pm$ 1.5	9.9 $\pm$ .7
63.0 <sup>(c)</sup>	21.1 $\pm$ 1.2	14.2 $\pm$ 1.2	9.9 $\pm$ 1.0

---

(a) extrapolated using the Frumkin equation with  $\alpha = 0.500$ .  $\Delta H_Z^\ddagger$  includes a contribution from the shift of  $\eta_Z$  with temperature.

(b) calc. from data of Post and Hiskey.

(c) points at 56 and 66° discarded.

average values of  $-\log i_0'$ , using a fixed value of  $\alpha$  (0.500). These values are shown in Fig. 10-2.

The differences between values of  $-\log i_0'$ , with  $\alpha$  fixed show the variation of overvoltage with temperature and composition as clearly as would the change in  $\eta$  at constant  $i$ , but, in addition, contain corrections for the influence of the diffuse double layer, and provide a self-consistent extrapolation to the reversible potential.

The temperature dependence of the corrected exchange current gives a quantity which is independent of parameters related to the potential:

$$\Delta H_0^\ddagger = -R \frac{d \ln i_0'}{d(1/T)} = \alpha h_H + \alpha F \frac{d(Q/T)}{d(1/T)}, \quad (2)$$

where  $h_H$  is the enthalpy of adsorption of a hydrogen atom on the electrode surface and  $Q$  is a parameter characteristic of the electrode material. Thus, changes in the heat of adsorption of hydrogen atoms on the surface would be expected to show up as changes in the enthalpy of activation  $\Delta H_0^\ddagger$ . Fig. 10-2 shows the plot of  $\log i_0'$  (with  $\alpha = 0.500$ ) as a function of  $1/T$ . The least-squares straight lines gave the values of  $\Delta H_0^\ddagger$  which are listed in Table 10-1, together with values of  $\Delta H_z^\ddagger$ , the enthalpy of activation at the zero-charge potential, and the values for mercury calculated from the data of Post and Hiskey [J. Am. Chem. Soc. 72, 4203 (1950)].

These results show that it is probable that the enthalpy of activation  $\Delta H_0^\ddagger$  is nearly independent of the amalgam composition; although a decrease of approximately 1 kcal/mole on going from mercury to the 63% amalgam is consistent with the data. Fig. 10-3 compares the quite significant trend of exchange current at constant temperature, with the almost insignificant trend of enthalpy of activation, as the composition of the amalgam is varied.

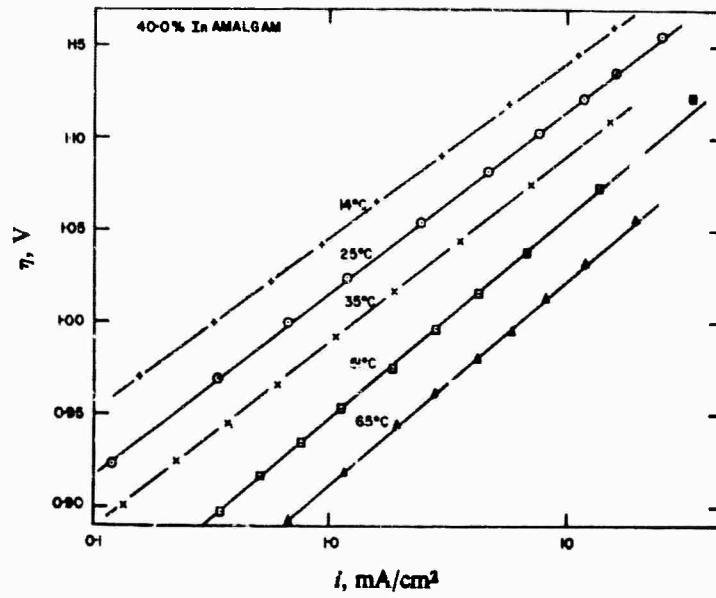


Fig. 10-1. Temperature dependence of hydrogen overvoltage on 40.0% Indium amalgam.

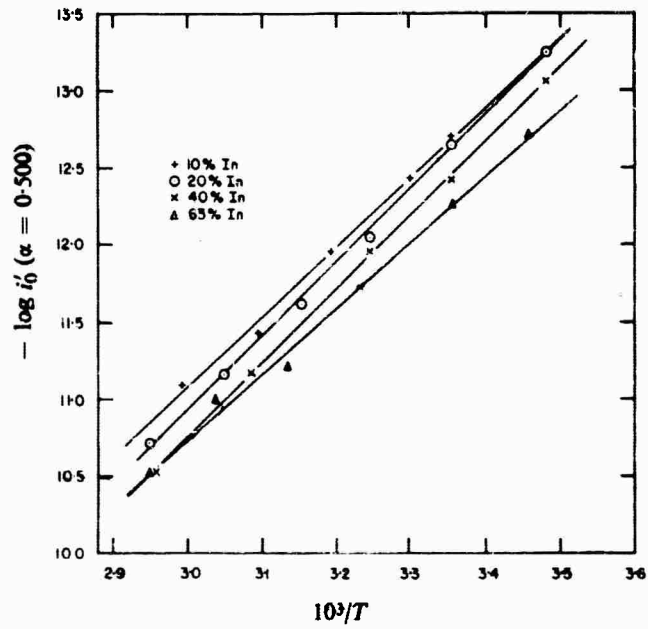


Fig. 10-2. Temperature dependence of exchange current. The lines were fitted by the method of least-squares, and were used to calculate the values of  $\Delta H_0^\ddagger$  listed in Table 10-1.

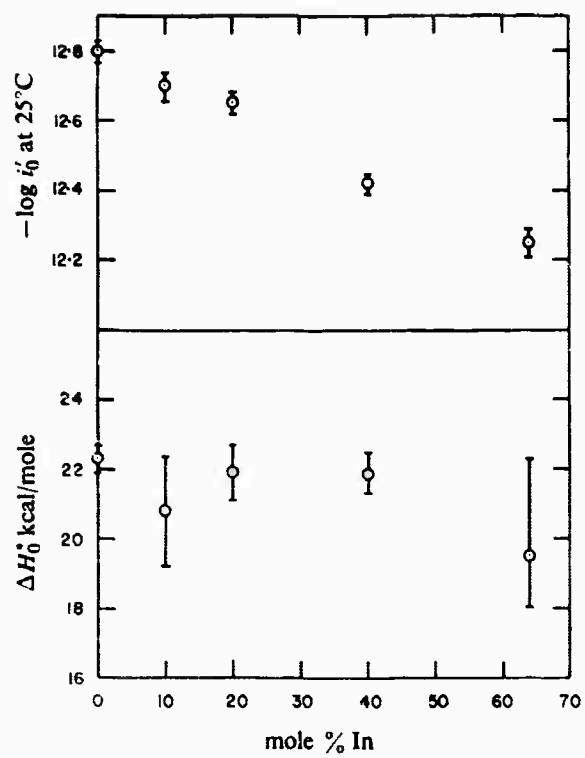


Fig. 10-3. Comparison of the variation in exchange current with composition and the variation in enthalpy of activation with composition.

According to the Frumkin theory of slow discharge reactions, the corrected exchange current is given by

$$\ln i'_0 = (1 - \alpha) \ln [H^+] - \frac{\alpha}{RT} g_H + Q, \quad (3)$$

where  $H^+$  is the concentration of hydrogen ion in the bulk of the solution,  $g_H$  is the free energy of desorption of a hydrogen atom from the electrode surface, and  $Q$  is a parameter which may depend on the composition of the electrode and the temperature.

If the change in  $-\log i'_0$  were due entirely to a change in  $g_H$ , the observed shift of 0.55 in  $-\log i'_0$  would correspond to a change in  $g_H$  of approximately 1.4 kcal/mole. If the entropy of adsorption of hydrogen atoms on the surface of the electrode were independent of composition, this variation could be ascribed entirely to a change in the enthalpy of adsorption  $h_H$ . Then eq. (2) predicts the  $\Delta H_O^\ddagger$  changes by approximately 0.7 kcal/mole provided that the temperature coefficient of  $Q$  is independent of composition. This estimate is consistent with the observed change in  $\Delta H_O^\ddagger$ .

Because of the large experimental error in  $\Delta H_O^\ddagger$ , however, we cannot unambiguously state how much of the variation in  $-\log i'_0$  can be ascribed to a variation in  $h_H$ . The enthalpy of adsorption of hydrogen atoms appears to be the primary factor, but contributions from the entropy of adsorption of hydrogen atoms, from the variation in the dipole structure of the double-layer at the interface, and from changes in the surface composition of the amalgam compared to its bulk composition, may all influence the rate of hydrogen evolution to a lesser extent.

## 11. The Potential of Zero Charge on Indium Amalgams in Perchlorate Solutions

James N. Butler

Presented at the Buffalo Meeting of the Electrochemical Society, October, 1965.

Submitted to J. Phys. Chem.

Indium amalgams provide one of the few systems other than mercury for which the zero-charge potentials can be measured by the streaming electrode method. We have made measurements on amalgams containing from 0 to 64% indium in perchloric acid solutions from 0.01 to 1.0 molar. These data are summarized in Fig. 11-1, and confirm the measurements made earlier (see parts 4 and 7 of this report).

To test whether the values obtained by the streaming electrode method corresponded to true zero-charge potentials, direct measurements of surface charge on the amalgams were made by observing the transient current as a spherical drop electrode was formed. By a suitable extrapolation to zero time, the surface charge can be measured directly [J. N. Butler and M. L. Meehan, J. Phys. Chem. 69, 4051 (1965)]. Zero-charge potentials obtained by this method are also shown in Fig. 11-1, and agree with the streaming electrode measurements.

For an ideally polarized electrode, the shift of zero-charge potential with electrolyte composition is given by the equation

$$\left( \frac{\partial E_z}{\ln a_+} \right)_q = \frac{RT}{F} \left[ 1 + 2 \left( \frac{\partial q_-}{\partial q} \right)_a \right]$$

where  $E_z$  is the potential with respect to an external, fixed reference electrode,  $a_+$  is the mean activity of the 1-1 electrolyte,  $q$  is the surface charge on the electrode,  $q_-$  is the charge in solution contributed by anions,  $R$  is the gas constant,  $T$  is the absolute temperature, and  $F$  the faraday constant. If there is no specific adsorption of ions at the electrode, the charge in the solution is entirely in the diffuse double-

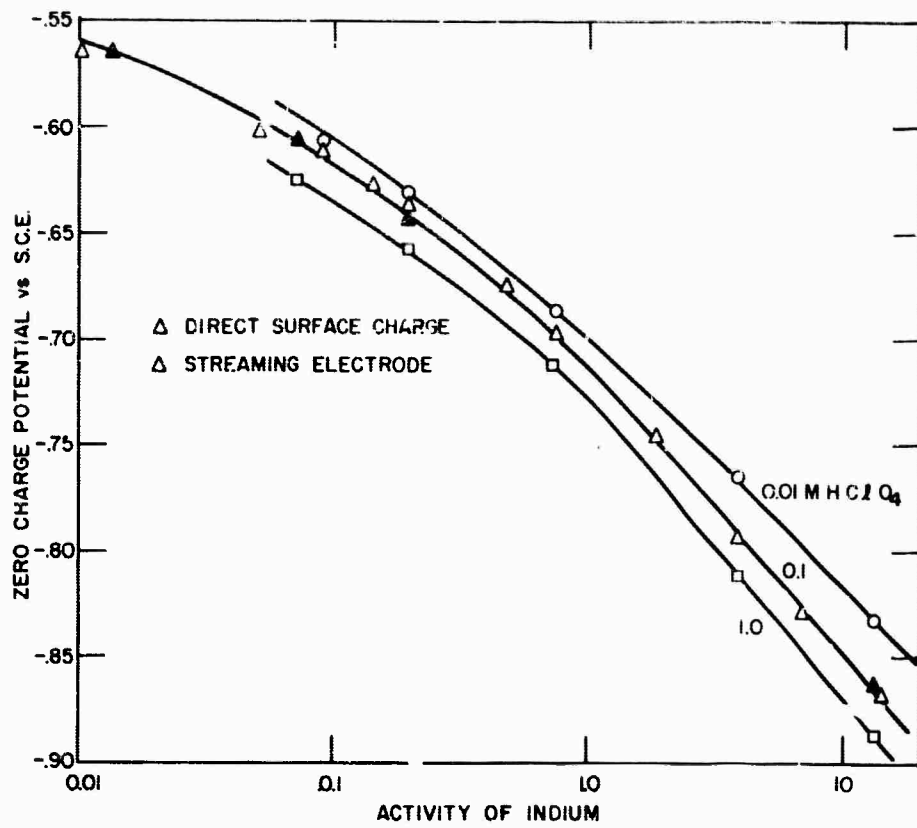


Fig. 11-1. Zero charge potential of indium amalgams in perchloric acid solution.

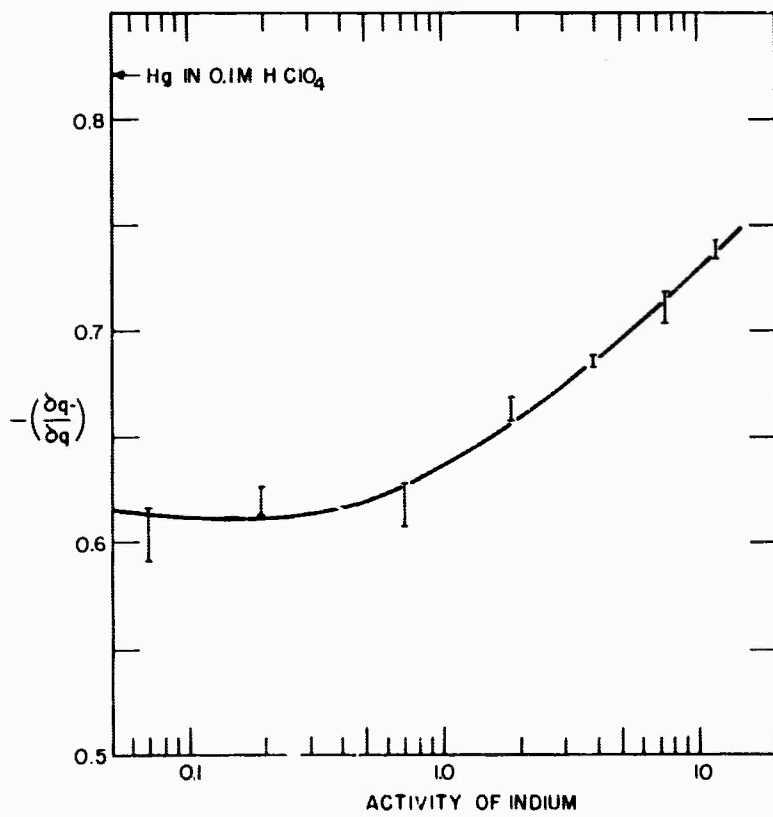


Fig. 11-2. Specific adsorption of perchlorate ion on indium amalgama.

layer, and the Gouy-Chapman theory may be used to calculate the dependence of  $q_-$  on  $q$ . At the potential of zero charge, this theory gives simply

$$\left(\frac{\partial q_-}{\partial q}\right)_{q=0} = -\frac{1}{2}$$

which says that  $E_z$  is independent of the electrolyte composition. Such a result is obtained for sodium fluoride solutions.

Our results for perchlorate solutions are shown in Fig. 11-2 where we have plotted the coefficient  $-(\partial q_-/\partial q)$ . The fact that it is larger than 0.5 indicates that the perchlorate ion is specifically adsorbed on the electrode, even at the potential of zero-charge. Note, however, that the indium amalgams show less specific adsorption of perchlorate than does mercury.

From measurements of the temperature dependence of the zero-charge potential in a cell without liquid junction, it is possible to obtain an entropy associated with the electrical double layer at the interface. For mercury in 1.0 M KCl, where there is considerable specific adsorption, this term is 0.72 mv/deg; for mercury in 0.1 M HClO<sub>4</sub>, where there is less specific adsorption, this term is 0.68 mv/deg; and for indium amalgams (20% and 40%) in 0.1 M HClO<sub>4</sub>, this term is 0.55 to 0.58 mv/deg. These results agree, in indicating a lower degree of specific adsorption on the amalgam than on mercury, with the variation of zero charge potential with electrolyte composition.

These results show that the large differences in double layer structure between mercury and the amalgams (see parts 7 and 8 of this report) must be attributed primarily to the orientation of solvent molecules in the aqueous phase and electronic dipoles in the metallic phase; and not to the specific adsorption of ions from the solution.

## 12. The Electrical Double Layer on Thallium Amalgam Electrodes

James N. Butler

Submitted as Technical Memorandum No. 16 (October, 1964).

Published: J. Electroanal. Chem. 9, 149-162 (1965).

In connection with our study of hydrogen overvoltage on thallium amalgams, we have made some measurements of double-layer capacity of thallium amalgam electrodes in 0.1 M HClO<sub>4</sub> at 25°C. We have also made a critical survey of the literature concerning the electrical double layer on thallium amalgams. In this paper, our experimental results are presented and compared with the literature values.

The methods were described previously (see part 7 of this report). The streaming-electrode method gives different values of the zero-charge potential depending on whether thallium ion is present in the solution or not. The values of Frumkin and Gorodetskaya [Z. Physik. Chem. 136, 451 (1928)] obtained in solutions containing the equilibrium amount of Tl<sup>+</sup> ion, were taken to be the most accurate, since the integrated capacity curves agreed with experimental electrocapillary curves, as can be seen in Fig. 12-1.

Our experimental values of capacity are shown in Fig. 12-2. By integrating these, and combining them with the data of Frumkin and Gorodetskaya, values of interfacial tension as a function of potential and composition were obtained. From this field of data, the surface excess of thallium in the amalgam was calculated as described in part 8 of this report. The results are shown in Fig. 12-3. Note that the surface excess is negative: the surface of the amalgam is deficient in thallium.

Although the surface excess of thallium is known, the absolute value of the surface concentration cannot be obtained without knowledge of the shape of the concentration profile in a direction perpendicular to the surface. If all the thallium were removed from the first atomic layer, but the concentration were equal to the bulk concentration out to that point, the observed surface deficiency could be accounted for almost exactly. Of course, such a concentration profile is absurd; but if one assumes that the

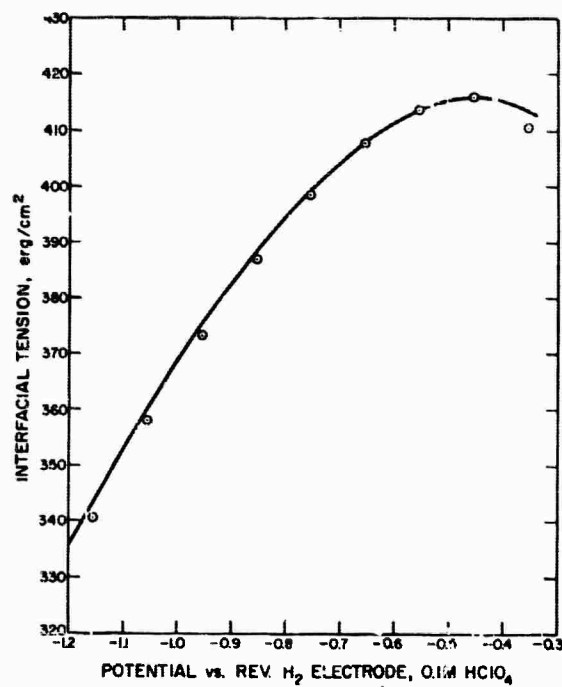


Fig. 12-1. Comparison of experimental interfacial tension measurements with values for 10% Tl amalgam obtained by integrating the capacity curve. The two sets of values were made to coincide at the electrocapillary maximum: —, integrated capacity curve (this work); O, experimental interfacial tension.

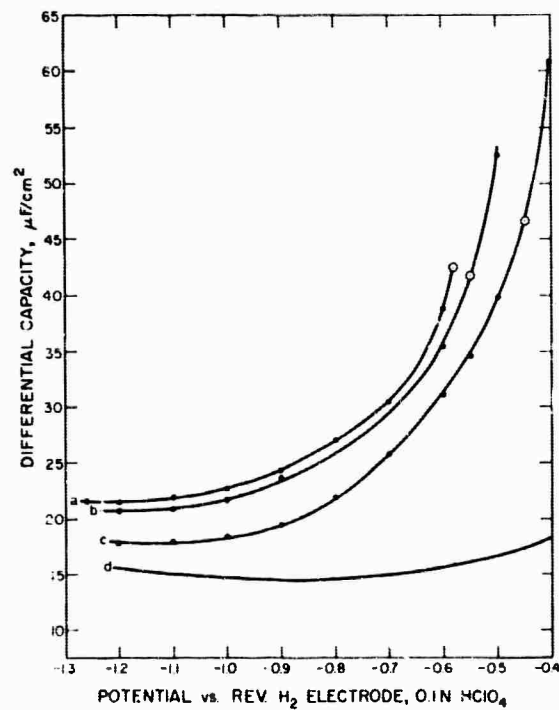


Fig. 12-2. Differential capacity of thallium amalgam electrodes: ●, experimental data; O, zero-charge point. (a), 40.5% Tl; (b), 31.2% Tl; (c), 10.1% Tl; (d), pure Hg.

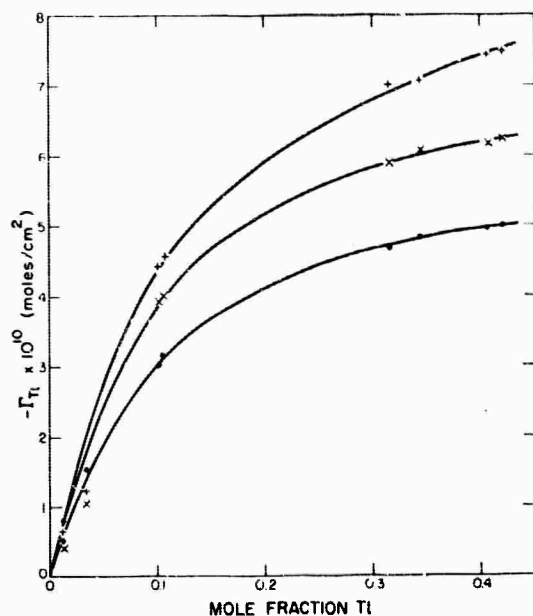


Fig. 12-3. Surface excess of thallium, with respect to mercury: +,  $\eta = 1.20$ ; X,  $\eta = 1.00$ ; ●,  $\eta = 0.80$ .

surface deficiency arises primarily in the first four or five atomic layers, one finds that the surface concentration is one-half to three-fourths of the bulk concentration, depending on the profile chosen.

Thus, it is rather unlikely that the observed similarity in hydrogen overvoltage between mercury and thallium amalgams (see part 13 of this report) is due entirely to a depletion of thallium at the surface. Although the surface concentration of thallium is certainly lower than the bulk concentration, the ratio of surface to bulk concentration is probably greater than 0.5, and is not very different for the different amalgams.

### 13. Hydrogen Overvoltage at a Dropping Thallium Amalgam Electrode

James N. Butler, Evelyn A. Barron-Apps, and Mary L. Meehan

Submitted as Technical Memorandum No. 17 (March, 1965)

Published: Trans. Faraday Soc. 61, 2509-2520 (1965).

To extend our studies of hydrogen overvoltage on indium amalgams to other liquid metal alloy systems, we have made a detailed study of hydrogen overvoltage on 10% and 40% thallium amalgams, including the temperature dependence. Using data on the properties of the electrical double layer (part 12 of this report) we have taken into account the influence of the diffuse double layer on the rate of hydrogen evolution.

The experimental method was that used in the studies of indium amalgams (parts 4 and 10 of this report). As can be seen from Fig. 13-1, only slight differences were observed between mercury and the thallium amalgams. The experimental measurements were fitted to the Frumkin equation, and the transfer coefficient was found to vary between 0.5 and 0.58, showing little trend with temperature or composition.

To observe the variations in the rate of hydrogen discharge free from the influence of the diffuse double layer, the transfer coefficient was fixed at  $\alpha = 0.50$ , and the corrected exchange current calculated. These results are shown in Fig. 13-2. From this temperature dependence, the enthalpy of activation was calculated, and the values obtained are summarized in Table 13-1.

Mercury and 10% thallium amalgam show enthalpies of activation which are the same within experimental error, but the values are clearly higher for the 40% thallium amalgam. The fact that discarding the two extreme points (in the 10% amalgam data) can change the values of enthalpy of activation by nearly 1.5 kcal/mole casts some doubt on the validity of the statistical limits of error. Thus, although the statistical analysis indicates a substantial probability that the enthalpy of activation is higher on 40% thallium amalgam than on mercury, the increase is not large, and may be within the experimental errors.

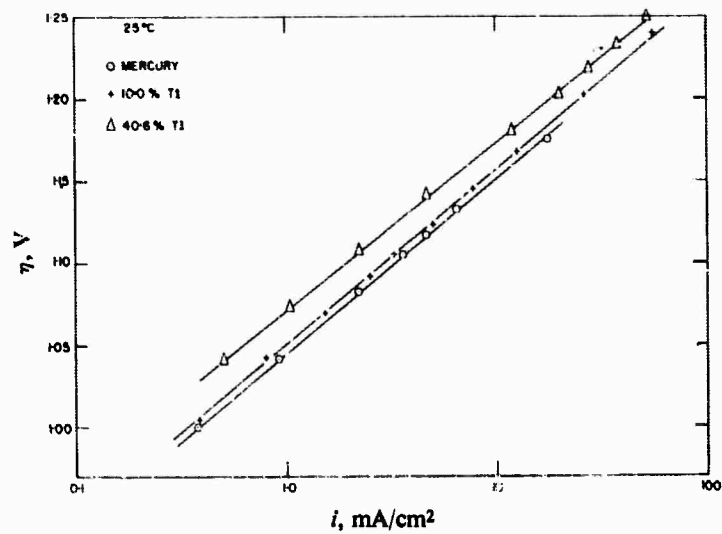


Fig. 13-1. Variation in hydrogen overvoltage with composition at 25°C.

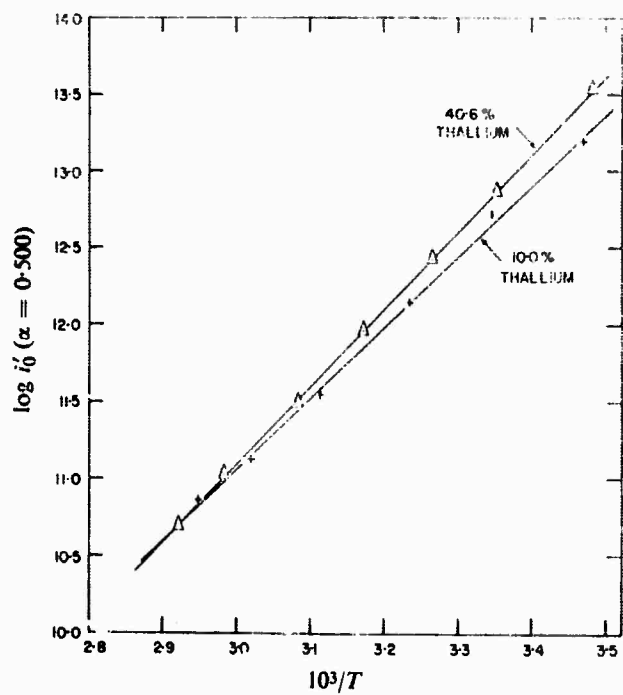


Fig. 13-2. Variation of exchange current with temperature and composition. The lines were fitted by the method of least-squares, and were used to calculate the values of  $\Delta H_0^\ddagger$  listed in Table 13-1.

TABLE 13-1

Enthalpy of Activation

	$\Delta H_0^\ddagger$ <u>(a)</u>	$\Delta H_Z^\ddagger$ <u>(a)</u>	$\Delta H^\ddagger$ <u>(<math>\eta = 1.00</math> V)</u>
mercury <sup>b</sup>	$22.3 \pm 0.4$	$20.4 \pm 0.4$	$11.0 \pm 0.4$
10.0% Tl amalgam	$21.2 \pm 1.1$	$16.0 \pm 1.1$	$9.1 \pm 1.0$
10.0% Tl <sup>c</sup>	$22.7 \pm 1.2$	$17.5 \pm 1.2$	$10.6 \pm 0.3$
40.6% Tl	$23.1 \pm 0.3$	$16.4 \pm 0.3$	$11.7 \pm 0.5$

---

<sup>a</sup> extrapolated using Frumkin's equation with  $\alpha = 0.500$ . No correction has been made for the shift of  $\eta_Z$  with temperature.

<sup>b</sup> calc. from data of Post and Hiskey [J. Am. Chem. Soc. 72, 4203 (1950)].

<sup>c</sup> points at 15° and 66° discarded.

14. Hydrogen Evolution and the Electrical Double Layer  
on Gallium and Gallium Alloy Electrodes

James N. Butler and Mary L. Meehan

Presented at the Cleveland Meeting of the Electrochemical Society, May, 1966.

Submitted to Trans. Faraday Soc.

Although studies of hydrogen evolution and the electrical double layer<sup>(1)</sup> have been made on pure gallium, no studies of this type have been extended to alloys of gallium which are liquid near room temperature. We have made measurements of hydrogen overvoltage in 0.1 M  $\text{HClO}_4$  at dropping liquid metal electrodes consisting of gallium, and alloys of gallium with mercury and indium. Although gallium-mercury alloys are liquid at 30°C, in the range from 2 atom % Hg to 97.5 atom % Hg the alloy separates into two liquid phases. Alloys of gallium with indium containing up to 20% In are liquid at 30°C.

Our overvoltage measurements at 1 ma/cm<sup>2</sup> on the various alloys are summarized in Table 14-1, together with previous measurements on mercury, indium, and indium amalgams for comparison. The introduction of either indium or mercury raises the overvoltage on gallium. The increase in overvoltage when 20% In is added to Ga is more than 70% of the increase between Ga and pure indium. The increase in overvoltage observed on an alloy containing 1.64% Hg is nearly 90% of the increase between Ga and pure mercury. In contrast, introduction of 0.5% of gallium in mercury has an almost undetectable effect.

Measurements of surface charge<sup>(2)</sup> in the electrical double layer on gallium-mercury and gallium-indium alloys showed small but significant changes from the properties of the electrical double layer on gallium. Using these values, corrections were made for the effect of the diffuse double layer on the hydrogen discharge reaction and corrected exchange currents and transfer coefficients were calculated. The variations of exchange current were qualitatively similar to the variations of overvoltage in Table 14-1, and the transfer coefficients varied between 0.5 and 0.6 with no particular trend.

TABLE 14-1

Hydrogen Overvoltage and Enthalpy of Activation  
in 0.1 M HClO<sub>4</sub>

Electrode	Overvoltage at 1 ma/cm <sup>2</sup> 35°C	$\Delta H_o^\ddagger$ kcal
Ga	.710	17.8 $\pm$ 1
20% In-Ga	.903	22.9 $\pm$ 1
In (s)	.95	14.1 (?)
<hr/>		
0.122% Hg-Ga	.747	
0.36%	.796	
1.64%	.973	
99.65%	1.020	
Hg	1.027	22.3 $\pm$ 0.4
<hr/>		
63% in-Hg	.974	19.5 $\pm$ 1.5

The temperature dependence of the corrected exchange current on gallium and the 20% indium-gallium alloy were measured, and the values obtained for the enthalpy of activation are summarized in Table 14-1. Note that although the enthalpy of activation on the indium-gallium alloy is nearly the same as for mercury, the overvoltage at a constant current is 100 mv lower - thus indicating large differences in the structure of the transition state which are probably attributable to the electronic structure of the metallic phase.

### References

1. K. Sabo and I. A. Bagotskaya, Dokl. Akad. Nauk SSSR 149, 139 (1963); 150, 128 (1963); Zh. Fiz. Khim. 37, 2581 (1963).  
A. N. Frumkin, N. S. Polyakovskaya, and N. B. Grigor'ev, Dokl. Akad. Nauk SSSR 157, 1455 (1964); Electrochim. Acta, 10, 793 (1965).
2. J. N. Butler and M. L. Meehan, J. Phys. Chem. 69, 4051 (1965).

15. On the Relation Between Heat of Adsorption of  
Hydrogen and Hydrogen Overpotential

A. C. Makrides

Submitted to J. Electrochem. Soc.

Suggested relations<sup>(1, 2)</sup> between the heat of adsorption of hydrogen,  $\Delta H_{\text{ads}}$ , as calculated from an equation due to Pauling<sup>(3, 4)</sup> and the hydrogen overpotential were examined using recent, accurate data for hydrogen evolution on Pb, In, Hg, Ga, Zn, Tl, and Cd. It was found that no relation in fact exists, the overpotential being unrelated to the calculated adsorption energy. The absence of such a correlation may be due to (a) a fundamental failure of the theoretical model on which it is based, or (b) a failure of the Pauling equation, or (c) neglect of the change in the adsorption energy of water for different metals. A qualitative argument is advanced to show that item (c) cannot be neglected and that it may in fact account for the absence of the expected dependence of overpotential on  $\Delta H_{\text{ads}}$ .

References

1. P. Ruetschi and P. Delahay, J. Chem. Phys. 23, 195 (1955).
2. B. E. Conway and J. O'M. Bockris, J. Chem. Phys. 26, 532 (1957).
3. L. Pauling, "Nature of the Chemical Bond", Cornell Univ. Press, Ithaca, 1948, p. 60.
4. D. D. Eley, Discussions Faraday Soc., 8, 34 (1950).

## B. Kinetics of Oxidation of Organic Fuels

### 16. Adsorption and Oxidation of Formic Acid on Smooth Platinum Electrodes in HClO<sub>4</sub> Solutions

S. B. Brummer and A. C. Makrides

Submitted as Technical Memorandum No. 8 (November, 1963).

Published: J. Phys. Chem. 68, 1448-1459 (1964).

The adsorption and oxidation of formic acid, a model organic fuel, on smooth Pt electrodes at 40°C was studied in HClO<sub>4</sub> solutions with anodic and cathodic chronopotentiometry and with potentiostatic, steady-state techniques. The oxidation rate at each potential was determined as a function of electrode preparation, pH (-0.3 to +1.55), and formic acid concentration (10<sup>-3</sup> to 1 M).

Anodic pre-treatment activates an electrode for subsequent oxidation of HCOOH. However, the oxidation rate at a given potential declines with time since pre-anodization (Fig. 16-1). This is because of the slow adsorption of a substance which interferes with the subsequent oxidation of HCOOH. The kinetics of adsorption of this blocking substance were determined with cathodic transients (H-atom co-deposition) and are much slower than would be expected from diffusion of formic acid molecules up to the electrode (Fig. 16-2). This suggests that the poisoning species is formed as the result of a reaction of the formic acid. The oxidation of HCOOH proceeds on the surface not occupied by this poisoning species, and is first-order in bare surface (Fig. 16-3).

The extent of coverage with this blocking species declines with increase in potential (see part 17 of this report) and is essentially zero at 0.7 volts. Anodic charging curves, when the adsorbate was oxidized, also showed that this adsorbate is unlikely to be HCOOH.

Currents for HCOOH oxidation were determined at each potential of interest at various times after pre-anodization. Current-potential curves follow the Tafel relation (Fig. 16-4) but the Tafel slope decreases with time after pre-anodization. The limiting value is close to 2.3RT/F. Above 0.45 volts, the current becomes independent of potential (Fig. 16-4).

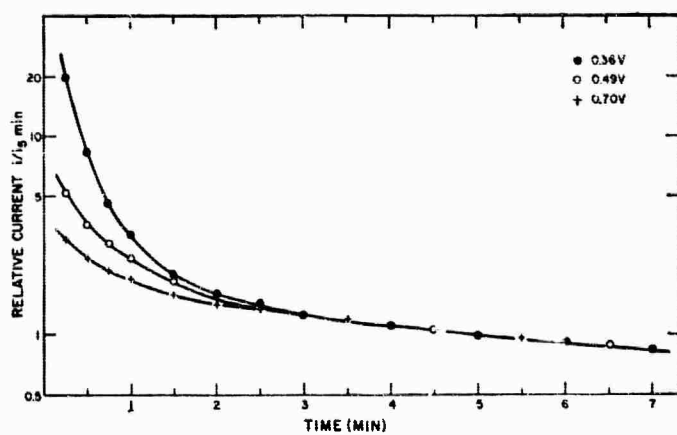


Fig. 16-1. Decline of rate of oxidation, at various potentials, as function of time since cleaning for 1 M HCOOH in 2 M HClO<sub>4</sub>.

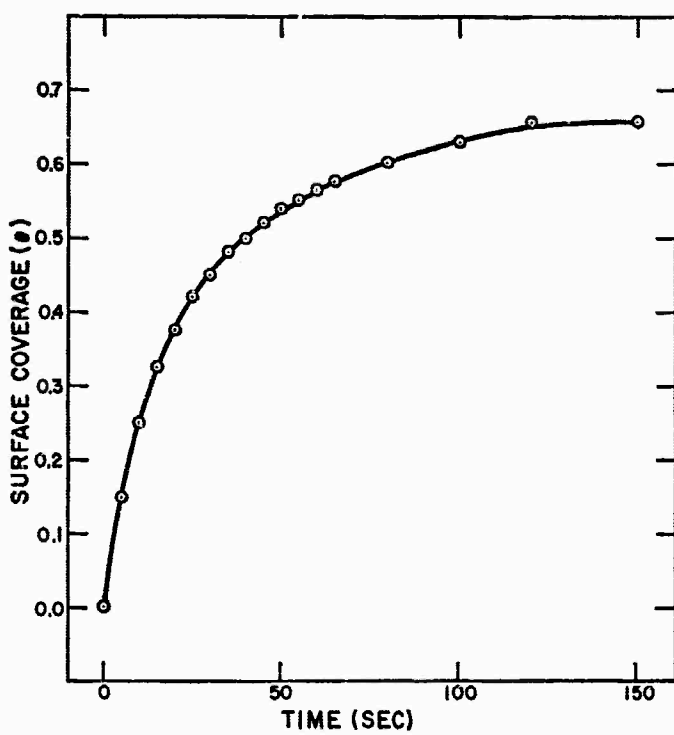


Fig. 16-2. Adsorption of HCOOH from 1 M HClO<sub>4</sub>, at 0.45 v., as a function of time.

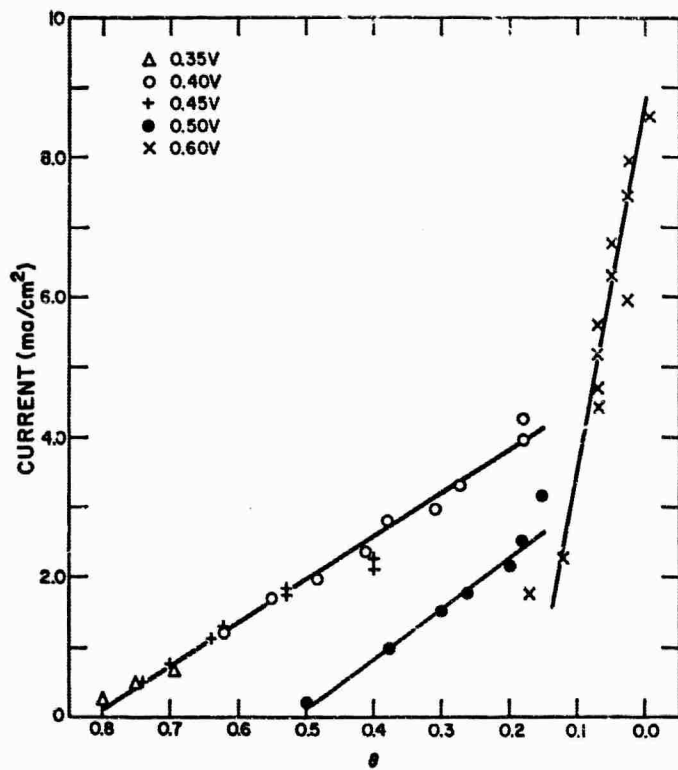


Fig. 16-3. Oxidation of HCOOH in 1 M HClO<sub>4</sub> at various potentials as a function of the coverage of the electrode.

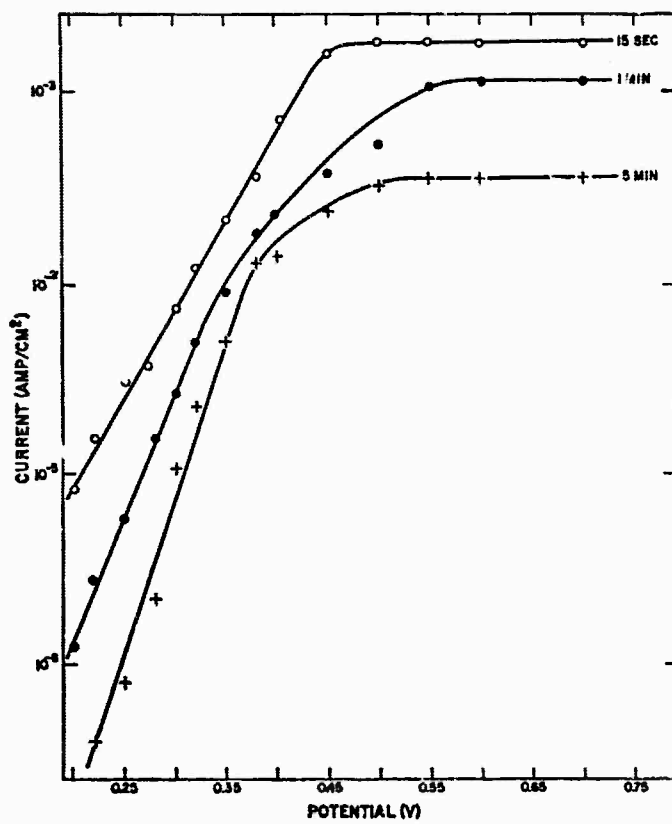
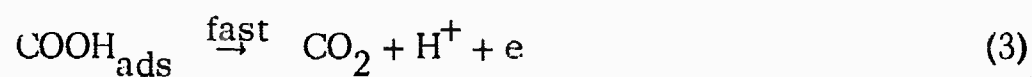
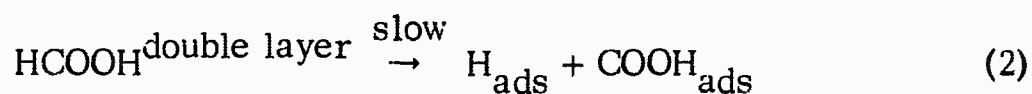
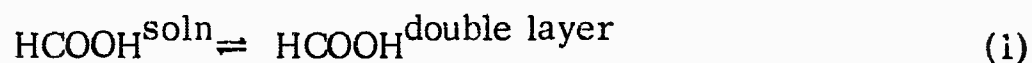


Fig. 16-4. Log current vs. potential for oxidation of 1 M HCOOH at pH 1.0.

This current plateau is not limited by diffusion in the solution. Similarly, the pH dependence of the oxidation rate at fixed potential versus the standard hydrogen electrode reaches a steady value at times longer than two minutes after the pre-anodization. This can be expressed as  $(\partial \log i / \partial \text{pH})_{\psi} = 1.0$ . The order of the reaction with respect to HCOOH is unity.

The following mechanism was suggested to account for these observations:



If it is assumed that the active surface area\*,  $\theta_A$ , is divided between free sites,  $\theta_F$ , those covered with hydrogen atoms,  $\theta_H$ , and those covered with some adsorbed blocking substance (not COOH),  $\theta_P$ , then

$$\theta_F = \theta_A - \theta_H - \theta_P \quad (5)$$

From (2)

$$i = \bar{k}(\text{HCOOH})^{\text{double layer}} \theta_F \quad (6)$$

where  $\bar{k}$  is a rate constant, and reaction (2) is assumed to take place only on free, active sites.  $\theta_A$  is taken to be independent of potential, and  $\theta_P$

\* Data of Fig. 16-3 indicate that some sites on the surface are more active for HCOOH oxidation.

was shown above to be independent of potential in the Tafel region, although not at higher potentials. If  $\theta_H$  is determined by the equilibrium



and if, in HCOOH solutions, it is given by

$$\theta_H = K(H^+) \exp - \left( \frac{\psi F}{RT} \right) \quad (8)$$

where  $K$  is the equilibrium constant of reaction and  $\psi$  is the potential of the electrode with respect to a hydrogen electrode in the same solution, then

$$i = \bar{k}(HCOOH)^{d.l.} [ \theta_A - \theta_P - K(H^+) \exp - \left( \frac{\psi F}{RT} \right) ] \quad (9)$$

It is clear that eq. (9) offers an approximate explanation of all the presently known facts. The Tafel slope,  $dE/d \log i$ , is approximately 60 mv., and  $(\partial \log i / \partial pH)$  is about 1.0 in the Tafel region. In addition, when  $\theta_H \rightarrow 0$ , as it is for  $E_\psi \gtrsim 0.35$  v., a limiting current is observed. The order of the reaction with respect to HCOOH is unity via eq. (1) and this equation also accounts for the apparent decline of the surface activity as the potential increases. The slowly adsorbing substance is formally included as  $\theta_P$ , and the fact that  $\theta_P$  is not very sensitive to concentration indicates why an order of unity with respect to HCOOH is observed even in the Tafel region. In the limiting current region, the pH dependence is small and may reflect some second-order effect on the rate of reaction (2).

17. The Use of Large Anodic Galvanostatic Transients  
to Evaluate the Maximum Adsorption on Platinum  
from Formic Acid Solutions

S. B. Brummer

Submitted as Technical Memorandum No. 13 (August, 1964).

Presented in part at the Washington Meeting of the Electro-  
Chemical Society, October, 1964.

Published: J. Phys. Chem. 69, 562-571 (1965).

In order to investigate the nature of the adsorbed species which poisons the low potential oxidation of HCOOH, further studies of the adsorption process on smooth Pt at 40°C were made with large anodic and cathodic galvanostatic transients.

During the application of a large anodic current,  $i_a$ , three processes contribute to the charge passed,  $Q_a$ . These are (I) oxidation of adsorbate, (II) oxidation of a species in solution, and (III) surface oxidation of the electrode. By applying a cathodic current,  $i_c$ , at various times during the anodic transient, it is possible to measure III directly and, from the charge passed in deposition of H atoms prior to H<sub>2</sub> evolution, one can follow changes in the concentration of adsorbed HCOOH. By varying  $i_a$ , one can assess the effect of II. It is found that the contributions of processes I, II, and III can be effectively separated. This method is illustrated in Fig. 17-1.

Typical results from the application of this novel technique are shown in Fig. 17-2. Here, we plot the fraction of the surface available for hydrogen deposition,  $\theta_H$ , as a function of the anodic stripping charge. The dotted region at high  $\theta_H$  indicates where electrode oxidation is first found, during the anodic transient. In general,  $\theta_H$  increases linearly with  $Q_a$ , indicating that the adsorbate has a constant oxidation state over its whole range of coverage: two electrons per site are released when the adsorbate is oxidized to CO<sub>2</sub>. The value of  $Q_a$  (with minor corrections) extrapolated to  $\theta_H = 1$  (a 'clean' electrode) is taken as  $Q_{\text{HCOOH}}^{\text{max}}$ , the

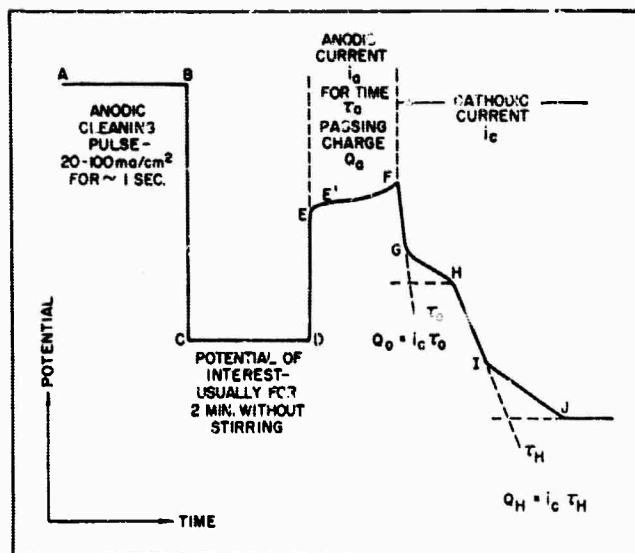


Fig. 17-1. Potential-time sequence used to clean the electrode and to make the measurements.

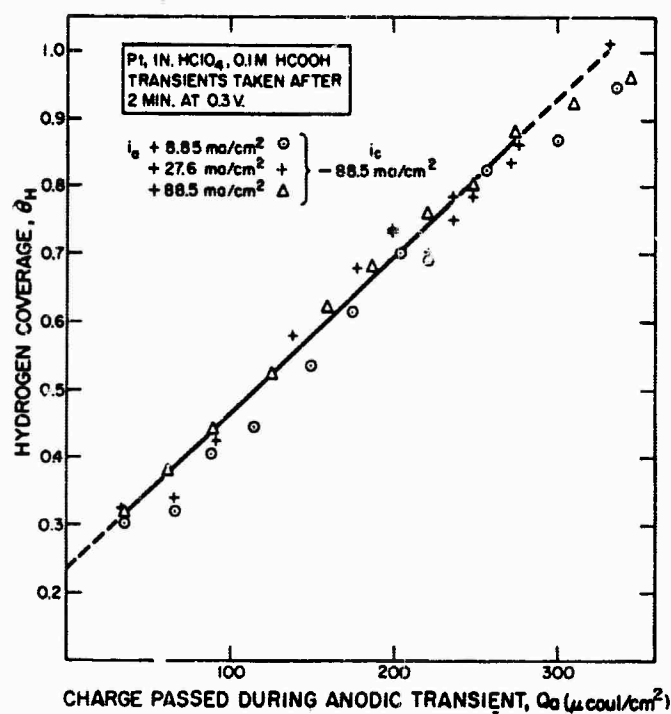


Fig. 17-2. Variation of  $\theta_H$  with  $Q_a$  in 0.1 M HCOOH. The measurements were taken from 0.3 v., 2 min. after cleaning pulse.

maximum adsorption from HCOOH solutions. This value (285 microcoulombs/real  $\text{cm}^2$ ) is too large to correspond to HCOOH itself, particularly as the adsorbed species has a maximum coverage of 73% of the surface (Fig. 17-3). Electrode coverage with this species which poisons HCOOH oxidation declines as the potential is raised above approximately 0.35 volts. The decline is more rapid at lower HCOOH concentrations. Coverage is essentially zero by approximately 0.7 volts.

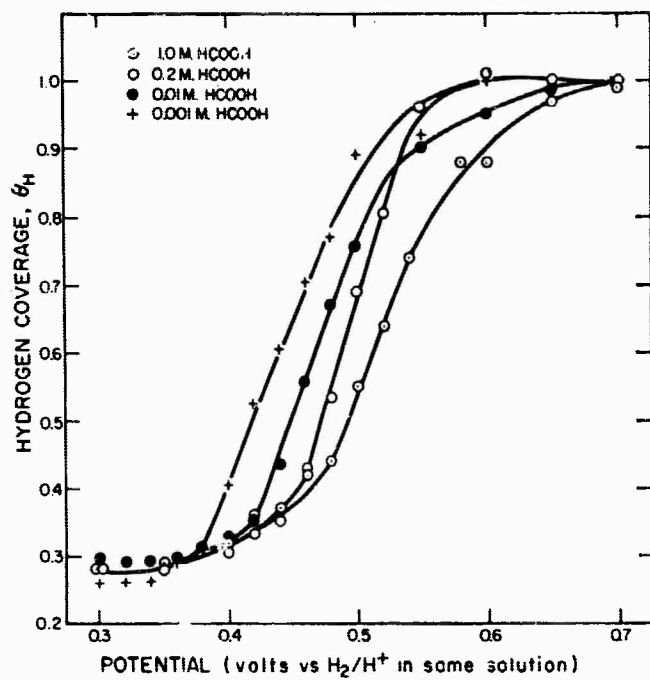


Fig. 17-3. Variation of  $\theta_H$  with electrode potential in HCOOH solutions. The measurements were taken 2 min. after cleaning pulse, usually with 50-ma./cm.<sup>2</sup> pulses.

18. Galvanostatic Transient Studies of Carbon Monoxide Adsorption on Platinum Electrodes

S. B. Brummer and J. I. Ford

Submitted as Technical Memorandum No. 14a (August, 1964).

Presented in part at the Washington Meeting of the Electrochemical Society, October, 1964.

Published: J. Phys. Chem. 69, 1355-1362 (1965).

In order to test suggestions that the adsorbed species which poisons the low potential oxidation of HCOOH is CO formed from decomposition of the HCOOH, the adsorption of CO on smooth Pt electrodes from solutions of 1 N HClO<sub>4</sub> saturated with 1 atm of CO at 40° was studied using anodic and cathodic galvanostatic transients. It is found that when a large anodic current,  $i_a$ , is applied to the electrode, the potential increases rapidly to  $\sim 1.2$  v. (vs. H<sup>+</sup>/H<sub>2</sub> in the same solution), falls to  $\sim 1.0$  v, slowly starts to increase again, and finally becomes almost steady. The charge passed in the various regions of this transient is insensitive to the current density in the range 2.3 to 147 ma/cm<sup>2</sup> and, also, to the starting potential, in the range 0.1 to 0.8 v.

As in the case of HCOOH, three processes contribute to the charge passed,  $Q_a$ , during the application of such a current. These are (I) oxidation of adsorbate, (II) oxidation of a species in solution, and (III) surface oxidation of the electrode. By applying a cathodic current,  $i_c$ , at various times during the anodic transient, it is possible to measure (III) directly. From the charge passed in deposition of H atoms prior to H<sub>2</sub> evolution,  $Q_H$ , one can follow changes in the concentration of adsorbed CO. The effect of (II) can be assessed by varying  $i_a$ .

It is found that  $\theta_H(Q_H/Q_H^{\max})$  increases almost linearly with  $Q_a$  and this relation is independent of  $i_a$  (Fig. 18-2). Oxidation of the electrode is impeded, even when the adsorbed CO has been removed, but does occur during the progress of (I) (Fig. 18-2). In addition, it is a function of  $i_a$ . Thus, the coincidence of the  $\theta_H - Q_a$  curves in Fig. 18-3 for the different current densities, does not mean that we are solely observing

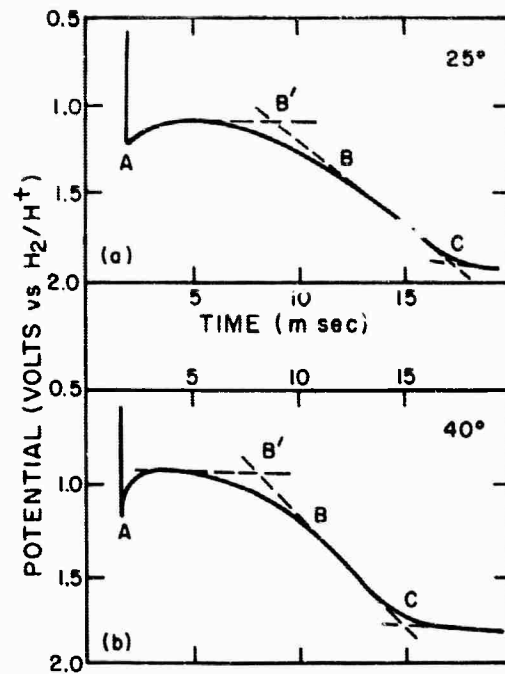


Fig. 18-1. Anodic galvanostatic transients taken from 0.3 v., 2 min. after cleaning pulse, with 1 atm. of CO, at  $\sim 50 \text{ ma./cm.}^2$ . At  $25^\circ$ , point B is not very well defined, but at  $40^\circ$  quite a sharp break is observed. The overshoot also is more pronounced at  $40^\circ$ .

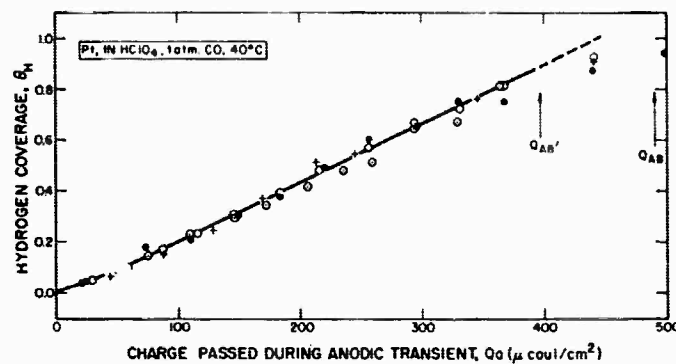


Fig. 18-2. Variation of  $\theta_H$  with  $Q_a$  for various current densities. Transients were taken from 0.3 v., 2 min. after cleaning pulse, with 1 atm. of CO. Anodic current densities:  $\circ$ , 2.35 ma./cm.<sup>2</sup>;  $\square$ , 7.35 ma./cm.<sup>2</sup>;  $\bullet$ , 73.5 ma./cm.<sup>2</sup>;  $+$ , 147 ma./cm.<sup>2</sup>; cathodic current density, 147 ma./cm.<sup>2</sup>.  $\theta_H$  values are slightly corrected according to dotted line in Figure 3a.

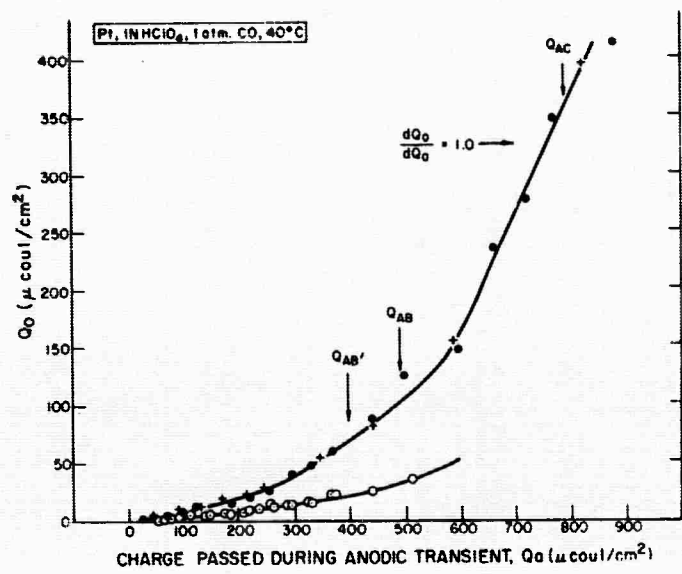


Fig. 18-3. Variation of  $Q_0$  with  $Q_a$  for various current densities. The transients were taken after 2 min. at 0.3 v. with 1 atm. of CO. Anodic current densities:  $\circ$ , 2.35 ma./cm.<sup>2</sup>;  $\square$ , 7.35 ma./cm.<sup>2</sup>;  $\bullet$ , 73.5 ma./cm.<sup>2</sup>; +, 147 ma./cm.<sup>2</sup>; cathodic current density, 147 ma./cm.<sup>2</sup>.

(I); there must also be a contribution from (II). The sum of (II) and (III) is evidently independent of  $i_a$ , and (II) is not limited by diffusion.  $Q_a$  is corrected for (II) and (III) from the measurements.

Then, it is found that 390  $\mu\text{coulombs/real cm}^2$  are required to oxidize all of the adsorbed CO. Of this, 60  $\mu\text{coulombs/cm}^2$  is weakly adsorbed and involves three electrons per Pt surface atom for oxidative removal. The remainder, from  $\theta_H = 0.1$  to  $\theta_H = 1.0$ , requires 1.77 electrons per site. This would correspond to  $\sim 23\%$  of the adsorbed CO in a doubly bonded or "bridged" structure. From cathodic charging curves it is found that the electrode is less than 2% bare at 0.3 v. The rate of adsorption of CO at low potentials is limited by diffusion in solution.

19. Comparison of Adsorbed Formic Acid and  
Carbon Monoxide on Platinum Electrodes

S. B. Brummer

Submitted as Technical Memorandum No. 14b (August, 1964).

Presented in part at the Washington Meeting of the Electrochemical Society, October, 1964.

Published: J. Phys. Chem. 69, 1363-1365 (1965).

A comparison is made between the properties of the adsorbed films formed on smooth platinum in HCOOH and CO-saturated solutions of HClO<sub>4</sub>. Both the coulometric behavior and the oxidation kinetics of the adsorbed films (compared at constant surface coverage, Fig. (19-1)) suggest that while they are similar they are not the same.

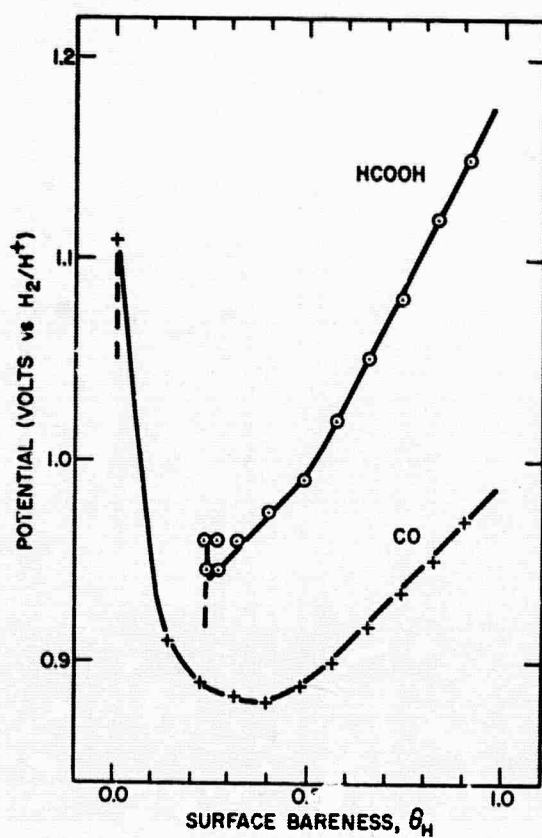


Fig. 19-1. The variation of potential with surface bareness during a  $14.7 \text{ ma./cm.}^2$  anodic galvanostatic transient. HCOOH measurement was taken in a  $0.2 \text{ M}$  solution in  $1 \text{ N HClO}_4$ . The CO measurement was made with  $1 \text{ N HClO}_4$  saturated with  $1 \text{ atm.}$  of CO.

## C. Oxygen Reduction

### 20. Electrochemical Behavior of Nickel Compounds II. Anodic Dissolution and Oxygen Reduction in Perchlorate Solutions

A. K. M. S. Huq, A. J. Rosenberg, and A. C. Makrides

Submitted as Technical Memorandum No. 3 (April, 1963).

Presented at the Boston Meeting of the Electrochemical Society, May, 1963,

Published: J. Electrochem. Soc. 111, 278-286 (1964).

The anodic dissolution of Ni, Si, and Sb and of the compounds NiSi, NiSb, NiAs, and NiS was studied in molar perchlorate solutions at pH 0.04 and 10.8. The results are shown in Figs. 20-1 - 20-7 and Table 20-1.

In all cases except with Si in acid solution, active dissolution at low anodic potentials is followed by a transition to a passive state where the anodic current density is nearly independent of potential. In acid solution, the critical potentials of NiSi, NiAs, and NiS are less positive than that of Ni and the critical currents are less by two to three orders of magnitude. The critical potential of NiSb is about the same as for Sb, but the critical current is substantially less. The anodic current in the passive region for the compounds is greater than for passive Ni. NiSi, NiAs, and NiS show a transpassive region in which Sb, As, and S are probably oxidized to ions of a high valence state. In alkaline solutions, NiSi, NiSb, and NiS show an active-passive transition at the same potential as pure Ni. However, the rate of oxidation of these compounds in the passive state is again considerably greater than for passive Ni. It is suggested that in acid solution the passive film on nickel compounds is either a mixed oxide or an oxide having the basic structure of the second element; in alkaline solution, nickel oxide is formed first but it probably has a different structure than the oxide formed on passive Ni. The difference between acid and alkaline solutions arises from the difference in the stability of nickel oxide in the two electrolytes. A stable, passive oxide on Ni is formed in acid solution only when the dissolution rate is sufficiently large to cause nickel hydroxide to precipitate at the

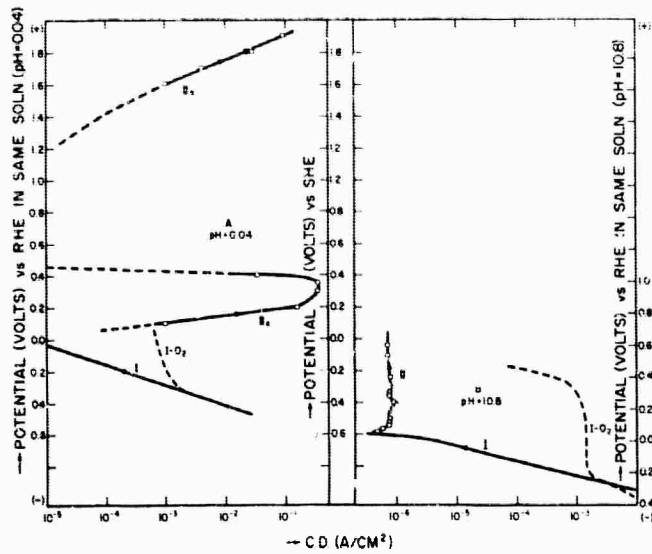


Fig. 20-1. Polarization curves for Ni. Fig. 1A, pH = 0.04 (1M HClO<sub>4</sub>): curve I, cathodic hydrogen evolution, curve IIa, anodic dissolution and passivation of Ni; curve IIb, transpassive region. Passivation current < 10<sup>-5</sup> amp/cm<sup>2</sup>. Curve I-O<sub>2</sub>, O<sub>2</sub> reduction - Tafel region masked by anodic dissolution of Ni at ~ 80 mv (vs. RHE). Fig. 1B, pH 10.8 (1M NaClO<sub>4</sub>): curve I-cathodic hydrogen evolution; curve II, initial anodic dissolution and passivation; curve I, O<sub>2</sub>, O<sub>2</sub> reduction - extends into passivation region.

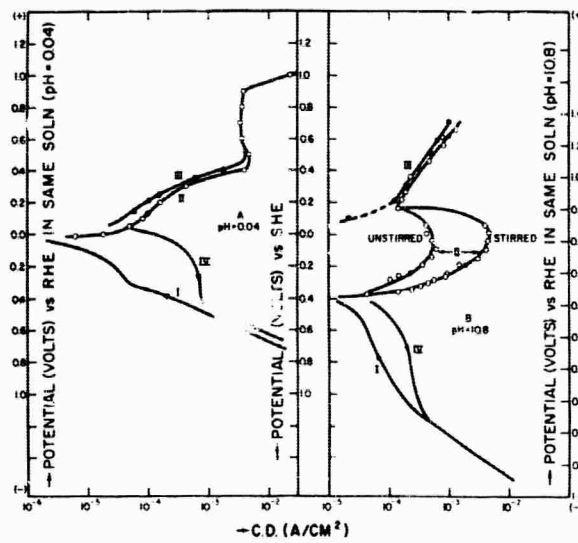


Fig. 20-2. Polarization curves for Sb. Fig. 2A, pH 0.04 (1M HClO<sub>4</sub>): curve I, cathodic hydrogen evolution; curve II, anodic current for dissolution and passivation, toward increasing potentials; curve III, anodic currents, toward decreasing potentials; curve IV, cathodic currents, toward decreasing potentials, following curve III; O<sub>2</sub> reduction not observed. Fig. 2B, pH 10.8 (1M NaClO<sub>4</sub>): curves I and IV, cathodic processes including hydrogen evolution; curve II, anodic dissolution and passivation, toward increasing potentials, stirring-dependent current in the active/passive transition region; curve III, reverse of curve II; no O<sub>2</sub> reduction observed.

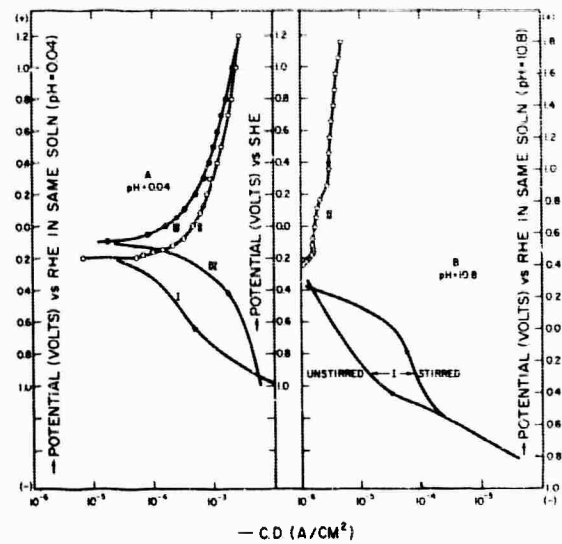


Fig. 20-3. Polarization curves for Si. Fig. 3A, pH 0.04 (1M HClO<sub>4</sub>); Fig. 3B, at pH 10.8 (1M NaClO<sub>4</sub>); passivation in alkaline solution: no O<sub>2</sub> reduction observed.

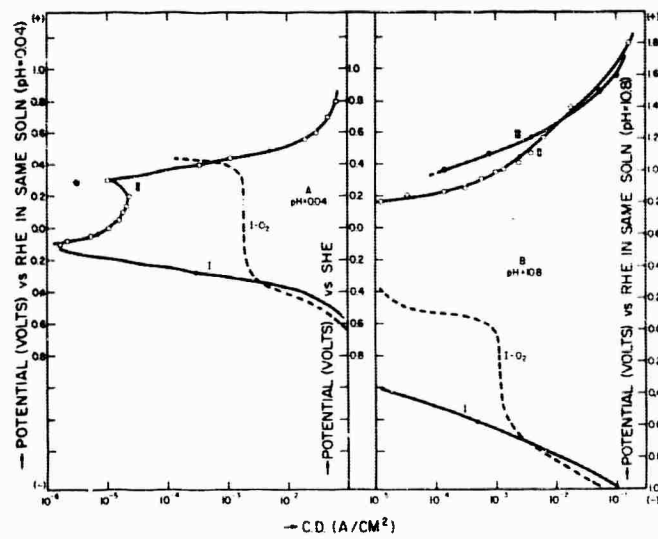


Fig. 20-4. Polarization curves for NiAs. Fig. 4A, pH 0.04 (1M HClO<sub>4</sub>): curve I, cathodic hydrogen evolution; curve II, anodic current for dissolution and passivation of NiAs; curve I-O<sub>2</sub>, cathodic O<sub>2</sub> reduction, Tafel region masked by anodic dissolution of NiAs. Fig. 4B, pH 10.8 (1M NaClO<sub>4</sub>): curve I, cathodic hydrogen evolution; curve II, anodic dissolution of NiAs, toward increasing potentials; curve III, same as II, toward decreasing potentials; curve I-O<sub>2</sub>, O<sub>2</sub> reduction.

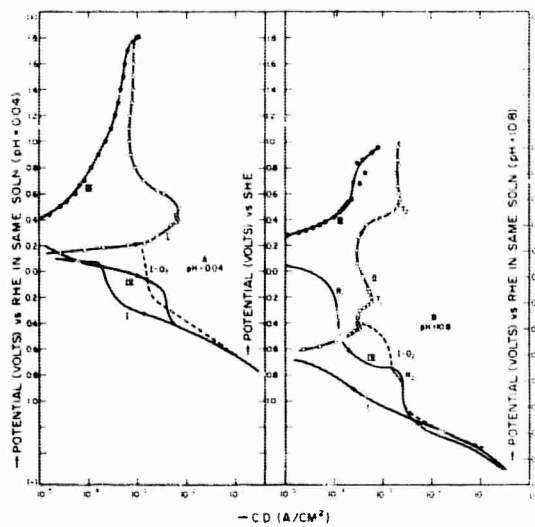


Fig. 20-5. Polarization curves for NiSb. Fig. 5A, pH 0.04 (1M HClO<sub>4</sub>): curves I and IV, cathodic processes including hydrogen evolution; curve II, (toward increasing potentials) anodic dissolution and active/passive transition; curve III, (toward decreasing potentials) anodic current with no active/passive transition; curve I-O<sub>2</sub>, O<sub>2</sub> reduction, Tafel region masked by anodic dissolution of electrode. Fig. 5B, pH 10.8 (1M NaClO<sub>4</sub>): curve I, cathodic hydrogen evolution; curve IV, oxide reductions (R<sub>1</sub> and R<sub>2</sub>) and hydrogen evolution; curve II, (toward increasing potentials) anodic currents, two transitions (T<sub>1</sub> and T<sub>2</sub>) observed; curve III, reverse of curve II; curve I-O<sub>2</sub>, O<sub>2</sub> reduction.

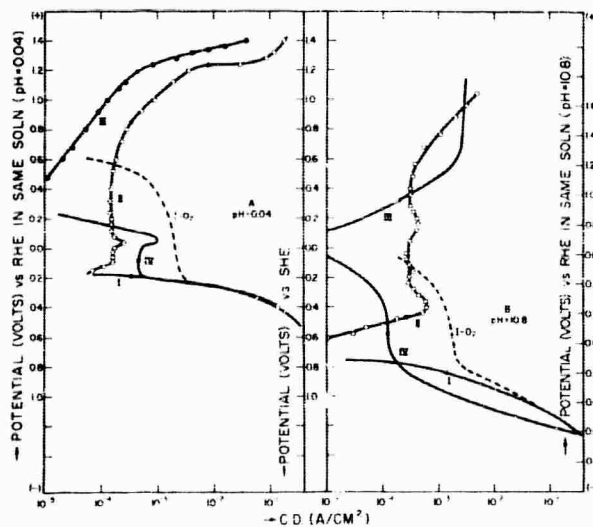


Fig. 20-6. Polarization curves for NiS. Fig. 6A, pH 0.04 (1M HClO<sub>4</sub>): curve I, cathodic hydrogen evolution; curve IV, oxide reduction and hydrogen evolution; curve II, (toward increasing potentials) anodic dissolution and passivation current; curve III, (toward decreasing potentials); curve I-O<sub>2</sub>, reduction currents for O<sub>2</sub>-reduction. Fig. 6B, pH 10.8 (1M NaClO<sub>4</sub>): curves I, II, III, and IV have same meanings as in Fig. 6A.

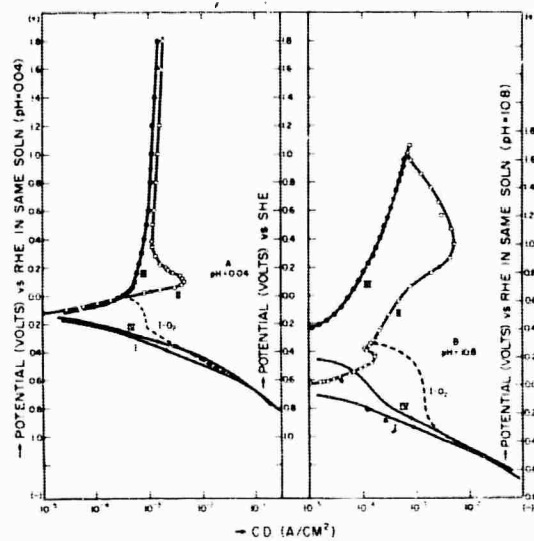


Fig. 20-7. Polarization curves for NiSi. Fig. 7A, pH 0.04 (1M HClO<sub>4</sub>): curves I and IV, cathodic hydrogen evolution; curves II and III, anodic currents for dissolution and passivation of NiSi; curve II, (traced toward increasing potentials) shows active/passive transition; curve I-O<sub>2</sub>, O<sub>2</sub> reduction, masked by anodic dissolution of electrode. Fig. 7B, pH 10.8 (1M NaClO<sub>4</sub>): curves I, II, III, and IV have same meanings as in Fig. 7A; curve II shows two transitions; curve I-O<sub>2</sub> shows pronounced O<sub>2</sub> reduction current.

TABLE 20-1

Summary of Results  
Molar Perchlorate Solutions of pH 0.04

	Passivation potential $E_t, v$	Critical C. D. $i_t, \text{amp/cm}^2$	C. D. in passive region $i_p, \text{amp/cm}^2$	Passive potential range $\Delta E_p, v$	$\Delta E_t / \Delta pH$
Ni	+0.3	$3 \times 10^{-1}$	$\sim 10^{-6}$	0.4 to 1.4	-0.074
Sb	+0.4	$4.5 \times 10^{-3}$	$3.5 \times 10^{-3}$	0.4 to 0.9	-0.041
Si	--	---	$\sim 10^{-3}$	---	---
NiAs	+0.2	$2.3 \times 10^{-5}$	$\sim 10^{-5}$	---	---
NiSb	+0.45	$7 \times 10^{-3}$	$7 \times 10^{-4}$	0.8 to 1.8	-0.082
NiS	-0.10	$1.5 \times 10^{-4}$	$1.5 \times 10^{-4}$	-0.1 to 0.7	-0.026
NiSi	+0.10	$4.5 \times 10^{-3}$	$\sim 10^{-3}$	0.4 to 1.8	-0.050

1M NaClO<sub>4</sub> at pH 1.8

	Passivation potential $E_t, v$	Critical C. D. $i_t, \text{amp/cm}^2$	C. D. in passive region $i_p, \text{amp/cm}^2$	Passive potential range $\Delta E_p, v$
Ni	-0.5	$10^{-6}$	$7 \times 10^{-7}$	---
Sb	-0.04	$5 \times 10^{-4}$ (unstirred) $5 \times 10^{-3}$ (stirred)	$\sim 10^{-4}$	---
Si	-0.16	$1.7 \times 10^{-6}$	$1.6 \times 10^{-6}$	-0.16 - 2.0
NiAs	--	$< 10^{-6}$	$< 10^{-6}$	---
NiSb	-0.44	$3 \times 10^{-4}$	$3 \times 10^{-4}$	-0.44 - 0.37
	(0.56)	$(2 \times 10^{-3})$	$(2 \times 10^{-3})$	(0.56 - 1.0)
NiS	-0.39	$6 \times 10^{-4}$	$3 \times 10^{-6}$	-0.39 - 0.56
NiSi	-0.44	$1.7 \times 10^{-4}$	$1.2 \times 10^{-4}$	---

electrode surface, a condition not fulfilled during the dissolution of any of the compounds. In general, the oxide of the companion element or a mixed oxide is more stable than nickel oxide in acid solution at low potentials. This situation is reversed in alkaline solution, and in this case the initial passive film is nickel oxide.

The order of electrocatalytic activity for oxygen reduction is  $\text{Ni} > \text{NiAs} > \text{NiSi}$  in acid solution, and  $\text{NiS} > \text{Ni} > \text{NiSi} \sim \text{NiSb} > \text{NiAs}$  in alkaline solution. The order in the activity of the materials remains essentially independent of pH except that NiSi is more active than NiAs in alkali and that the reverse is true in acid. A significant observation is that  $\text{O}_2$  reduction takes place in the potential region in which the materials are generally passive and are covered with surface oxides. The observed differences between these compounds indicate that the presence of the negative element (Si, S, Sb, As) modifies the nature of the surface oxide to produce changes in the electrocatalytic activity.

## 21. Kinetics of Redox Reactions on Passive Electrodes

A. C. Makrides

Submitted as Technical Memorandum No. 2 (April 1963).

Presented in part at the Washington Meeting of the Electrochemical Society, October, 1964.

Published: J. Electrochem. Soc. 111, 392-400 (1964).

The formation of a surface oxide is an important factor in the kinetic of oxygen evolution and oxygen reduction on practically all metallic electrodes. In general, a superficial oxide is expected to change the specific interaction of oxygen (or of reaction intermediates) with the electrode to alter the potential distribution between metal and electrolyte, and to modify the dissolution kinetics of the metal. The change in the kinetics of dissolution has been studied in detail, since it is the characteristic phenomenon in passivity. However, relatively little work has been done on the effects of oxide films on electrochemical reactions other than corrosion reactions. The general features of electrode processes on superficially oxidized metals are examined in this paper using as a model a simple, one-electron redox reaction.

Aside from specific effects, e. g. , changes in the energy of adsorption of reactants or of intermediates, superficial oxides may influence the kinetics of an electrochemical reaction by providing a barrier to electron transfer between the metal and an ion or molecule at the oxide/electrolyte interface. With thick films, the oxide is the electrode, the underlying metal serving merely as a contact. The chemical character of the bulk oxide and its electrical properties, e. g. , its semi-conducting properties, enter then into the description of its electrode characteristics. At the other extreme, very thin oxide films may be considered as simply providing a barrier through which electrons must tunnel in order to participate in the reaction. The upper limit for tunneling is about 30 Å; conduction through the oxide is necessary for electron transfer with thicker films. However, if the film is only 100-200 Å, its electrical characteristics are influenced strongly by the underlying

metal, and this interaction may be important in the description of the electrode behavior of superficially oxidized electrodes.

A simple way of examining the general electrochemical effects of surface oxides is to compare the kinetics of an elementary electron transfer reaction on oxide-covered and oxide-free electrodes. Specific effects, e. g. , adsorption, should be at a minimum for the redox couple chosen. The  $\text{Fe}^{+++}/\text{Fe}^{++}$  couple was selected in this study because its kinetic behavior on oxide-free electrodes is straightforward. Furthermore, since its reversible potential falls in about the middle of the potential region over which a number of common metals and alloys are passive, both the oxidation of ferrous ion and the reduction of ferric ion can be followed without gross interference from corrosion reactions.

Overpotential measurements for the  $\text{Fe}^{+++}/\text{Fe}^{++}$  couple on passive Ni, Fe, and Ti, were carried out in solutions of fixed ionic strength but of varying pH. The results are given in Figs. 21-1 - 21-4 and Table 21-I.

Tafel lines were generally obtained with exchange currents between  $10^{-7}$  and  $10^{-5}$  amp/cm<sup>2</sup> and cathodic transfer coefficients of about 0.45. The anodic transfer coefficients were less, particularly with Ti and Fe electrodes. A limiting anodic current, which was unrelated to diffusion of  $\text{Fe}^{++}$  ion in solution, was observed under certain conditions on Fe and Ti. The contribution of ionic current to the total current through the film is negligible in most cases. In general, the passive film has rectifying properties, the easy direction of electron flow being from metal to solution. This rectification is additional to the usual Faradaic rectification observed with most electrochemical reactions. The apparent transfer coefficients, calculated from the anodic and cathodic polarization curves, yield sums significantly less than unity.

The polarization behavior of the  $\text{Fe}^{+++}/\text{Fe}^{++}$  couple on passive Ni, and Ti can be summarized by an expression of the form (potentials in units of  $RT/F$ )

$$i = i_0 \{ \exp [ - \alpha_f (E - E_{rev}) ] - \exp [ \beta_r (E - E_{rev} - V) ] \}$$

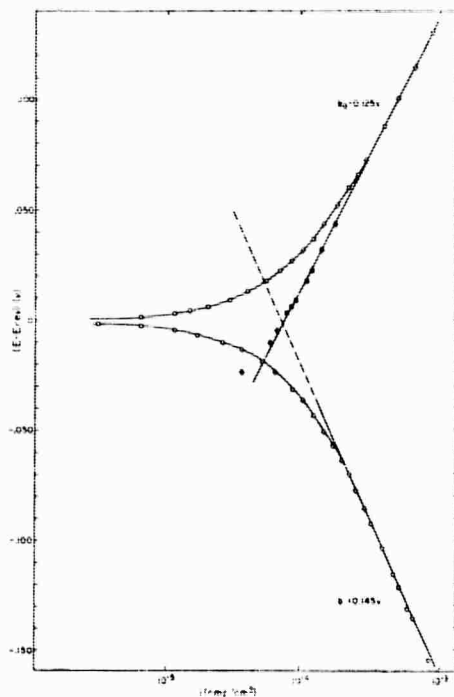


Fig. 21-1. Polarization curves for the  $\text{Fe}^{3+}/\text{Fe}^{2+}$  couple (0.05M) on Ni electrodes in  $\text{M MgSO}_4$  at  $\text{pH} = 2.3$  and at  $30^\circ\text{C}$ . Current densities corresponding to the full circles are calculated from  $i_{\text{ox}} = i_{\text{appl}} + i_{\text{red}}$  where  $i_{\text{red}}$  is given by the extrapolated cathodic curve.

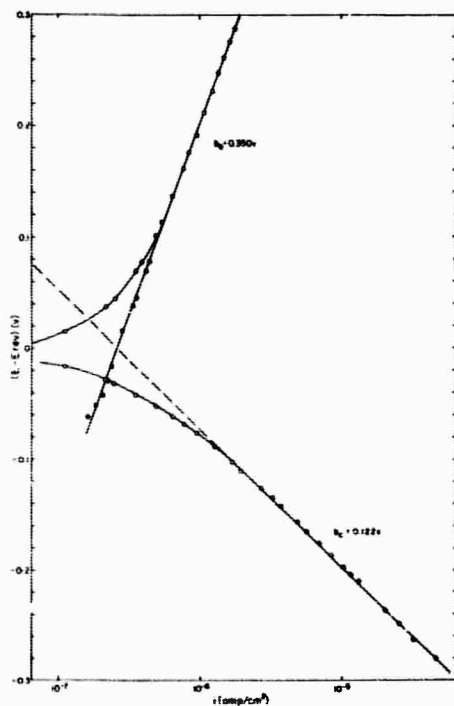


Fig. 21-2. Polarization curves for the  $\text{Fe}^{3+}/\text{Fe}^{2+}$  couple (0.05M) on Ti electrodes in  $\text{M MgSO}_4$  at  $\text{pH} = 2.3$  and at  $20^\circ\text{C}$ . Current densities corresponding to the full circles are calculated from  $i_{\text{ox}} = i_{\text{appl}} + i_{\text{red}}$  where  $i_{\text{red}}$  is given by the extrapolated cathodic curve.

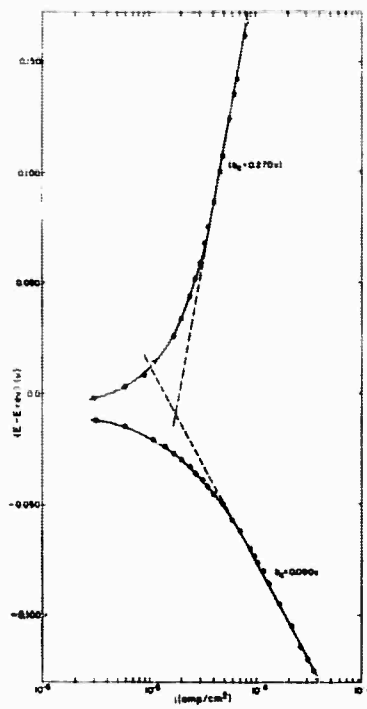


Fig. 21-3. Polarization curves for the  $\text{Fe}^{+++}/\text{Fe}^{++}$  couple on Fe electrodes at  $40^\circ\text{C}$ . The solution was 0.30M in  $\text{Fe}^{+++}$ , 0.03M in  $\text{Fe}^{++}$ , and M/20 in  $\text{H}_2\text{SO}_4$  and M/10 in  $\text{Na}_2\text{SO}_4$ . The anodic curve was obtained after the electrode was kept for 30 min at 0.20v vs. Eref for  $\text{Fe}^{+++}/\text{Fe}^{++}$ .

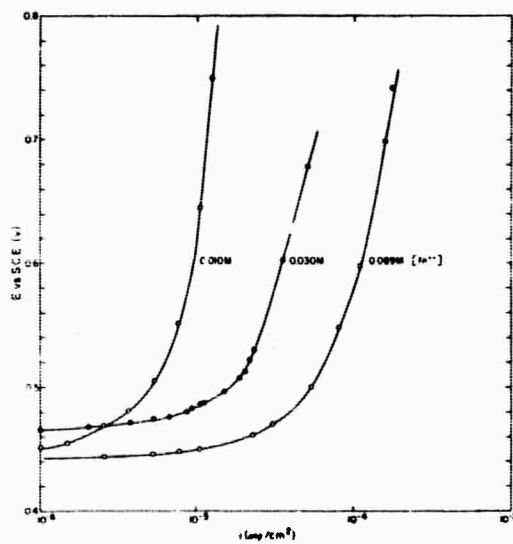


Fig. 21-4. Anodic polarization curves for the  $\text{Fe}^{+++}/\text{Fe}^{++}$  couple on iron in  $0.3\text{M MgSO}_4$  at  $\text{pH} = 1.45$ . The  $\text{Fe}^{+++}$  concentration was 0.3M. The current was kept constant at each value shown until the potential changed by less than 1 mv in 5 r.n.

TABLE 21-1

Nickel<sup>a</sup>

pH	T, °C	$E_{\text{corr}}, \text{V}$	$i_0$ extrapolated from cathodic 2 curve, amp/cm <sup>2</sup>	$i_0$ from $\left(\frac{\partial i}{\partial E}\right)$ (E - E <sub>rev</sub> ) = 0		$\alpha_c$	$\alpha_a$	$\alpha_c + \alpha_a$
				$(i_0)_c$	$(i_0)_a$			
2.3	10	-0.0003	2.6 x 10 <sup>-5</sup>	2.5 x 10 <sup>-5</sup>	2.5 x 10 <sup>-5</sup>	0.415	0.484	0.90
	20	-0.0006	4.55 x 10 <sup>-5</sup>	4.4 x 10 <sup>-5</sup>	4.4 x 10 <sup>-5</sup>	0.40	0.495	0.90
	20	-0.0012	7.6 x 10 <sup>-5</sup>	7.45 x 10 <sup>-5</sup>	7.15 x 10 <sup>-5</sup>	0.41	0.49	0.90
0.35	30	-0.0006	8.6 x 10 <sup>-5</sup>	8.6 x 10 <sup>-5</sup>	7.5 x 10 <sup>-5</sup>	0.46	(0.60)	--
							(0.375)	
0.00	0	-0.0003	5.0 x 10 <sup>-5</sup>	-----	-----	0.47	--	--
	10	-0.0008	8.0 x 10 <sup>-5</sup>	-----	-----	0.47	--	--
	20	-0.0005	11. x 10 <sup>-5</sup>	10.2 x 10 <sup>-5</sup>	8.0 x 10 <sup>-5</sup>	0.47	--	--
	30	-0.001	14. x 10 <sup>-5</sup>	12.8 x 10 <sup>-5</sup>	7.0 x 10 <sup>-5</sup>	0.47	(0.33)	--

<sup>a</sup> All solutions  $C_{\text{Fe}^{+++}} = C_{\text{Fe}^{++}} = 0.050\text{M}$  and  $\text{M MgSO}_4$ .

Here  $V$  is the potential drop within the oxide and is, in general, a function of the current density. The results suggest that  $V$  is proportional to  $E$ , i. e.

$$V = (E - E_{rev})$$

In this case

$$i = i_0 \left\{ \exp[-\alpha_r(E - E_{rev})] - \exp[(\beta_r)(1 - \gamma)(E - E_{rev})] \right\}$$

Consequently

$$\alpha_c + \alpha_a = (\alpha_r) + \beta_r(1 - \gamma) = 1 - \gamma\beta_r$$

with an apparent stoichiometric number of

$$v = \frac{i_0}{i} \left/ \left( \frac{\partial i}{\partial E} \right) \right|_{(E - E_{rev})=0} = 1 - \gamma\beta_r$$

These equations are followed by passive Ni at pH = 2.3 and by Ti at pH = 1.5 and for  $T \leq 20^\circ\text{C}$ . The coefficient  $\gamma$  is 0.15 for Ni and 0.60 for Ti. Fe, Ni at low pH, and Ti at higher temperatures show a more complicated behavior on anodic polarization.

These results demonstrate the existence of a potential drop across the passive, oxide film, the magnitude of this potential being dependent on the thickness and composition of the film.

22. Kinetics of the Ferric-Ferrous Reaction on  
Iron-Chromium Alloys

A. C. Makrides

Submitted as Technical Memorandum No. 4 (June, 1963).

Presented in part at the Washington Meeting of the Electrochemical Society, October, 1964.

Published: J. Electrochem. Soc. 111, 400-407 (1964).

The kinetics of the  $\text{Fe}^{+++}/\text{Fe}^{++}$  couple on superficially oxidized electrodes present a number of interesting features. In general, the exchange currents are low ( $\sim 10^{-6}$  amp/cm<sup>2</sup>), the transfer coefficients have unusual values and sums less than unity, and the anodic and cathodic curves are generally asymmetrical. These features appear to be basic to an electrode covered with a thin oxide (i. e. , a passive electrode) and not to be related to the specific nature of the redox couple. They are probably connected with electronic processes within the surface oxide and are expected, therefore, to occur with any redox reaction taking place at such an electrode. In particular, they undoubtedly play a major role in oxygen evolution and reduction on electrodes which form surface oxides in the relevant potential region.

A study of the kinetics of the  $\text{Fe}^{+++}/\text{Fe}^{++}$  reaction on passive Fe, Ni, and Ti electrodes was presented in a previous paper (1). This redox couple was chosen as a model reaction because its kinetics are straight-forward on oxide-free electrodes and because both oxidation of  $\text{Fe}^{++}$  and reduction of  $\text{Fe}^{+++}$  can be followed over a relatively wide potential range.

A detailed study of the redox kinetics of the  $\text{Fe}^{+++}/\text{Fe}^{++}$  reaction on Fe-Cr alloys is presented here. These alloy electrodes, which show the same general features as other superficially oxidized electrodes, are convenient experimentally, since they have small dissolution rates in acid solutions. In addition to the usual experimental quantities required for a more or less complete characterization of a redox reaction (Tafel parameters, reaction order, pH dependence, and temperature coefficient), the

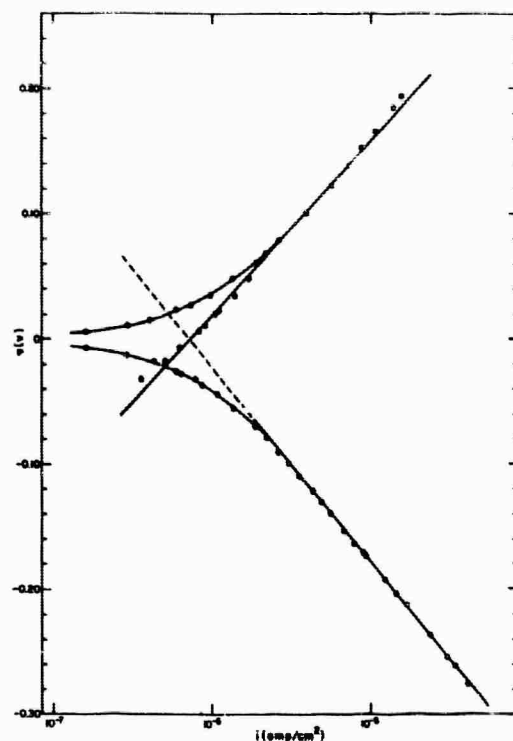


Fig. 22-1. Polarization curves of the  $\text{Fe}^{3+}/\text{Fe}^{2+}$  couple (0.050M) on passive Fe-Cr in M  $\text{MgSO}_4$  at pH = 2.2. Solid circles are calculated from  $i_a = i_c \pm i_{\text{appl}}$  where  $i_c$  is the extrapolated cathodic current and  $i_{\text{appl}}$  the externally applied current (30°C).

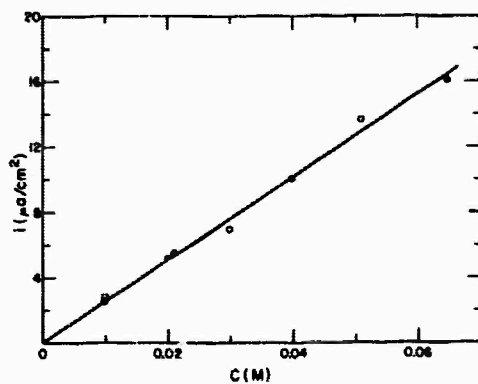


Fig. 22-2. Current at a fixed potential as a function of the concentration of ferrous or ferric ions —○— oxidation of  $\text{Fe}^{2+}$  at 0.600v vs. SCE; —●— reduction of  $\text{Fe}^{3+}$  at 0.200v vs. SCE (30°C).

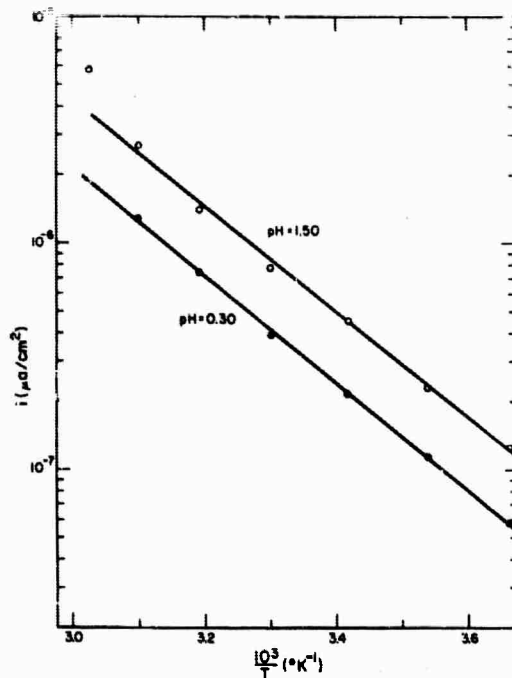


Fig. 22-3. Temperature coefficient of exchange current (extrapolated from the cathodic curve) for  $\text{Fe}^{+++}/\text{Fe}^{++}$  (0.50M) in  $\text{M MgSO}_4$ .

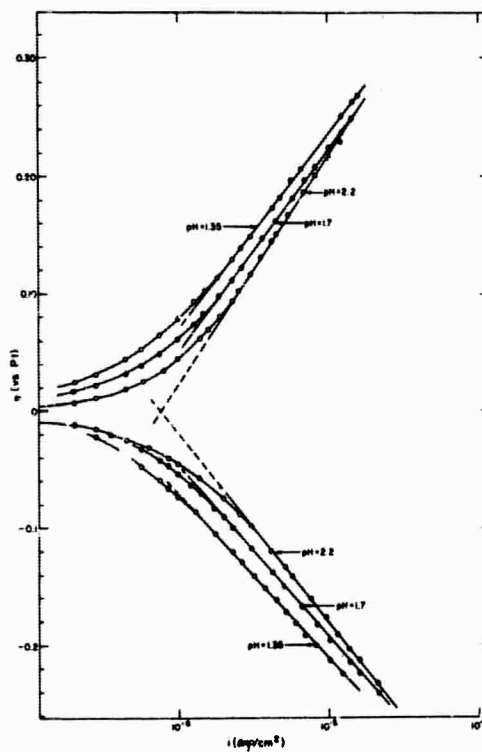


Fig. 22-4. Polarization curves of the  $\text{Fe}^{+++}/\text{Fe}^{++}$  couple (0.10M) on passive Fe-Cr in  $\text{M MgSO}_4$  at different pH (30°C).

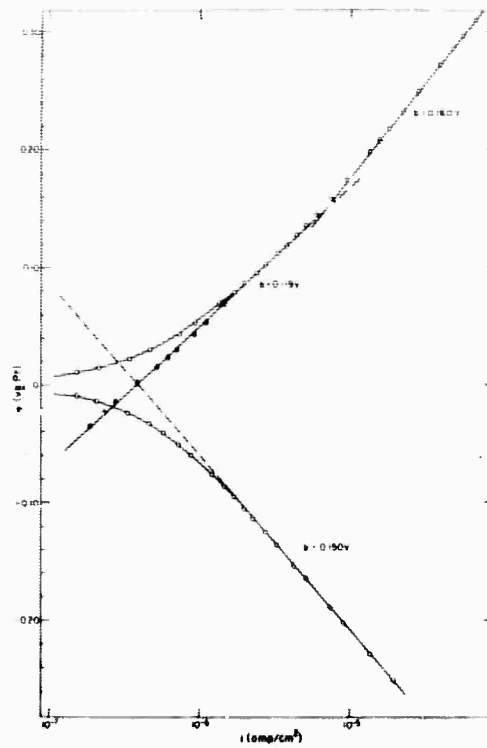


Fig. 22-5. Anodic polarization curve for  $Fe^{2+}$  oxidation on passive Fe-Cr alloy after cathodic pulsing. Measurements were made 24 hr after pulsing.

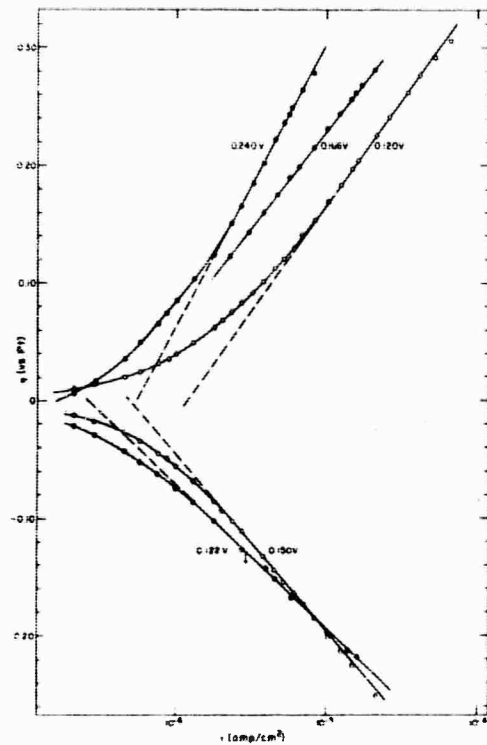


Fig. 22-6. Effect of anodic (dark circle) and cathodic (open circle) pulsing on polarization curve of the  $Fe^{3+}/Fe^{2+}$  couple (0.10M) on passive Fe-Cr in  $M MgSO_4$  at  $pH = 1.35$ . Curve corresponding to (dash half da  $\Delta$  circle dash) was obtained with electrodes which had not been pulsed ( $30^\circ C$ ). Arrows show points at which potential begins to drift in indicated direction. Measurements in these potential ranges were made rapidly and do not correspond to a steady state.

TABLE 22-1

$\text{Fe}^{+++}/\text{Fe}^{++}$  on Passive Fe-Cr  
T = 30.0°C

T = 30.0°C

<u><math>\text{Fe}^{+++}</math>, M/liter</u>	<u><math>\text{Fe}^{++}</math>, M/liter</u>	<u>pH<sup>a</sup></u>	<u><math>\alpha_c</math></u>	<u><math>\alpha_a</math></u>
$5.0 \times 10^{-3}$	$5.0 \times 10^{-3}$	0.30	0.40	0.37
$5.0 \times 10^{-2}$	$5.0 \times 10^{-2}$	0.30	0.38	0.37
$1.0 \times 10^{-1}$	$1.0 \times 10^{-1}$	1.35	0.43	0.36
$5.0 \times 10^{-2}$	$5.0 \times 10^{-2}$	1.5	0.40	0.35
$1.0 \times 10^{-1}$	$1.0 \times 10^{-1}$	1.7	0.41	0.35
$1.0 \times 10^{-1}$	$1.0 \times 10^{-1}$	2.1	0.38	0.30
$1.4 \times 10^{-2}$	$5.0 \times 10^{-3}$	0.60 <sup>b</sup>	0.42	0.38
$4.1 \times 10^{-2}$	$5.0 \times 10^{-3}$	0.60 <sup>b</sup>	0.40	0.38
$5.0 \times 10^{-2}$	$5.0 \times 10^{-2}$	0.30	0.40	{ 0.58 <sup>c</sup> 0.37
$5.0 \times 10^{-2}$	$5.0 \times 10^{-2}$	1.35	0.42	0.58 <sup>c</sup>
Avg $\alpha_c = 0.40 \pm 0.01$ $\alpha_a = 0.36 \pm 0.02$				

<sup>a</sup> All solutions M in  $\text{MgSO}_4$  except where noted.

<sup>b</sup> No  $\text{MgSO}_4$  added.

<sup>c</sup> Two Tafel slopes on anodic polarization; data not included in average  $\alpha_c$  or  $\alpha_a$ .

dependence of the kinetics on the electrochemical conditioning of the surface film (e. g. , "deforming") was also determined. The results are presented in Figs. 22-1 - 22-6 and Table 22-I.

Tafel behavior is generally observed with exchange currents of the order of  $10^{-6}$  amp/cm<sup>2</sup> ( $C_{\text{Fe}^{+++}} = C_{\text{Fe}^{++}} = 0.050\text{M}$ ), a cathodic transfer coefficient of 0.40, and an anodic transfer coefficient of 0.36. The electrochemical reaction order is unity both for oxidation of  $\text{Fe}^{++}$  and reduction of  $\text{Fe}^{+++}$ ; the heat of activation at the reversible potential is 10.8 kcal/mole.

The results show that an appreciable fraction of the total potential drop on anodic polarization occurs within the passive film. This potential drop is probably associated with changes in the average oxidation state of cations between the inner and outer layers of the surface oxide. The electrochemical characteristics of the film depend on the pH of the solution, probably because of the migration of protons into the passive film. A change in the kinetics of  $\text{Fe}^{++}$  oxidation which occurs in the trans-passive region of the Fe-Cr alloy is due to the production of  $\text{Fe}^{+3}$  or  $\text{Cr}^{+6}$  ions in the inner oxide layer.

### 23. Surface Oxidation of Gold Electrodes

S. B. Brummer and A. C. Makrides

Submitted as Technical Memorandum No. 6 (October, 1963).

Presented at the New York Meeting of the Electrochemical Society, October, 1963.

Published: J. Electrochem. Soc. 111, 1122-1128 (1964).

Most metals form stable surface oxides in the potential range where oxygen can be reduced. Therefore, a study of the electrochemical properties of surface oxides is a necessary step in the detailed study of the mechanism of oxygen reduction.

The surface oxides formed on electropolished gold by potentiostatic anodization in the range 1.2 – 1.85 v vs.  $H^+/H_2$  were studied by galvanostatic reduction at current densities between 10 and 1000  $\mu a/cm^2$ . Molar perchlorate solutions of pH 0.06 to 2.8 were employed.

Typical cathodic chronopotentiograms, taken after 5 minutes of constant potential anodization, are shown in Fig. 23-1. A notable feature of these curves is that the oxide is reduced at virtually a constant potential, although its "thickness" is only 1-2 monolayers.

The amount of oxide on the electrode increases with potential above 1.3 volts (Fig. 23-2), but is independent of pH at a fixed potential against the reversible hydrogen electrode (RHE) as can be seen from Fig. 23-3.

Current-potential curves constructed from the chronopotentiograms determined at various current densities follow Tafel curves with a slope of 39 to 42 mv/decade (Fig. 23-4). The Tafel slope is independent of the potential of formation of the oxide  $E_a$ , and of pH, but the exchange current of the reduction depends both on  $E_a$  and on pH. The order of the reduction reaction with respect to hydrogen ions is 1.4.

The following mechanism was proposed to account for the main experimental findings:

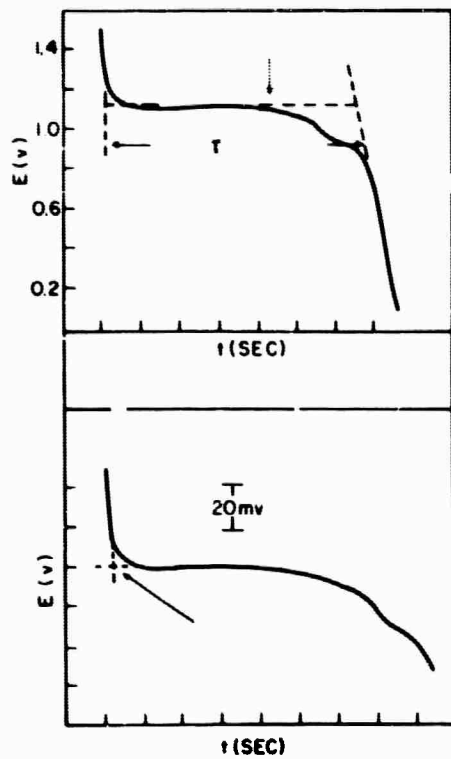


Fig. 23-1. Typical cathodic chronopotentiogram in 1N HClO<sub>4</sub> after 5 min of anodization at controlled potential. Arrow in upper figure indicates ~ 0.8 monolayer of O<sup>2-</sup> remaining on surface. Arrow in lower figure indicates the potential corresponding to the reduction of the oxide.

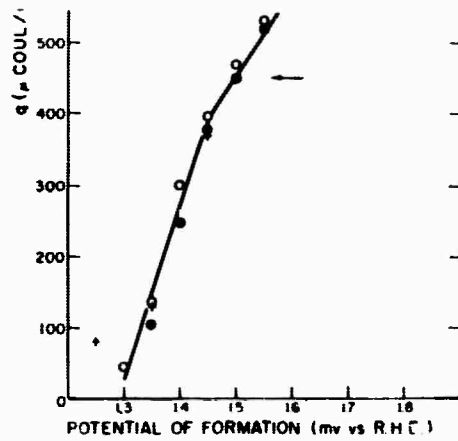


Fig. 23-2. Variation of cathodic charge with the potential of anodization in 1N HClO<sub>4</sub>. Open and closed circles are from different experiments in the present study. Crosses are from the results of Laitinen and Chao (J. Electrochem Soc. 108, 726(1961)). The arrow indicates a monolayer.

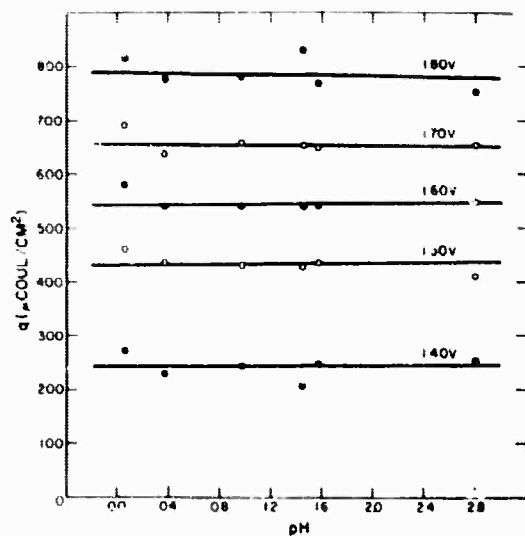


Fig. 23-3. Charge vs. pH at various potentials of formation.

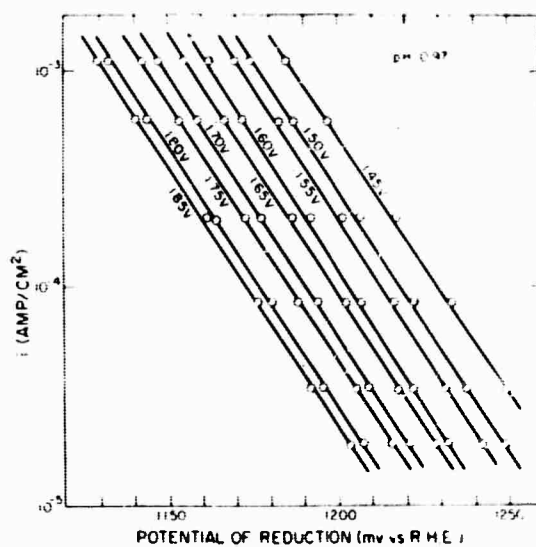
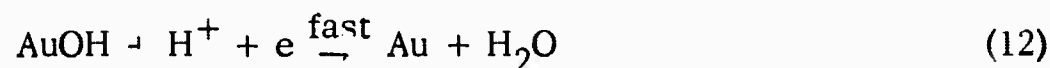
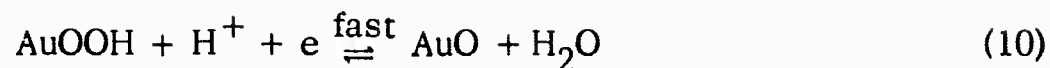


Fig. 23-4. Current-potential curves for reduction of films formed at various potentials.



where AuO is written as the Au<sup>II</sup> oxidation state and AuOH as the Au<sup>I</sup> oxidation state, but either of these may be hydrated. The rate equation is

$$i = 3k_{\text{II}}(\text{AuO})(\text{H}^+) \exp -\frac{\alpha\psi F}{RT} \quad (13)$$

where  $\alpha$ , the transfer coefficient, is  $\sim 0.5$ , and  $\psi$  is the potential. We can solve for (AuO) by assuming that reaction (I) is fast and is in equilibrium at all potentials. Then

$$\begin{aligned} \xrightarrow{k_{\text{I}}} (\text{AuOOH})(\text{H}^+) \exp -\frac{\beta\psi F}{RT} = \\ k_{\text{I}}(\text{AuO})(\text{H}_2\text{O}) \exp \frac{(1-\beta)\psi F}{RT} \end{aligned} \quad (14)$$

and

$$(\text{AuO}) = K(\text{AuOOH})(\text{H}^+) \exp -\frac{\psi F}{RT} \quad (15)$$

where K is a constant equal to  $k_{\text{I}}/k_{\text{I}}(\text{H}_2\text{O})$ . Then the final rate equation is

$$i = 3k_{\text{II}}K(\text{AuOOH})(\text{H}^+)^2 \exp -\frac{(1+\alpha)\psi F}{RT} \quad (16)$$

If the surface oxide AuOOH is thought of as a well-defined and essentially homogeneous solid, its activity will remain constant although its concentration declines during reduction. This would account for the initial flatness of the galvanostatic reduction curve. If  $\alpha$ , in Eq. 16, is 0.5, the Tafel slope is 39 mv, in good agreement with experiment.

The pH dependence,  $(\partial \log i / \partial \text{pH})_E$ , as given by Eq. 16 is -2. This result is only in moderate agreement with the experimental observation of  $(\partial \log i / \partial \text{pH})_E = -1.39$ .

Further experiments with this system have showed that certain cations in solution, viz.  $\text{Mg}^{+2}$ , considerably alter the kinetics of reduction of the oxide although the amount of oxide at any given potential is essentially the same. These effects probably result from specific adsorption of cations which modifies the double layer structure at the oxide-solution interface and may be crucial in determining the electrocatalytic properties of superficial oxides present during the cathodic reduction of  $\text{O}_2$ .

24. Ageing Effects on Thin Anodic Oxide Films on  
Gold in N HClO<sub>4</sub>

S. B. Brummer

Submitted as Technical Memorandum No. 20 (June, 1965).

Presented at the Toronto Meeting of the Electrochemical Society, May, 1964.

Published: J. Electrochem. Soc. 112, 633-636 (1965).

The properties of anodic oxide films on Au in 1N HClO<sub>4</sub> were studied as a function of time (2 sec to 5 min) and of potential of formation (1.45 to 1.85 v vs. Pt, H<sup>+</sup>/H<sub>2</sub> in the same solution).

Over the range observed (10-20% of the total oxide) the oxide grows slowly with time, apparently according to Elovich kinetics (Fig. 24-1) although the constants are potential-dependent.

The oxides formed at longer times at a given potential are harder to reduce (Fig. 24-2). This "ageing" effect is greatest at the lower potentials of formation despite the greater thickness of the oxide at the higher potentials and despite the larger change in the amount of oxide at the higher potentials.

The triangular sweep method should not be used in the quantitative investigation of these thin oxides, partly because the oxide is formed over a range of potentials, but mainly because of this ageing effect. Thus, oxides formed during a triangular sweep are easier to reduce than expected from the potential of formation, because of lack of ageing. They are also less homogeneous (reduced over a wider range of potentials) as shown in Fig. 24-3.

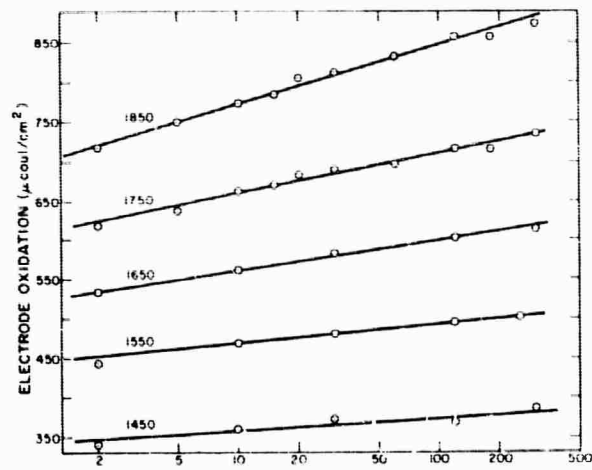


Fig. 24-1. Growth of oxide at various potentials (mv vs. R. H. E.) as a function of time.

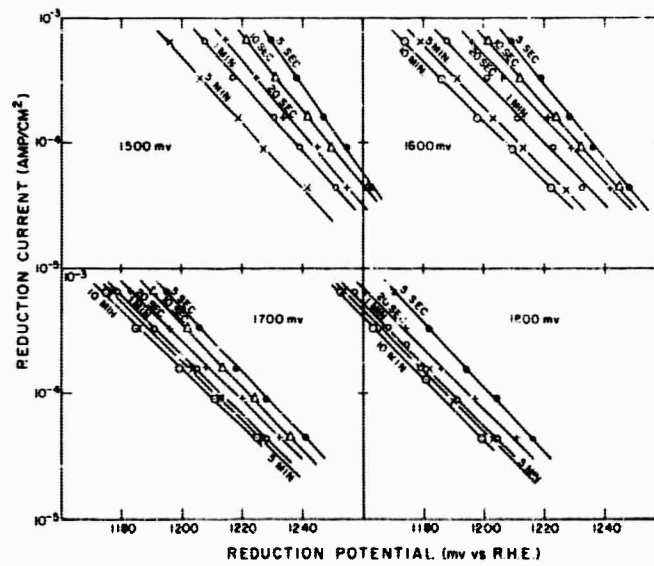


Fig. 24-2. Current-potential curves for the reduction of oxides, as a function of time and potential of formation.

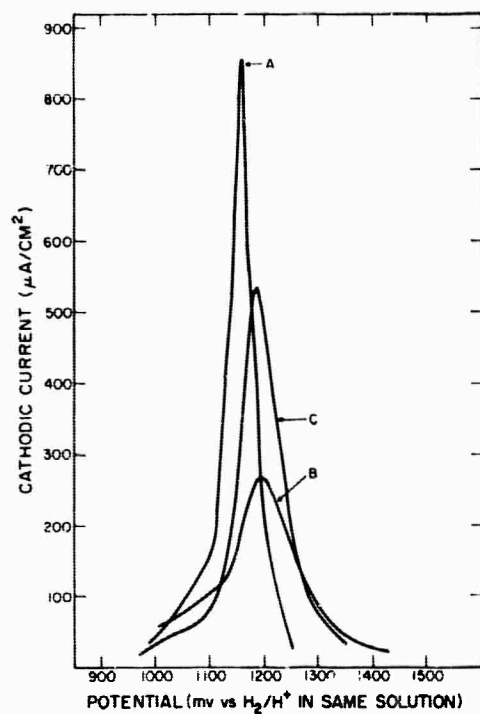


Fig. 24-3. Current-potential curves for the reduction of oxides, made with linear potential sweeps of 0.14 v/sec. Curve A, oxide reduced after 5 min at 1500 mv; curve B, oxide formed and reduced during triangular potential sweep, reversed at 1500 mv; curve C, triangular sweep reversed at  $\sim 1600$  mv, such that  $Q_A = Q_C$ .

**BLANK PAGE**

## DOCUMENT CONTROL DATA - R&amp;D

(Security classification of title, body of abstract and indexing annotation must be entered when the overall report is classified)

1. ORIGINATING ACTIVITY (Corporate author)  Tyco Laboratories, Inc.		2a. REPORT SECURITY CLASSIFICATION  Unclassified	
		2b. GROUP	
3. REPORT TITLE  Electrochemistry of Fuel Cell Electrodes			
4. DESCRIPTIVE NOTES (Type of report and inclusive dates) Final - Date: April 1, 1962 - October 15, 1965			
5. AUTHOR(S) (Last name, first name, initial)  MAKRIDES, A.C.; BRUMMER, S. B.; BUTLER, J.N.			
6. REPORT DATE 11/15/1965		7a. TOTAL NO. OF PAGES 113	7b. NO. OF RXFS
8a. CONTRACT OR GRANT NO. Nonr-3765(00)		9a. ORIGINATOR'S REPORT NUMBER(S)  None assigned	
b. PROJECT NO. 9800			
c. Task No. NR 359-443		9b. OTHER REPORT NO(S) (Any other numbers that may be assigned this report)	
d.			
10. AVAILABILITY/LIMITATION NOTICES  Reproduction in whole or in part is permitted by the U. S. Government. Distribution of this document is unlimited.			
11. SUPPLEMENTARY NOTES		12. SPONSORING MILITARY ACTIVITY  Office of Naval Research Materials Sciences Division	
13. ABSTRACT  This report is an extended abstract of the main results on a program which dealt with electrochemistry of fuel cell reactions, and included studies on the hydrogen reaction, the oxidation of organic fuels, and oxygen reduction. The clarification of the role of the electrode in catalyzing fuel cell reactions was the central theme of this work.  In order to establish the relation of electrocatalytic activity to electrode composition it is necessary first to understand in detail the mechanism of the reaction of interest. The simplest reaction studied was the hydrogen reaction, and in this case, it was possible to show that electrocatalytic activity is dependent on the electronic structure rather than the surface composition of the electrode. The oxidation of organic fuels and oxygen reduction are more complicated reactions and the work with these reactions was directed primarily towards elucidating their kinetics and mechanisms.  A summary of the main experimental results, of the conclusions reached, and of the implications of these studies in the development of fuel cells is given in Section II of this report. Detailed abstracts of the work done under this contract, and published in various journals, are given in Section III.			

14. KEY WORDS	LINK A		LINK B		LINK C	
	ROLE	WT	ROLE	WT	ROLE	WT
Electrochemistry; Electrode Kinetics; Fuel Cells Oxygen Electrode; Hydrocarbon Electrodes; Hydrogen Electrode; Hydrocarbon Oxidation Amalgam Electrodes; Oxide Electrodes; Platinum Electrode; Electrochemical Double Layer; Potentials of Zero Charge; Nickel Electrodes; Nickel Intermetallic Electrodes; Platinum Amalgam Electrodes; Indium Amalgam Electrodes; Thallium Amalgam Electrodes; Formic Acid Oxidation; Electrocatalysis						

**INSTRUCTIONS**

1. **ORIGINATING ACTIVITY:** Enter the name and address of the contractor, subcontractor, grantee, Department of Defense activity or other organization (*corporate author*) issuing the report.
- 2a. **REPORT SECURITY CLASSIFICATION:** Enter the overall security classification of the report. Indicate whether "Restricted Data" is included. Marking is to be in accordance with appropriate security regulations.
- 2b. **GROUP:** Automatic downgrading is specified in DoD Directive 5200.10 and Armed Forces Industrial Manual. Enter the group number. Also, when applicable, show that optional markings have been used for Group 3 and Group 4 as authorized.
3. **REPORT TITLE:** Enter the complete report title in all capital letters. Titles in all cases should be unclassified. If a meaningful title cannot be selected without classification, show title classification in all capitals in parenthesis immediately following the title.
4. **DESCRIPTIVE NOTES:** If appropriate, enter the type of report, e.g., interim, progress, summary, annual, or final. Give the inclusive dates when a specific reporting period is covered.
5. **AUTHOR(S):** Enter the name(s) of author(s) as shown on or in the report. Enter last name, first name, middle initial. If military, show rank and branch of service. The name of the principal author is an absolute minimum requirement.
6. **REPORT DATE:** Enter the date of the report as day, month, year, or month, year. If more than one date appears on the report, use date of publication.
- 7a. **TOTAL NUMBER OF PAGES:** The total page count should follow normal pagination procedures, i.e., enter the number of pages containing information.
- 7b. **NUMBER OF REFERENCES:** Enter the total number of references cited in the report.
- 8a. **CONTRACT OR GRANT NUMBER:** If appropriate, enter the applicable number of the contract or grant under which the report was written.
- 8b, 8c, & 8d. **PROJECT NUMBER:** Enter the appropriate military department identification, such as project number, subproject number, system numbers, task number, etc.
- 9a. **ORIGINATOR'S REPORT NUMBER(S):** Enter the official report number by which the document will be identified and controlled by the originating activity. This number must be unique to this report.
- 9b. **OTHER REPORT NUMBER(S):** If the report has been assigned any other report numbers (*either by the originator or by the sponsor*), also enter this number(s).
10. **AVAILABILITY/LIMITATION NOTICES:** Enter any limitations on further dissemination of the report, other than those

imposed by security classification, using standard statements such as:

- (1) "Qualified requesters may obtain copies of this report from DDC."
- (2) "Foreign announcement and dissemination of this report by DDC is not authorized."
- (3) "U. S. Government agencies may obtain copies of this report directly from DDC. Other qualified DDC users shall request through \_\_\_\_\_."
- (4) "U. S. military agencies may obtain copies of this report directly from DDC. Other qualified users shall request through \_\_\_\_\_."
- (5) "All distribution of this report is controlled. Qualified DDC users shall request through \_\_\_\_\_."

If the report has been furnished to the Office of Technical Services, Department of Commerce, for sale to the public, indicate this fact and enter the price, if known.

11. **SUPPLEMENTARY NOTES:** Use for additional explanatory notes.
12. **SPONSORING MILITARY ACTIVITY:** Enter the name of the departmental project office or laboratory sponsoring (*paying for*) the research and development. Include address.
13. **ABSTRACT:** Enter an abstract giving a brief and factual summary of the document indicative of the report, even though it may also appear elsewhere in the body of the technical report. If additional space is required, a continuation sheet shall be attached.

It is highly desirable that the abstract of classified reports be unclassified. Each paragraph of the abstract shall end with an indication of the military security classification of the information in the paragraph, represented as (TS), (S), (C), or (U)

There is no limitation on the length of the abstract. However, the suggested length is from 150 to 225 words.

14. **KEY WORDS:** Key words are technically meaningful terms or short phrases that characterize a report and may be used as index entries for cataloging the report. Key words must be selected so that no security classification is required. Identifiers, such as equipment model designation, trade name, military project code name, geographic location, may be used as key words but will be followed by an indication of technical content. The assignment of links, roles, and weights is optional.